Fall 2023

Load Determination, Strengthening, and Behavior Study of Prestressed Concrete Channel Bridge Girders in South Carolina

Elhussien Khaled Elbatanouny

Load Determination, Strengthening, and Behavior Study of Prestressed Concrete Channel Bridge Girders in South Carolina

by

Elhussien Khaled Elbatanouny

Bachelor of Science
Helwan University, 2017

Master of Science
University of South Carolina, 2021

Submitted in Partial Fulfillment of the Requirements

For the Degree of Doctor of Philosophy in

Civil Engineering

College of Engineering and Computing

University of South Carolina

2023

Accepted by:

Paul Ziehl, Major Professor

Robert Mullen, Committee Member

Fabio Matta, Committee Member

Thomas Cousins, Committee Member

Ann Vail, Dean of the Graduate School

Dedication

To my family and friends for their love, support, and encouragement.

Acknowledgments

My deepest gratitude is to my advisor, Dr. Paul Ziehl for his invaluable mentorship and continuous support throughout this research endeavor. Dr. Ziehl's expertise and patience have been instrumental in shaping this dissertation. I am also grateful to Dr. Ziehl for providing the necessary resources, facilities, and funding that enabled me to pursue this Ph.D. program.

I would like to thank the members of my dissertation committee, Dr. Robert Mullen, Dr. Fabio Matta, and Dr. Thomas Cousins for their valuable insights, feedback, and expertise. Their critical evaluation and suggestions have immensely contributed to the refinement of this research work.

I am also grateful to my research team: Dr. Li Ai, Dr. Laxman KC, and Alex Henderson for all the assistance they have provided during my research. Their efforts are appreciated. I consider each one of you a dear and close friend.

I am eternally grateful to my wife, Menna. Thank you for all the support and encouragement when I needed them most. You believed in me in times when I did not believe in myself. Your love and support have always lit my way.

I want to express my deepest gratitude to my mother, Fatma Shaltout. Your unwavering support, encouragement, and belief in me have been the pillars of my journey. I know that completing this dissertation is a dream of yours. I hope I can be the man you have always wanted me to be.

I want to express my gratitude to my brother, Mohamed Elbatanouny. You have always been my idol and the person I look up to. Despite your busy schedule, you have consistently taken the time to guide and support me. You serve as an excellent example of hard work and intelligence, and on top of that, you are an exceptional father.

Thanks to my sister, Hadeer Elbatanouny. You have always been an inspiration to me. Your achievements in your career have consistently motivated me. I hope you continue to achieve even greater success in your life, and I am truly proud of all that you have accomplished.

Thanks to all my family and friends back in Egypt. Your support and encouragement were always appreciated. You have always been there for me, even though we are miles apart right now.

Finally, thanks to God, “Allah’, nothing can be accomplished without his will.

Abstract

The South Carolina Department of Transportation (SCDOT) is currently engaged in a multi-year effort to assess the structural integrity of its inventory of over 9,000 bridges. This assessment process is expected to result in an increase in the number of bridges that require load postings, repairs, or replacements across South Carolina. This could potentially lead to adverse economic repercussions due to restricted truck routes, bridge closures, repair work, and the need for bridge replacements. To alleviate the escalating costs associated with these challenges, it is imperative to explore methods aimed at reducing the need for load postings and bridge closures or replacements.

This study is a part of an ongoing multi-year research investigation, which is being funded and supported by SCDOT. The study has three main objectives: (a) to investigate methods to strengthen the skinny-leg channel girder bridges to reduce the number of load postings, (2) utilize acoustic emission (AE) parameters for condition assessment of in-service bridges and determine the condition factor for load ratings of the bridges, and (3) extend the use of AE to determine the vehicle loads on the bridges while monitoring the deterioration. Three studies were performed to fulfill the objectives.

The first study addresses the existing gap in research by investigating different methods for strengthening prestressed skinny-leg girder bridges. Aluminum alloys possess desirable properties that make them attractive as external reinforcement materials. However, while previous studies have investigated the use of aluminum alloys on reinforced concrete members, there is a lack of investigation on their use on full-scale

prestressed concrete bridge girders. To address this gap, this study investigates the feasibility of utilizing aluminum alloy channels as an external reinforcement material on full-scale prestressed concrete bridge girders. Nine girders obtained from decommissioned bridges in South Carolina were tested under monotonic loading to failure. The test program consisted of six unstrengthened girders, one strengthened with bonded aluminum channels (SE), one strengthened with bonded and bolted aluminum channels (SEB), and one strengthened with bolted aluminum channels (SB). The results indicate that externally anchoring aluminum alloy channels with bolts was the most effective strengthening method in terms of practicality and higher increase in the moment capacity.

The second study proposes a data-driven condition assessment for in-service bridges using acoustic emission. The study aims to utilize AE parameters to assess the condition of the girders and to determine the condition factor used in the load rating of the bridges. Six prestressed concrete channel bridge girders, which were originally used in 30-ft span bridges constructed in the 1960s, were subjected to flexural tests at the University of South Carolina (USC). Acoustic emission (AE) was used to monitor the girders during the tests. The girders were visually inspected prior to testing and each girder was assigned a condition rating based on the Specifications for the National Bridge Inventory (SNBI). Intensity analysis charts were developed based on the collected AE data. The charts may detect if the girders are operating within the specified design criteria and are calibrated to theoretical cracking load and findings of cumulative signal strength analysis. In addition, the charts may assess the deterioration regardless of the initial girder condition, which can be utilized to determine the condition factor of the girders for load rating purposes.

The innovation of the third study lies in presenting a potential approach for predicting the vehicle loads on prestressed concrete girder bridges from the collected AE data. To achieve this goal, three improved machine learning algorithms based on artificial neural networks (ANN), AdaBoost, and random forest were adopted to analyze the AE data. An ensemble training strategy was employed to eliminate the imbalance issue while training machine learning models. The AE data was collected by conducting a flexural test on a full-scale prestressed concrete girder. In this study, load determination is considered a classification problem. The loading procedure was divided into load steps and the AE signals were classified to their corresponding load steps. The results show that the improved random forest algorithm outperformed the improved ANN and AdaBoost algorithms in classifying AE hits to their corresponding load steps.

Table of contents

Dedication iii

Acknowledgments iv

Abstract vi

Table of contents ix

List of Tables xii

List of figures xiv

List of symbols xvii

Chapter 1 Introduction 1

1.1 Background 2

1.2 Research Significance 6

1.3 Objectives 7

1.4 Layout of dissertation 9

Chapter 2 Literature review 11

2.1 Load rating 12

2.2 Review of literature relevant to strengthening methods utilizing aluminum alloys 15

2.3 Review of literature relevant to condition assessment using acoustic emission 18

2.4 Review of literature relevant to the prediction of load using acoustic emission 20

Chapter 3 Full-Scale Experimental Investigation of Prestressed Concrete Channel Bridge Girders Strengthened with Aluminum Alloy Channels 22

3.1 Abstract 23

3.2 Introduction 24
3.3 Literature Review 26
3.4 Research Significance 29
3.5 Experimental Program 30
3.6 Visual Inspection 40
3.7 Results and discussion 45
3.8 Summary and comparison 53
3.9 Conclusions 56
Chapter 4 Condition Assessment of Prestressed Concrete Channel Bridge Girders Using Acoustic Emission and Data-Driven Methods 59
4.1 Abstract 60
4.2 Introduction 61
4.3 Acoustic emission 63
4.4 Experimental procedure 65
4.5 Visual Inspection 70
4.6 Results and discussion 74
4.7 Conclusions 79
Chapter 5 An Automated Load Determination System for Bridges based on Acoustic Emission and Machine Learning Techniques 81
5.1 Abstract 82
5.2 Introduction 83
5.3 Experimental Setup 87
5.4 Data Processing and Methodology 93

5.5 Results and Discussion 104

5.6 Conclusions and recommendations 115

Chapter 6 Summary and Conclusions 117

6.1 Summary 118

6.2 Conclusions of each study 119

6.3 General conclusions 122

6.4 Recommendations and Future Work 123

References 126

Appendix A - Material Testing Results 135

Appendix B - Calculations 141

Appendix C - Machine Learning Models 158

Appendix D - Condition Assessment 165

List of Tables

Table 3.1 Specimens designation 32

Table 3.2 Details of the aluminum channel section 33

Table 3.3 Details of aluminum threaded rods 35

Table 3.4 Details of steel threaded rods 36

Table 3.5 Approximate conversion in selecting $\emptyset c$ [7] 40

Table 3.6 Condition rating of each girder 44

Table 3.7 Summary of test results of unstrengthened girders 48

Table 3.8 Summary of test results of strengthened girders. 52

Table 3.9 Comparison of the test results 56

Table 4.1 Approximate conversion in selecting $\emptyset c$ [7] 70

Table 4.2 Summary of condition state of each girder 73

Table 5.1 Limitations of the second filter [86] 94

Table 5.2 AE signal parameters 94

Table 5.3 Accuracies of the three algorithms 112

Table A.1 Concrete compression test results 136

Table A.2 Equivalent specified strength results (fc, eq') 137

Table A.3 Calculations of equivalent specified strength (fc, eq') 138

Table A.4 Ultimate tensile strength for strands tested. 139

Table B.1 Moment capacity for different material properties 149

Table B.2 LRFR Strength I design load ratings (inventory) 151

Table B.3 LFR design load ratings (inventory) 152

Table B.4 Materials cost for strengthening of the girders. 155

List of figures

Figure 1.1 Photograph of a precast prestressed concrete channel bridge girders [4] 3
Figure 1.2 Typical cross-section of skinny-leg channel girder (SCDOT drawing)..... 4
Figure 1.3 Rating factors (RF) of the skinny-leg channel girder bridges [5] 4
Figure 3.1 Photographs of a precast prestressed concrete channel bridge girders [4]..... 25
Figure 3.2 Typical cross-section of skinny leg-channel girder (SCDOT drawing)..... 25
Figure 3.3 Rating factors (RF) of the skinny-leg channel girder bridges [5] 26
Figure 3.4 Dimensions and reinforcement details of the girders..... 31
Figure 3.5 Cross-sections of the girders; left) with end diaphragms, right) without end diaphragms..... 32
Figure 3.6 Strengthening schemes: a) SE, b) SEB, and c) SB..... 33
Figure 3.7 (left) surface preparation by needle gun; (right) Epoxy was applied, and the aluminum channels were placed. 34
Figure 3.8 Aluminum channels bonded and bolted with aluminum threaded rods. 35
Figure 3.9 Aluminum channels bolted with steel threaded rods..... 36
Figure 3.10 Test setup of the girders 37
Figure 3.11 Photos of the test setup of the girders..... 38
Figure 3.12 Various strand deterioration conditions..... 40
Figure 3.13 Existing deterioration of the girders..... 44
Figure 3.14 Moment versus midspan displacement for the unstrengthened girders..... 46
Figure 3.15 Failure modes of the unstrengthened girders..... 47

Figure 3.16 Moment versus midspan displacement for the strengthened girders..... 50
Figure 3.17 Failure modes for the strengthened girders 51
Figure 3.18 Moment versus midspan displacement for the girders 55
Figure 4.1 Dimensions and reinforcement details of the girders 66
Figure 4.2 Elevation (top) and plan view (bottom) of girders test setup 67
Figure 4.3 Elevation (top) and plan (bottom) instrumentation layout 68
Figure 4.4 Photos of the test setup of the girders..... 69
Figure 4.5 Load vs time 70
Figure 4.6 Existing deterioration for the girders..... 73
Figure 4.7 CSS and Load curves versus time for girders in good condition 74
Figure 4.8 CSS and Load curves versus time for girders in poor condition 75
Figure 4.9 Intensity analysis chart (girders in good condition) 77
Figure 4.10 Intensity analysis chart (girders in poor condition)..... 78
Figure 5.1 Dimensions and reinforcement details of girder 88
Figure 5.2 Test setup of the girder 89
Figure 5.3 Photos of the test setup of the girder 90
Figure 5.4 Load vs Time 91
Figure 5.5 Schematic of acoustic emission parameters [85]..... 92
Figure 5.6 AE sensors configuration 93
Figure 5.7 Amplitude and load vs time for the test..... 96
Figure 5.8 Balanced training (BT) and testing for the machine learning models..... 97
Figure 5.9 Decision-making process..... 98
Figure 5.10 Three-layer artificial neural network..... 99

Figure 5.11 Mechanism of a backpropagation network 100
Figure 5.12 The architecture of the AdaBoost algorithm 102
Figure 5.13 The architecture of the random forest 104
Figure 5.14 Output of BT-ANN 106
Figure 5.15 Output of BT-AdaBoost 108
Figure 5.16 Output of BT-random forest 110
Figure 5.17 The confusion matrixes of (a) GTANN; (b) GTAdaBoost; (c) GTRF 111
Figure 5.18 Evaluation of load steps (a) GT-ANN; (b) GT-AdaBoost; (c) GT-RF 113
Figure 5.19 Comparison of F1 scores 114
Figure A.1 Strands extracted from specimens 139
Figure B.1 Typical Channel Cross-Section (SCDOT drawing) 142
Figure B.2 Strain versus time for aluminum channels at midspan for girder (SEB) 156
Figure B.3 Strain versus time for aluminum channels at midspan for girder (SB) 157
Figure C.1 Output of BT-SVM 160
Figure C.2 The maximum probability a) BT-RF; b) BT-SVM 161
Figure C.3 Output of random forest trained on data from five girders and tested on another girder 162
Figure C.4 Output of random forest trained on data from eight girders 163
Figure C.5 Output of random forest trained on data from nine girders and tested on random sample 164
Figure D.1 Intensity analysis chart (girders in good condition) 167
Figure D.2 Intensity analysis chart (girders in poor condition) 168

List of symbols

RF	Rating Factor
C	Capacity (LRFD)
DC	Dead load effect due to structural components and attachments
DW	Dead load effect due to wearing surface and utilities.
P	Permanent loads other than dead loads
LL	Live load effect
IM	Dynamic load allowance
γ_{DC}	LRFD load factor for structural components and attachments
γ_{DW}	LRFD load factor for wearing surfaces and utilities.
γ_P	LRFD load factor for permanent loads other than dead loads = 1.0
γ_{LL}	Evaluation live load factor
$\emptyset_c$	Condition factor
$\emptyset_s$	System factor
$\emptyset$	LRFD resistance factor
f'_c	Specified compressive strength of concrete.
f_{pu}	Specified ultimate tensile strength of prestressing strands.
f_{py}	Specified yield strength of prestressing strands.
f_{yA}	Specified yield strength of aluminum alloy channels

B Width of the top flange

t_s Flange thickness

t_w Web thickness

h Girder thickness

b_{wb} Bottom web width

b_{wu} Upper web width

A_g Cross-section area

I_g Moment of inertia

y_{bs} Distance between the centroid of prestressing strands to bottom fiber.

d_{ps} Distance between the centroid of prestressing strands to top fiber.

A_{ps} Area of prestressing strands

E_{ps} Modulus of Elasticity of prestressing strands

E_A Modulus of Elasticity of aluminum alloy channels

A'_s Area of steel bars

f'_y Specified yield strength of steel bars.

M_{cr} Cracking moment

M_n Nominal moment capacity

ε_s Strain in the steel reinforcing bars.

E_s Modulus of Elasticity of steel bars

c Depth of neutral axis

M_n Nominal moment capacity

Chapter 1

Introduction

1.1 Background

Bridges are integral to the aging infrastructure throughout the United States. The state of South Carolina relies significantly on its numerous bridges for community connectivity, trade, and transportation. The state ranks 26th in the nation in bridge inventory, with more than 9,000 bridges. Most bridges were designed utilizing the H-10 or H-15 loading standards. In comparison, the current loading standard of HL-93, is much greater [1], [2]. The South Carolina Department of Transportation (SCDOT) manages approximately 90% of all bridges. On average, the bridges in this area are 40 years old, approaching the 50-year service level, with 6.8% being load posted, 11% being structurally deficient, and 0.33% being reported closed [3]. This is a direct outcome of bridge deterioration and overloading due to their long service lives and increased vehicle loads.

The SCDOT is currently engaged in a multi-year effort to assess the structural integrity of its inventory of over 9,000 bridges. This assessment process is expected to result in an increase in the number of bridges that require load postings, repairs, or replacements across South Carolina. This could potentially lead to adverse economic repercussions due to restricted truck routes, bridge closures, repair work, and the need for bridge replacements. To alleviate the escalating costs associated with these challenges, it is imperative to explore methods aimed at reducing the need for load postings and bridge closures or replacements.

Initial findings from the effort have identified prestressed concrete channel girder bridges as one of the problematic superstructure types. Out of the 9,481 bridges in South Carolina, 377 are prestressed channel girder bridges. These bridges were built between 1950 and 2000 with the majority being built in the 1960s. These bridges typically consist

of multiple spans and are supported by timber pile substructures. Figure 3.1 presents field picture of prestressed concrete channel bridge girders.

Figure 1.1 Photograph of a precast prestressed concrete channel bridge girders [4]

The prestressed concrete channel girders can be separated into two categories: skinny-leg channel girders and wide-leg channel girders. There are 103 skinny-leg channel girder bridges and 274 wide-leg channel girder bridges in South Carolina. This dissertation will focus on skinny-leg channel girders. The name comes from the cross-section shape that creates a channel along the span length. They are comprised of channel sections with a span length of 30 ft. The bridge cross-section typically consists of ten or more girders. Each girder is 30.5 in. or 33 in. wide. The girders are tied together by transverse tie rods at quarter points along the span. The thickness of the flanges is 5 in., while the web thickness tapers down to 2.5 in. at the bottom with five prestressing strands on each leg. Figure 1.2 depicts a typical cross-section drawing of a skinny-leg channel girder obtained from an SCDOT drawing.

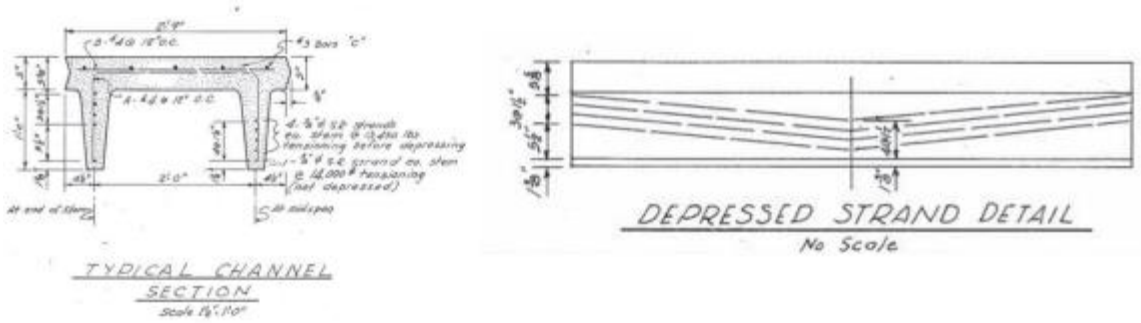

Figure 1.2 Typical cross-section of skinny-leg channel girder (SCDOT drawing)

The skinny-leg channel girder bridges are designed for H15-44 loading criteria, which is lower than the design vehicles used in current design standards (HL-93). The SCDOT conducted load ratings of these bridges, using the typical EV-3 truck as the controlling vehicle in the rating process. Among these bridges, almost all the skinny-leg channel girder bridges have a load rating factor (RF) below 1, indicating the need for load postings, repairs, or replacements due to capacity limitations (Figure 1.3) [5].

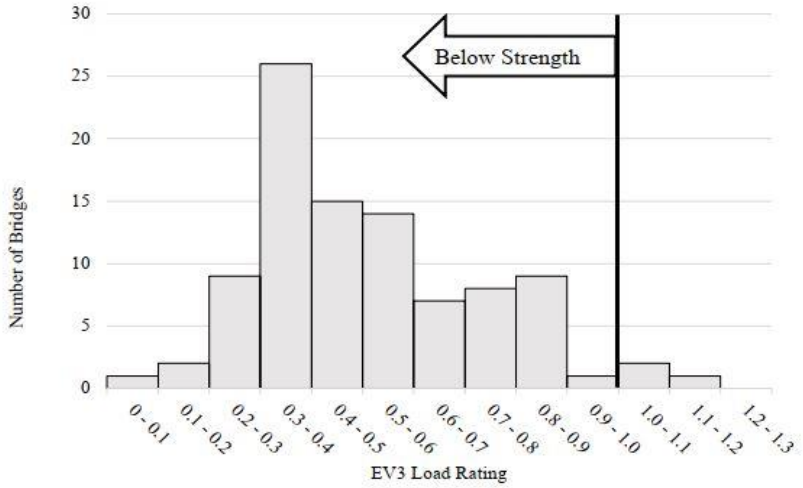

Figure 1.3 Rating factors (RF) of the skinny-leg channel girder bridges [5]

Laboratory testing on the skinny-leg channel girders was a collaborative effort involving Clemson University and the University of South Carolina. This study, however, specifically examines the investigations conducted at the University of South Carolina, with the primary goal of addressing a particular challenge related to reducing load

restrictions on these bridges. In many cases, repairing and strengthening the sections with deficiencies presents a cost-effective and structurally efficient solution. Nevertheless, there has been a lack of substantial research dedicated to the design and implementation of repair and strengthening strategies for this class of structures. The motivation of this study is to explore strengthening techniques for skinny-leg girder bridges that are cost-effective and easily implemented in the field to extend their lifespan.

Furthermore, the deterioration of concrete bridges is a crucial issue. Most in-service bridges have experienced various levels of deterioration. Visual inspection is primarily used in the United States by bridge owners to evaluate the condition, however, this method is not well suited for detecting concealed defects or those located in areas that are not easily accessible [6]. In addition, visual inspections are conducted periodically, typically every 2 years [7]. The condition of the bridges may experience alterations during this period. However, in some cases, bridge inspectors are sent to the structure on an increased frequency, resulting in a more time-consuming and labor-intensive process [8]. Furthermore, the efficiency of bridge inspection procedures can be subjective to the expertise of the inspector [9]–[11]. To overcome these challenges, an alternative approach is to develop and install a structural health monitoring (SHM) system. When well-designed and properly implemented, the SHM system can effectively replace the frequency of manual inspections, often resulting in cost savings. Once critical structural parameters are identified for a structure's performance, sensors that can continuously monitor its condition can be installed. This not only provides a more objective set of performance measurements but also allows for more frequent data collection, enabling precise and convenient tracking of historical trends. Furthermore, it offers immediate warning to the owner if specific

structural thresholds are exceeded. Engineers can monitor current and historical trends from a centralized location, reducing the necessity for unscheduled on-site inspections, unless the collected data suggests otherwise. In addition, it provides site-specific data on the condition of bridges for maintenance funding prioritization.

Nondestructive approaches such as acoustic emission (AE) have been utilized in monitoring bridge degradation [12], [13]. AE was chosen over other methods due to its high sensitivity for detecting stress waves resulting from material changes, such as the formation of cracks [14]. Furthermore, being a passive non-destructive testing method, AE is a feasible candidate for structural health monitoring. The motivation for this study is to propose an SHM system utilizing AE that can evaluate the condition of the in-service bridges and determine the condition factor for load rating applications. In addition, this study explores the feasibility of predicting the vehicle loads that pass over the bridges from the collected AE data. Correlating AE criteria with load demand can provide meaningful insight into the extent of structural deterioration occurring in the structure. In addition, bridge loads are subject to a great deal of uncertainty, primarily due to live loads. One effective way to decrease uncertainty is to assess live loads and conduct load ratings by obtaining site-specific traffic data [15].

1.2 Research Significance

One specific superstructure type, prestressed skinny-leg girders, is addressed in this study. The first study addresses the existing gap in research by investigating different methods for strengthening prestressed skinny-leg girder bridges. Aluminum alloys possess desirable properties that make them attractive as external reinforcement materials. However, while previous studies have investigated the use of aluminum alloys on

reinforced concrete members, there is a lack of investigation on their use on full-scale prestressed concrete bridge girders. To address this gap, this study investigates the feasibility of utilizing aluminum alloy channels as an external reinforcement material on full-scale prestressed concrete bridge girders.

The second and third studies propose a data-driven condition assessment for in-service bridges using acoustic emission. The second study aims to utilize AE parameters to assess the condition of in-service bridges and to determine the condition factor used in the load rating of the bridges. The study also presents deterioration quantification charts based on the collected AE data. In addition, the third study explores a potential approach for estimating the vehicle loads on prestressed concrete girder bridges from the collected AE data while monitoring the deterioration.

The output of this work proposes potential strengthening methods for prestressed skinny-leg channel girder bridges that are cost-effective and easier to implement in the field to reduce the number of load-posted bridges. Furthermore, this work develops condition assessment tools for the evaluation of the current condition of bridges and estimates the condition factor for load rating purposes. In addition, this work extends the use of AE to predict the vehicle loads on prestressed girder bridges from the collected AE data while monitoring the deterioration. This approach may potentially provide site-specific data for load and traffic conditions for load rating applications.

1.3 Objectives

This study is a part of an ongoing multi-year research investigation, which is being funded and supported by SCDOT. The study presented has three main objectives: (a) to investigate methods to strengthen the skinny-leg channel girder bridges to reduce the

number of load postings, (2) to utilize acoustic emission (AE) parameters for condition assessment of in-service bridges, and (3) to develop a potential approach for predicting vehicle loads that pass over bridges from the AE data collected while monitoring the bridge. To fulfill these objectives, three independent research studies were performed to achieve the goals. Each study had its own specific set of objectives, which can be summarized as follows:

1.3.1 Full-Scale Experimental Investigation of Prestressed Concrete Channel Bridge Girders Strengthened with Aluminum Alloy Channels

In this study, four-point bending tests were conducted on the prestressed skinny-leg channel girders until failure to study their flexural behavior before and after strengthening. The objectives of this study were:

- Evaluate the prestressed skinny-leg channel girders' existing deterioration and its effect on the moment capacity.
- Evaluate and investigate strengthening methods utilizing aluminum alloy channels externally bonded or bolted to the girders.

1.3.2 Condition Assessment of Prestressed Concrete Channel Bridge Girders Using Acoustic Emission and Data-Driven Methods

In this study, AE sensing was employed to evaluate the condition state of prestressed skinny-leg channel girders. The main objectives of this study were:

- Utilize AE parameters for condition assessment of the prestressed skinny-leg channel bridge girders.
- Quantify the deterioration in the girders observed during visual inspection using AE parameters.

- Determine the condition factor of the girders.

1.3.3 An Automated Load Determination System for Bridges Based on Acoustic Emission and Machine Learning Techniques

In this investigation, machine learning models were developed and implemented for predicting the vehicle loads that pass over prestressed skinny-leg girder bridges from the collected AE data. The primary objectives of this study were:

- The classification of acoustic emission (AE) hits to their corresponding load steps.
- Develop an optimized method for predicting vehicle loads that pass over prestressed concrete channel bridge girders from the collected AE data.

1.4 Layout of dissertation

Six chapters are included in the dissertation. Chapter 1 serves as an introduction, providing background information, motivation, research significance, objectives, and layout of the dissertation. Chapter 2, titled "Literature Review," introduces background information from published literature. Chapter 3, Chapter 4, and Chapter 5 were prepared in the format of journal articles. Therefore, some essential explanations may be repeated.

In Chapter 3, “Full-Scale Experimental Investigation of Prestressed Concrete Channel Bridge Girders Strengthened with Aluminum Alloy Channels”, a study that presents nine prestressed skinny-leg channel girders obtained from decommissioned bridges in South Carolina which were tested under monotonic loading to failure. The test program was comprised of six unstrengthened girders, one strengthened with bonded aluminum channels (SE), one strengthened with bonded and bolted aluminum channels (SEB), and one strengthened with bolted aluminum channels (SB). This chapter

demonstrates the feasibility of utilizing aluminum alloy channels as an external reinforcement material on full-scale girders.

Chapter 4 is titled “Condition Assessment of Prestressed Concrete Channel Bridge Girders Using Acoustic Emission and Data-Driven Methods”. This chapter presents an effort to use non-destructive evaluation techniques, particularly AE, to evaluate the condition state of prestressed skinny-leg channel bridge girders. Six girders were subjected to flexural tests at the University of South Carolina. AE was used to monitor the girders during the tests. The study presents deterioration quantification charts based on the collected AE data.

Chapter 5 is titled “An Automated Load Determination System for Bridges Based on Acoustic Emission and Machine Learning Techniques”. This chapter presents a potential approach for predicting the vehicle loads on prestressed concrete girder bridges from the collected AE data while monitoring the deterioration. Three improved machine learning algorithms based on artificial neural networks (ANN), AdaBoost, and random forest were adopted to analyze the AE data. The AE data was collected by conducting a flexural test on a full-scale prestressed concrete girder. The results obtained from all the models are discussed in this chapter.

Chapter 6 includes a summary of the work carried out in the dissertation as well as conclusions based on this study. Moreover, within this chapter, recommendations for further research are also provided.

Chapter 2

Literature review

2.1 Load rating

Bridge load rating is the process of determining the safe load-carrying capacity of a bridge using analytical methods, experimental methods, or a combination of both. Bridges are evaluated to ensure that they have an adequate reserve structural capacity to meet the anticipated live load requirements, with a safety margin [16]. In cases where the reserve structural capacity is insufficient to support the anticipated live load demands, measures such as load posting, rehabilitation, or closure of the bridge may be necessary to guarantee public safety.

Load rating is governed by the American Association of State Highway and Transportation Officials Manual for Bridge Evaluation (AASHTO MBE). SCDOT adheres to the load rating requirements specified in the AASHTO MBE, with certain adjustments tailored to align more effectively with the state's bridge infrastructure. The AASHTO MBE manual provides three distinct methodologies for load rating bridges: Allowable Stress rating (ASR), Load Factor Rating (LFR), and Load and Resistance Factor Rating (LRFR). Among these methodologies, the LRFR stands out as the most recently developed approach for load rating. It sustains a consistent level of reliability by considering the structural deterioration that occurs over time utilizing a condition factor, in contrast with the other methods. The outcomes of the LRFR method are conveyed in the form of a rating factor. The LRFR equation for load rating analysis is:

$$RF = \frac{C-(\gamma_{DC})(DC)-(\gamma_{DW})(DW)-(\gamma_P)(P)}{(\gamma_{LL})(LL+IM)} \quad \text{(Eq.1)}$$

where:

$RF =$ Rating Factor

$C =$ Capacity (LRFD)

DC = Dead load effect due to structural components and attachments

DW = Dead load effect due to wearing surface and utilities.

P = Permanent loads other than dead loads

LL = Live load effect.

IM = Dynamic load allowance

γ_{DC} = LRFD load factor for structural components and attachments

γ_{DW} = LRFD load factor for wearing surfaces and utilities.

γ_P = LRFD load factor for permanent loads other than dead loads

γ_{LL} = Evaluation live load factor

and for strength limit states:

$C = \emptyset_c \emptyset_s \emptyset R_n$ (Eq.2)

$\emptyset_c$ = Condition factor

$\emptyset_s$ = System factor

$\emptyset$ = LRFD resistance factor

R_n = Nominal member resistance

Bridges subjected to evaluation using the LRFR method undergo comprehensive assessments that involve the application of various live load models. Three distinct procedures are employed: design load rating, legal load rating, and permit load rating. These procedures utilize design live loads, legal loads, and permit loads, respectively for evaluating the bridges. Design load rating holds particular significance as it acts as the primary assessment to determine whether a bridge needs to be posted. There are two distinct sub-classes of design load rating, known as inventory and operating levels. The inventory load rating is associated with a reliability level that surpasses that of the

operating load rating. In cases where the inventory rating factor is less than one, the operating rating factor must be checked. When the operating rating factor is less than one, the bridge must undergo separate evaluations for each truck specified in the legal load rating. This process is crucial for determining the appropriate load posting requirements of the bridge.

The computation of the rating factor according to the LRFR method using equations (Eq.1 and Eq.2), entails the determination of several factors. Most of these factors can be updated in alignment with established codes, guidelines, and bridge specifications. However, the condition factor requires a visual inspection of the bridge. This inspection process is characterized by its time-consuming nature, labor-intensive requirements, and a substantial reliance on the expertise of the inspectors. An alternative approach involves the development and implementation of an SHM system, capable of determining the condition factor based on collected data. This method not only offers objectivity but also enables the continuous and real-time updating of load rating assessments.

Currently, bridges are load rated using specified material properties from old bridge drawings. This method can underestimate the actual capacity of a bridge. Gunter et al. [4] performed a laboratory test on a decommissioned prestressed wide-leg channel bridge girder. The results revealed that the experimental moment capacity was higher than the AASTO calculations. This was attributed to the higher than specified material properties.

A series of experimental tests were conducted on prestressed skinny-leg girders obtained from decommissioned bridges in South Carolina[17]. The primary goal of this thesis was to contribute to the reduction of load-bridges by acquiring a deeper

understanding of the relationship between deterioration and capacity. Thirteen girders were tested at full scale for flexural resistance in the laboratory. The girders sustained deterioration throughout their service life. Spalling, cracking, and section loss were observed for most of the girders which led to several feet of an exposed strand(s). In addition, some girders contained visibly corroded strand(s). The condition of the girders was then assessed and categorized based on the Specifications for the National Bridge Inventory (SNBI) condition rating. Each girder was assigned a condition rating ranging from 0 to 9, based on the observed deterioration. The results revealed that the girders in good condition (NBI 6 or higher) had higher experimental moment capacity than the nominal capacity. This was attributed to the higher than specified material properties. In addition, the girders in poor condition (NBI 4 or lower) had lower experimental moment capacity than the nominal capacity. This was attributed to the deterioration observed prior to testing. The findings from this study highlight the potential discrepancy between specified and actual material properties, which could lead to inaccuracies in load ratings. Additionally, this research emphasizes the importance of inspection methods as a viable means to anticipate the effects of deterioration on the moment capacity,

2.2 Review of literature relevant to strengthening methods utilizing aluminum alloys

Several research studies have been carried out to improve the flexural strength of reinforced concrete (RC) beams utilizing aluminum alloy (AA) as an external reinforcement material.

Rasheed et al. [18] conducted an experimental investigation to validate the feasibility and practicality of using AA plates as external reinforcement for enhancing the strength of reinforced concrete beams. The study assessed the performance of RC beams

strengthened with AA plates, both with and without the addition of carbon fiber reinforced polymers (CFRP) sheets acting as end-anchors. Ten RC beams were cast and tested under monotonic loading to failure. The beams were 10 in. thick, 5 in. wide, and 6 ft. long. One specimen served as a control specimen. The remaining beams were strengthened by attaching AA plates to the soffit using epoxy adhesive. Four strengthened beams had no end anchorages. Four strengthened beams had end anchorages, in the form of U-wrap CFRP sheets, which were applied in either a single-layer or double-layer configuration. In addition, one strengthened beam had three double-layer U-wrap CFRP sheets (one at mid-span and two at the ends).

The results of the study demonstrated that all strengthened beams exhibited a substantial increase of 13% to 40% in flexural strength compared to the control specimen. The authors reported that the strengthened beams without end anchors failed primarily in flexure with full debonding of AA plates, whereas the strengthened beams with end anchors failed due to localized debonding of AA plates and flexure. Moreover, strengthened beams without end anchorages showed a ductile response lower than the control specimen. However, end anchorages were observed to enhance the ductility of the strengthened beams to comparable levels of ductility of the control specimen. The authors reported that the strengthened beam having the extra midspan anchorage has the lowest ductility.

Abuodeh et al. [19] investigated the effectiveness of using mechanically fastened (MF) aluminum alloy (AA) plates for flexural strengthening of RC members. The test program involved preparing 16 RC beams, one left unstrengthened, one strengthened with an externally bonded plate using epoxy, four strengthened with mechanically fastened

plates, and the remaining beams strengthened with epoxy-bonded and mechanically fastened plates of varying sizes, spacing, and layout. The beams were 10 in. thick, 5 in. wide and 6 ft. long. The results of the study demonstrated that all strengthened beams exhibited an increase that ranged between 16% to 35% in flexural strength compared to the unstrengthened beam. It was concluded that implementing epoxy and end anchor bolts is a viable approach to enhance the strength and ductility of reinforced concrete beams strengthened with aluminum alloy plates. In addition, analytical predictions were made to assess the advantages of using mechanically fastened systems. The authors concluded that the use of end anchors eliminated premature failure modes. Hence, the flexural capacity of the strengthened beams can be predicted following the design procedures in ACI 318-19 code.

Zhang et al. [20] conducted a study to investigate the use of aluminum alloy plates in the bolted side-plating (BSP) retrofitting technique for RC beams. The study aimed to examine the effects of several factors such as plate thickness, plate height, bolt spacing, anchoring techniques, and prestressing on the flexural strength, stiffness, and ductility of the beams. The test program involved conducting experiments on seven specimens with different configurations of aluminum plates and bolts. The beams were 14 in. thick, 8 in. wide, and 9 ft. long. The results of the study demonstrated that all strengthened beams exhibited an increase that ranged between 40% to 67% in flexural strength compared to the unstrengthened beam. However, all the strengthened beams demonstrated lower ductility than the unstrengthened beam. The study results show that increasing the thickness of aluminum plates and reducing the spacing of the bolts can significantly increase the

flexural capacity and stiffness of the beams. In addition, the prestressing of the AA plates recovered the deflection of the RC beam for 60% under service loading.

2.3 Review of literature relevant to condition assessment using acoustic emission

Elbatanouny et al. [21] employed AE to monitor eight prestressed concrete beams subjected to cyclic load testing (CLT). The primary objective of the research was to investigate the utilization of AE in assessing structural deterioration, serving as a supplement to conventional measurements used to evaluate the condition of a structure, following the acceptance criteria for CLT. The test program included eight prestressed concrete T-beams, each spanning 16 ft. Five specimens were pre-cracked, with varying levels of corroded tendons, while the remaining specimens served as control specimens. Four specimens exhibited a crack width of 0.016 in., while one specimen achieved a crack width of 0.032 in. The simply supported specimens were tested in a four-point bending test setup. Load application was carried out using cycles of increasing magnitudes. Sixteen AE sensors were mounted on each specimen. AE was monitored continuously throughout the load testing.

Signal strength, energy, and amplitude were the three parameters used in establishing the AE evaluation criteria. Signal strength was of the AE hits used in the intensity analysis evaluation method. Intensity analysis was performed on all the specimens and only the AE data collected during the loading phase was used in this analysis. Intensity analysis evaluation charts were developed to assess the deterioration in the specimens. The results demonstrated that the method was successful in quantifying the existing deterioration in the specimens.

Energy associated with AE hits was used in the relaxation ratio evaluation method. Data collected during both the loading and unloading phases contributed to this analysis. The method is based on the impact of cracks present in a specimen. The relaxation ratio is computed as the ratio between the energy recorded during unloading and the energy recorded during loading. The presence of higher AE energy during the unloading phase, compared to the loading phase, serves as an indicator of deterioration. The results indicated that the relaxation ratio could detect a transition in the cracking behavior, shifting from micro-cracking (invisible) to macro-cracking (visible). However, this observation primarily applied to control specimens. No clear trend was observed for the pre-cracked specimens.

The amplitude of the AE hits was used in the b-value evaluation method. The b-value serves as an indication of degradation in the integrity of the specimen and is associated with the formation of cracks. When cracks begin to form, there is an increase in the number of hits with high magnitude, resulting in a reduction in the magnitude of the b-value. The results revealed that the b-value analysis offered an early warning of deterioration accumulation in both the control and pre-cracked specimens. The authors concluded that utilizing AE data in conjunction with traditional load-deflection response data enables a better evaluation of structural health.

Anay et al. [22] applied AE for the evaluation of the condition of a single-span prestressed concrete bridge during a proof test. This county-owned bridge, located in southern New Mexico, had no design plans. The bridge was composed of nine double-tee beams, each measuring 33 in. wide, 19.5 in. thick, and 32 ft. long. Based on National Bridge Inventory (NBI) condition ratings, the superstructure received a condition rating of 6 (out

of 9). Eight AE sensors were mounted on the stem of the middle beam, with four positioned near the support (shear region) and the other four positioned at midspan (moment region). The decision to instrument only the middle beam with AE sensors was made due to its higher strain levels than the other beams observed during a diagnostic test.

The results indicated that the analysis of the cumulative signal strength (CSS) can effectively identify the onset of crack formation. This parameter served as an indicator of the susceptibility of the bridge to crack, both in the shear and moment regions. This was achieved by comparing the abrupt changes in CSS slopes observed in both regions. Moreover, intensity analysis provided insights into the extent of deterioration under specific loading conditions. The results highlighted a higher level of deterioration in the shear region compared to the moment region. AE was able to detect deterioration, whereas conventional instrumentation failed to reveal localized deterioration. The authors concluded that AE has the potential to be utilized as the primary instrumentation for proof testing, especially when monitoring crack growth during testing is of primary concern.

2.4 Review of literature relevant to the prediction of load using acoustic emission

Recently, K C et al. [23] investigated the potential of utilizing AE to predict vehicle loads on bridges. Two precast flat slabs were tested under a four-point bending test. The slabs were obtained from decommissioned bridges in rural areas of South Carolina. The slabs were 8.25 in. thick, 5.5 ft. wide, and 15 ft. long. The loading on the slabs was stepwise cyclic. Three load steps with a step size of 10 kip were performed, and AE data was collected during the test. The goal was to classify the AE data into their corresponding load steps.

The first endeavor in classification analysis involved the extraction of single attribute data from the test, with the aim of assessing if the attribute was a reliable indicator for classifying the AE hits into their respective load steps. This involved the examination of three AE parameters - rise time, amplitude, and energy - through basic statistical analysis to assign the AE hits to their corresponding load steps. The authors determined that although certain statistical differences were observed, classifying AE hits into their respective load steps through a single attribute analysis posed significant challenges. Consequently, this finding prompted the development of a machine-learning model capable of examining several attributes for the purpose of categorizing AE hits into their corresponding load steps.

The authors employed the artificial neural network (ANN) algorithm by simultaneously analyzing 13 AE parameters. The results revealed the feasibility of ANN in classifying the AE hits to their corresponding load steps with an acceptable accuracy of 86%. However, in this study, the classification was done on two load steps with a step size of 10 kip, and only the ANN algorithm was implemented. Moreover, this study is limited to precast RC flat slab bridges. Using AE to predict the vehicle loads on other typical bridges, such as girder bridges, was not studied.

Chapter 3

Full-Scale Experimental Investigation of Prestressed Concrete Channel Bridge Girders Strengthened with Aluminum Alloy Channels[1]

[1]E. Elbatanouny, A. Henderson, L. Ai, Laxman K C, B. Ross, T. Cousins, P. Ziehl. Full-Scale Experimental Investigation of Prestressed Concrete Channel Bridge Girders Strengthened with Aluminum Channels. To be submitted to Construction and Building Materials.

3.1 Abstract

South Carolina has over 9,000 bridges in its inventory, many of which were designed for H10 or H15 truckloads. The South Carolina Department of Transportation (SCDOT) identified prestressed concrete channel bridge girders as one superstructure type that has difficulty meeting sufficient load ratings related to flexure. Hence, it is imperative to explore strengthening methods for these girders. Aluminum alloys possess desirable properties that make them attractive as external reinforcement materials. However, while previous studies have investigated the use of aluminum alloys on reinforced concrete members, there is a lack of investigation on their use on full-scale prestressed concrete bridge girders. To address this gap, this study investigates the feasibility of utilizing aluminum alloy channels as an external reinforcement material on full-scale prestressed concrete channel bridge girders. The main goal of this paper is to reduce the number of load-posted bridges in the state of South Carolina. Nine girders obtained from decommissioned bridges in South Carolina were tested under monotonic loading to failure. The test program consisted of six unstrengthened girders, one strengthened with bonded aluminum channels (SE), one strengthened with bonded and bolted aluminum channels (SEB), and one strengthened with bolted aluminum channels (SB). Before testing, a visual inspection of the girders was conducted to identify any existing deterioration, and each girder was given a condition rating based on the Specifications for the National Bridge Inventory (SNBI). The results indicate that externally anchoring aluminum alloy channels with bolts was the most effective strengthening method in terms of practicality and higher increase in the moment capacity. Moreover, the results also revealed that the measured

moment capacities of the girders varied based on the extent of the existing deterioration observed through visual inspection.

Keywords: Bonding; Anchorage; Aluminum Alloy Channels; Full-scale tests; Prestressed Concrete, Flexural Strengthening; Bridges.

3.2 Introduction

Regular inspections and load tests are conducted on bridges to assess the condition of their components and determine whether they have enough structural capacity to support anticipated live load demands with an appropriate safety margin. This process is referred to as load rating. If the reserve structural capacity is inadequate, actions such as load posting, rehabilitation, or bridge closure may be taken to ensure public safety [16]. In South Carolina, the transportation infrastructure consists of multiple bridges in fair condition (47%) due to structural issues, such as outdated design loads and bridge deterioration. On average, the bridges are approximately 40 years old, approaching the 50-year service level, with 6.8% being load posted, 11% being structurally deficient, and 0.33% being reported closed [3].

The South Carolina Department of Transportation (SCDOT) is currently in the process of load rating its entire inventory of bridges. In South Carolina, there are approximately 9,400 highway bridges; out of those, 377 bridges are prestressed concrete channel girders built during the 1960's [24]. These bridges typically consist of multiple spans and are supported by timber pile substructures. Figure 3.1 presents field picture of prestressed concrete channel bridge girders.

Figure 3.1 Photographs of a precast prestressed concrete channel bridge girders [4]

The prestressed concrete channel girders can be separated into two categories: skinny-leg channel girders and wide-leg channel girders. There are 103 skinny-leg channel girder bridges and 274 wide-leg channel girder bridges. This study will focus on skinny-leg channel girders. Figure 3.2 shows a typical cross-section of a skinny-leg channel girder obtained from an SCDOT drawing. The name comes from the cross-section shape that creates a channel along the span length. They are comprised of precast prestressed concrete channel sections with a span length of 30 ft. The bridge cross-section typically consists of ten or more girders. Each girder is 30.5 in. or 33 in. wide. The girders are tied together by transverse tie rods at quarter points along the span. The thickness of the flanges is 5 in., while the web thickness tapers down to 2.5 in. at the bottom.

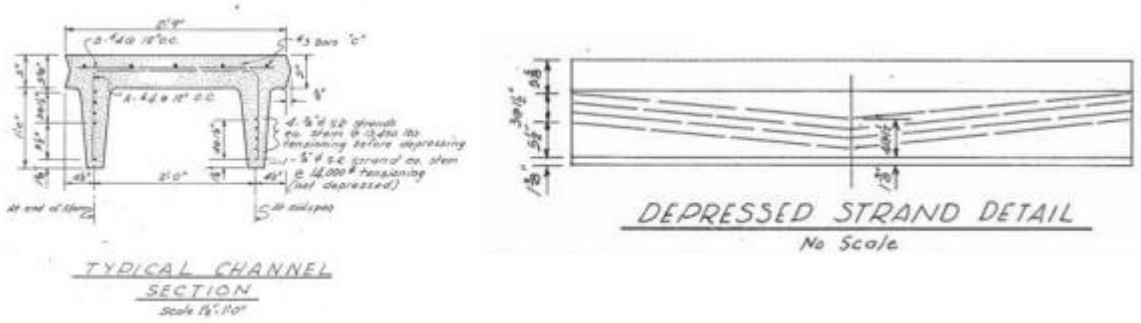

Figure 3.2 Typical cross-section of skinny-leg channel girder (SCDOT drawing)

The skinny-leg channel girder bridges are designed for H15-44 loading criteria, which is lower than the design vehicles used in current design standards (HL-93). The SCDOT conducted load rating of these bridges, using the typical EV-3 truck as the controlling vehicle in the rating process. Among these bridges, almost all the skinny-leg channel girders have a load rating factor (RF) below 1, indicating the need for load postings due to capacity limitations (Figure 3.3) [5]. Hence, the capacity of these bridges needs to be increased to satisfy current load demands and to decrease the number of load-posted bridges. The primary focus of the SCDOT is to assess the current state of these bridges and use cost-effective and easily implemented strengthening techniques to extend their lifespan.

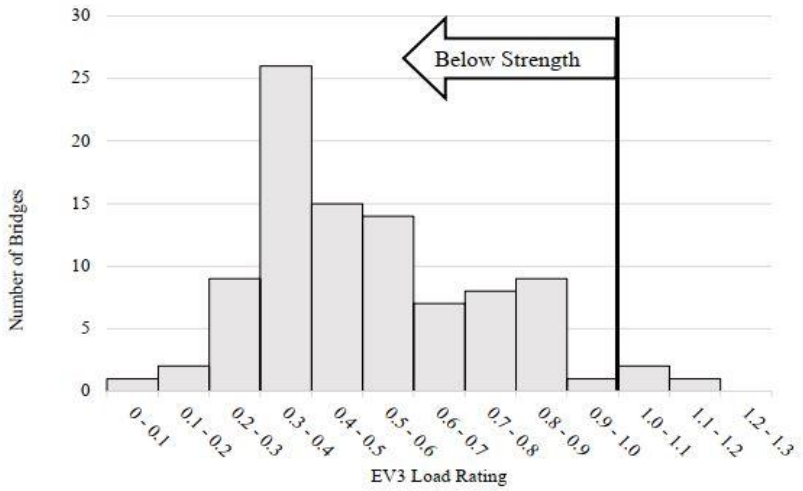

Figure 3.3 Rating factors (RF) of the skinny-leg channel girder bridges [5]

3.3 Literature Review

Structural strengthening may be necessary for a bridge for several reasons. These could include deterioration caused by environmental conditions, accidents, extreme loading, or the requirement to withstand increased vehicle loads [25]. As a result, various strengthening materials and techniques emerged in the last decades. Steel and Fiber

reinforced polymers (FRP) have been used as externally bonded reinforcement for this purpose. As flexural reinforcement, steel plates and FRP sheets are usually bonded and may be anchored to the soffit or the sides of the beams to increase the flexural capacity [26]–[35].

Steel was utilized as an external reinforcement material due to its high tensile strength, ductility, and low cost. However, the susceptibility of steel to corrosion and its heavy weight made steel less attractive to use as an external reinforcing material. As a result, FRP emerged and has been the dominant external reinforcement material, primarily due to its superior tensile strength (5 times that of steel), lightweight, versatility, and corrosion resistance. However, the brittle behavior with no well-defined yield point, high cost, and rapid deterioration of FRP under high temperatures have driven researchers to seek alternative materials [18], [36]. As a result, aluminum alloys (AA) have emerged as potential candidates for external reinforcement applications. Aluminum alloys (AA) possess desirable characteristics such as their high tensile strength, lightweight (one-third the weight of steel), high ductility, and reasonable cost [18], [19], [36], [37].

Several studies have been conducted to enhance the flexural capacity of reinforced concrete beams utilizing AA as an external reinforcing material. Rasheed et al. [18] conducted a study to validate the potential and practicality of employing Aluminum Alloy (AA) plates as an externally bonded reinforcement strengthening material for RC beams. The behavior of AA-strengthened beams was evaluated with and without carbon fiber reinforced polymers (CFRP) sheets (U-wrap) acting as end-anchors and spaced throughout the specimens. Ten RC beams were cast and tested. One beam was a control specimen without strengthening (CB). The remaining beams were strengthened by externally

bonding AA plates to the soffit of the beams using epoxy adhesive. All strengthened beams showed a higher increase in flexure strength than the control specimen in the 13% to 40% range. The authors reported that the strengthened beams without end anchorages failed primarily in flexure with full debonding along the length of the beam, whereas beams with end anchorage failed by localized debonding and flexure. Moreover, strengthened beams without end anchorages showed a ductile response slightly lower than the control specimen. However, end anchorages were observed to enhance the ductility of the strengthened beams to comparable levels of ductility of the control specimen.

Abuodeh et al. [19] investigated the effectiveness of using mechanically fastened (MF) aluminum alloy (AA) plates for flexural strengthening of reinforced concrete (RC) members. The test program involved preparing 16 RC beams, one left unstrengthened, one strengthened with an externally bonded plate, and the remaining beams strengthened with mechanically fastened plates of varying sizes, spacing, and layout. The results showed that all the beams with mechanically fastened plates exhibited increased strength and ductility compared to externally bonded plates. In addition, analytical predictions were made to assess the advantages of mechanically fastened systems. It was concluded that implementing epoxy and anchor bolts is a viable approach to enhance the strength and ductility of reinforced concrete beams strengthened with aluminum alloy plates.

Zhang et al. [20] conducted a study to investigate the use of aluminum alloy plates in the bolted side-plating (BSP) retrofitting technique for reinforced concrete (RC) beams. The study aimed to examine the effects of several factors such as plate thickness, plate height, bolt spacing, anchoring techniques, and prestressing on the flexural strength, stiffness, and ductility of the beams. The test program involved conducting experiments on

seven specimens with different configurations of aluminum plates and bolts. The study results show that increasing the thickness of aluminum plates, using adhesive bonding, and reducing the spacing of the bolts can significantly increase the flexural capacity and secant stiffness of the beams. In addition, prestressing of the AA plates recovered the deflection of the RC beam up to 60% under service loading.

3.4 Research Significance

There are several materials and techniques available to enhance and improve the flexural capacity of bridges, but each option has its own set of limitations. However, aluminum alloys have been identified as a promising external reinforcement material due to their high strength, lightweight, and reasonable cost. Although previous studies have investigated the use of aluminum alloys on reinforced concrete members, there has been a lack of investigation into their use on prestressed concrete bridge girders. To fill this gap, this paper explores the feasibility of utilizing aluminum alloy channels as an external reinforcement material on full-scale prestressed concrete channel bridge girders. The primary goal of this paper is to contribute to the reduction of load posted bridges in the state of South Carolina. The study involved conducting laboratory tests to document the strength of in-situ channel bridge girders and evaluate potential strengthening schemes. The current paper adds to the body of knowledge by reporting on the experimental behavior of prestressed concrete channel girders strengthened by attaching aluminum channels to the sides of the webs using three different schemes. In addition, the moment capacities of the girders are calculated based on the design methods in the AASHTO [7] and compared with the experimental results.

3.5 Experimental Program

3.5.1 Test Specimens

Nine prestressed concrete channels, which were originally used in 30-ft span bridges constructed in the 1950's and 1960's, were subjected to flexural tests at the University of South Carolina (USC). These girders had been stored in SCDOT facilities after their roughly 30 – 40 year service life. The dimensions and reinforcement details of the girders are shown in Figure 3.4 and were based on SCDOT drawings. The existing drawings of the girders indicate that the typical longitudinal reinforcement includes five No. 3 bars and ten 3/8 in. prestressing strands. The prestressing strands are draped downward at the midspan, except for the bottom strand. The top four strands were prestressed with 13,450 lb. during release, whereas the bottom strands were prestressed with 14,000 lb. In the transverse direction, the girders were reinforced with No. 4 bars and No. 4 stirrups spaced at 12 in. on center. In addition, the specified compressive strength of the concrete and the yield strength of the deformed steel bars were 5,000 psi and 40,000 psi, respectively. The specified ultimate strength of the prestressing strands was 250,000 psi.

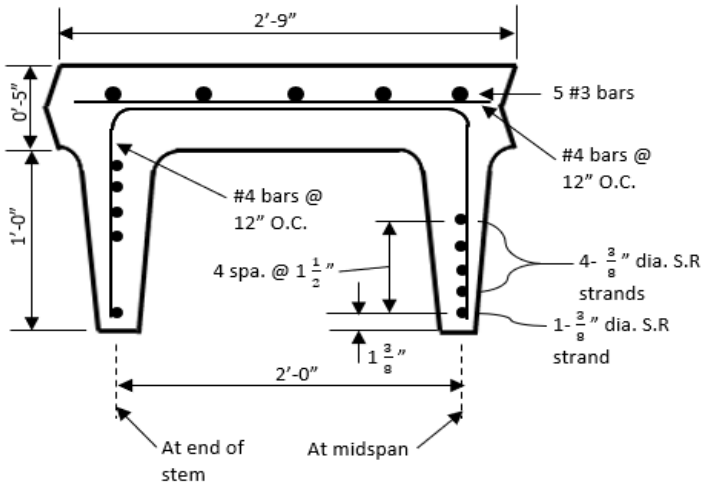

Figure 3.4 Dimensions and reinforcement details of the girders

Some of the girders were characterized by the presence of end diaphragms, while some had no end diaphragms, as shown in Figure 3.5. However, the cross-sections and reinforcement details of these girders matched with the existing plans for both girders with and without an end diaphragm. The experimental program was divided into two groups of specimens; an unstrengthened reference group (URG) and a group strengthened with aluminum alloy (AA) channels (SG). The URG consisted of six specimens that were tested to evaluate the performance of the unstrengthened girders and to serve as benchmarks for comparison with the strengthened girders. The SG consisted of three specimens that were strengthened in flexure by externally bonding or bolting aluminum alloy (AA) channels to the web sides. Table 3.1 presents the test program followed in this study. The unstrengthened specimens were identified by the letter “U” followed by the specimen number, whereas the strengthened specimens were identified by the letter “S” followed by the bonding technique of the AA channels, where “E” refers to bonding with epoxy and “B” refers to anchoring with bolts.

Figure 3.5 Cross-sections of the girders; left) with end diaphragms, right) without end diaphragms

Table 3.1 Specimens designation

Specimen Designation	End diaphragm	Strengthening (Yes/No)	Note
U1	Yes	No	Reference
U2	Yes	No	Reference
U3	Yes	No	Reference
U4	Yes	No	Reference
U5	Yes	No	Reference
U6	No	No	Reference
SE	Yes	Yes	Strengthened with AA channels bonded with epoxy to the web sides
SEB	Yes	Yes	Strengthened with AA channels bonded with epoxy and anchored at the ends and midspan with aluminum bolts to the web sides
SB	No	Yes	Strengthened with AA channels anchored at the ends with steel bolts to the web sides

3.5.2 Strengthening Procedures

Three methods of applying AA channels to the web sides were investigated in this study, as shown in Figure 3.6. Table 3.2 presents the details of the 6061-T6 aluminum channel sections used in this study, as reported by the manufacturer. The aluminum channels had a specified yield strength of 40 ksi. SikaDur-30 is the epoxy adhesive used

in this study to bond the AA channels to the concrete surfaces. It has a compressive strength, flexural strength, and shear strength of 8600 psi, 6800 psi, and 3600 psi, respectively. The mechanical and physical properties of the epoxy can be found in the product datasheet provided by the manufacturer [38].

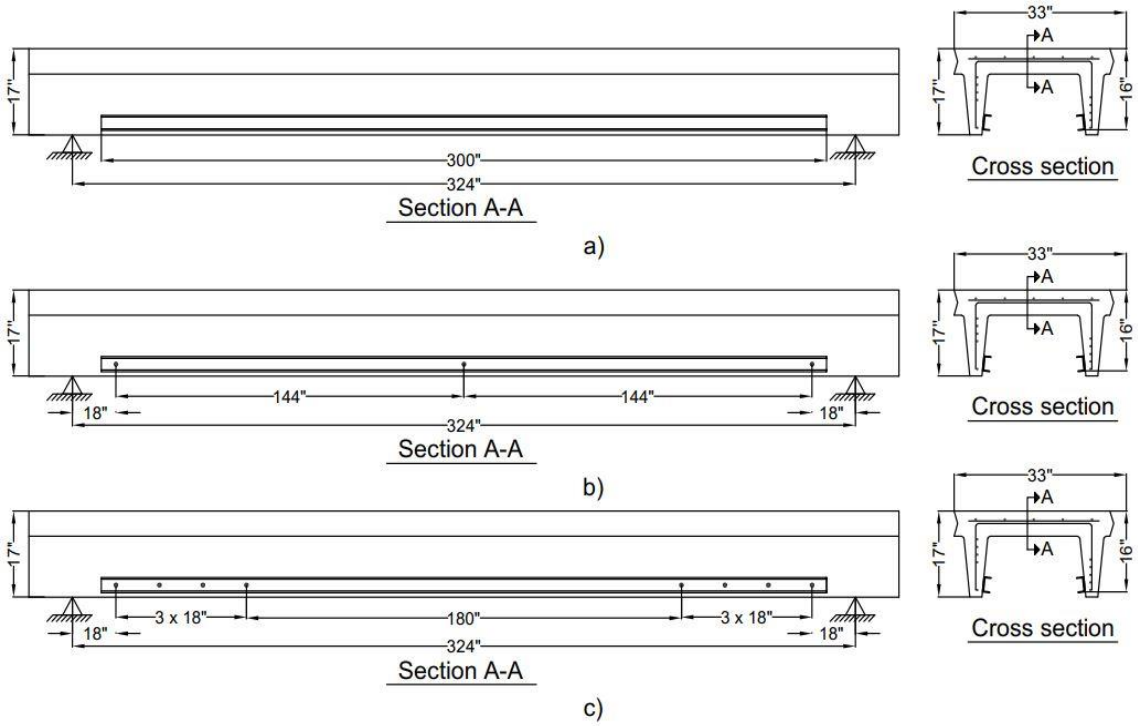

Figure 3.6 Strengthening schemes: a) SE, b) SEB, and c) SB

Table 3.2 Details of the aluminum channel section

Designation	Area (in^2)	Depth (in)	Weight (lb./ft)	Flange		Web Thickness (in.)	Yield Strength (ksi)
				Width (in.)	Thickness (in.)		
6061-T6 CH3X258	1.410	3.000	1.729	1.498	0.170	0.258	40.000

3.5.2.1 Girder (SE)

The girder was strengthened by bonding two 25 ft. long AA channel sections to the sides of the webs using epoxy adhesive. Prior to applying the epoxy adhesive, the surfaces of the concrete and AA channels were roughened to enhance the bond with the epoxy. The concrete surfaces were prepared by needle scaling method utilizing a needle gun to attain

a minimum concrete surface profile (CSP) 3 as recommended [38]. In addition, the surface preparation for AA channels was carried out by sanding them with 400-grit sandpaper on only one side of the AA channels attached to the epoxy. Once the surfaces were prepared, the epoxy adhesive was applied on both surfaces, and the AA channels were pressed in place. Figure 3.7 presents photographs of the installation of AA channels for girder SE. The girder was tested after 7 days of applying epoxy.

Figure 3.7 (left) surface preparation by needle gun; (right) Epoxy was applied, and the aluminum channels were placed.

3.5.2.2 Girder (SEB)

The girder was strengthened by bonding two 25 ft. long AA channel sections to the sides of the legs using epoxy adhesive. In addition, each AA channel was anchored at the ends and midspan by 0.625 in. aluminum threaded rods 6061. Table 3.3 presents the details of the 6061-T6 aluminum threaded rods as provided by the manufacturer. Drilled holes with a diameter of 0.75 in. were formed in the AA channels. Then, the Ground Penetrating Radar (GPR) was used to locate the prestressing strands and to determine the size of the rebar. These locations were then marked and used to coordinate hole drilling locations to avoid damaging any prestressing strands and avoid galvanic corrosion. Next, holes with a

diameter of 0.75 in. were drilled through the girder webs and cleaned thoroughly with an air compressor. Then, the same surface preparation procedures as girder SE were followed. Once the surfaces were prepared, the epoxy adhesive was applied on both surfaces, and the AA channels were anchored with aluminum threaded rods. The aluminum threaded rods were secured using aluminum hex nuts tightened using a 2 ft. wrench. Figure 3.8 displays photographs of the installation of AA channels for girder SEB. The girder was tested after 7 days of applying epoxy.

Table 3.3 Details of aluminum threaded rods

Designation	Diameter (in.)	Yield Strength (ksi)	Tensile Strength (ksi)	Shear Strength (ksi)
Aluminum Threaded Rod 6061-T6	0.625	40	45	30

Figure 3.8 Aluminum channels bonded and bolted with aluminum threaded rods.

3.5.2.3 Girder (SB)

The girder was strengthened by attaching two 25 ft. long AA channel sections to the sides of the legs. Each AA channel was anchored at each end by four 0.625 in. diameter steel ASTM A193 Grade B7 threaded rods. Table 3.4 presents the details of the steel threaded rods as provided by the manufacturer. The spacing between the bolts was 18 in. and 6 in. from the end of the aluminum channel, as shown in Figure 3.6c. Drilled holes

with a diameter of 0.75 in. were formed in the AA channels. Then, the Ground Penetrating Radar (GPR) was used to locate the prestressing strands and determine the rebar's size. These locations were then marked and used to coordinate hole drilling locations to avoid damaging any prestressing strands. Next, holes with a diameter of 0.75 in. were drilled through the girder webs and cleaned thoroughly with an air compressor. Next, the AA channels were anchored with steel threaded rods. Finally, the steel threaded rods were secured in place using steel hex nuts tightened using a 2 ft. wrench. Figure 3.9 presents photographs of the installation of AA channels for girder SB.

Table 3.4 Details of steel threaded rods

Designation	Diameter (in.)	Yield Strength (ksi)	Tensile Strength (ksi)	Shear Strength (ksi)
Steel ASTM A193 Grade B7 threaded rod	0.625	105	125	70

Figure 3.9 Aluminum channels bolted with steel threaded rods.

3.5.3 Test Setup

The girders were subjected to monotonic loading until failure. The girders were simply supported and tested in flexure under four-point loading, as shown in Figure 3.10.

The girders were supported on two concrete blocks that were made to test heavy bridge girders. To minimize friction during the load application, the girders were positioned over neoprene bearing pads that were nine inchwide and placed above the concrete blocks. Two structural steel members supported the spreader beam, each resting on two neoprene bearing pads, forming four contact points. These points were intentionally positioned directly above the girder legs to establish a four-point bending test setup, as indicated in Figure 3.10. The center of one support to the other is 27 ft. long, with 1.5 ft. of overhang at each end. This was done to eliminate uneven bearing issues due to some girders missing concrete at the ends of their 30 ft. lengths.

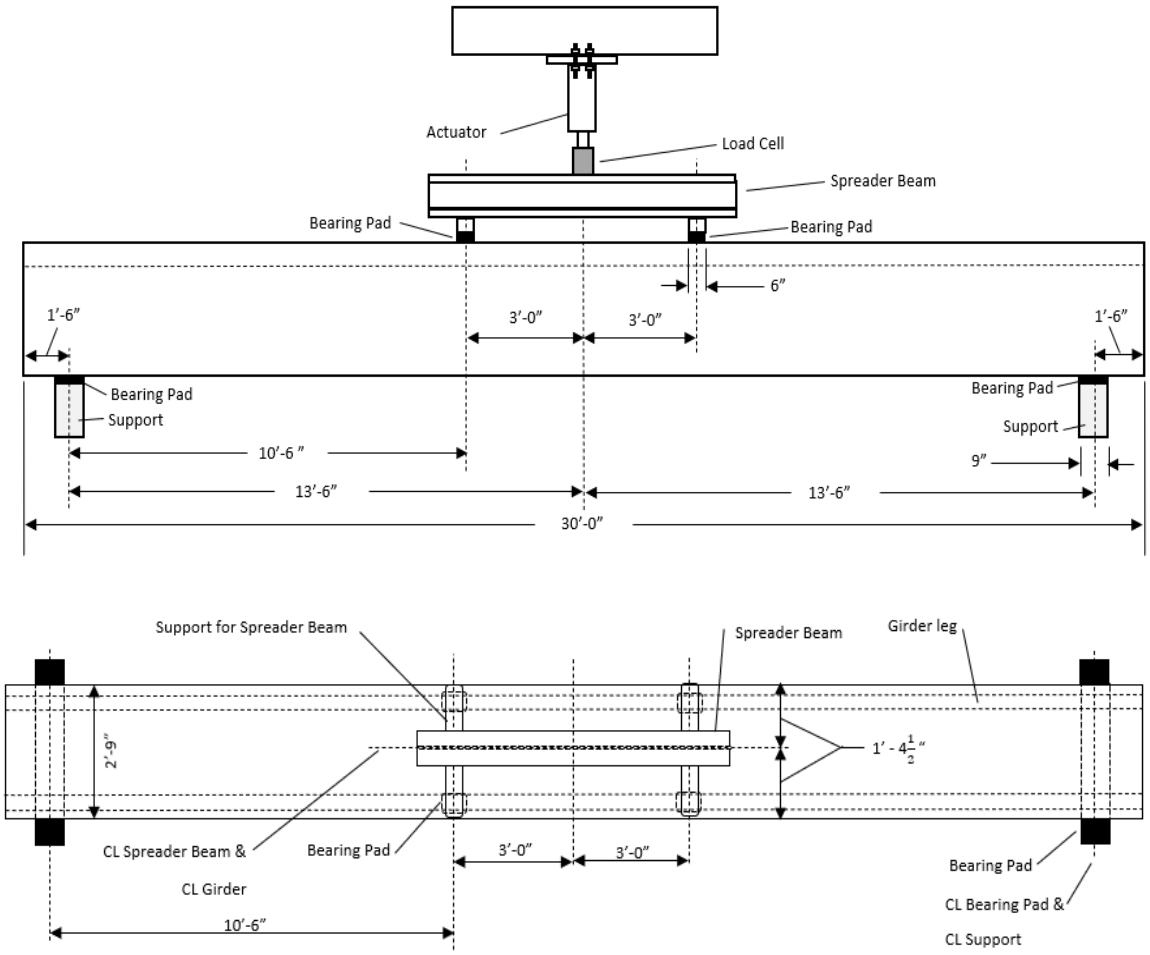

Figure 3.10 Test setup of the girders

Vertical displacement at the quarter-spans and the mid-spans of the girders were measured using string potentiometers during the testing. Strain gauges were placed on the AA channels at midspan, in the case of strengthened girders. The load application was carried out using a hydraulic actuator, and the load values were monitored using a calibrated load cell and pressure gauge. The load cell used had a capacity of 250 kip. Throughout the loading process, data was continuously recorded by a data acquisition system with 32 channels. Figure 3.11 shows photographs from the test setup of the girders.

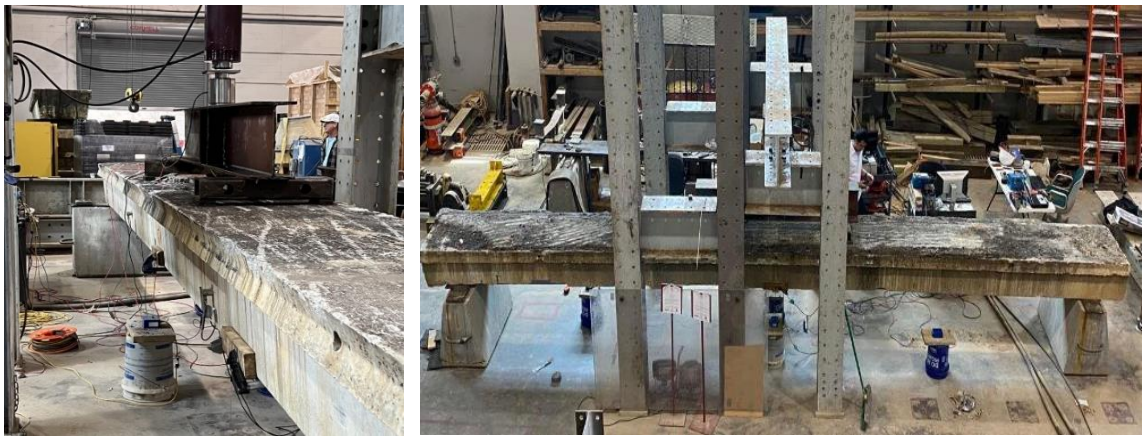

Figure 3.11 Photos of the test setup of the girders

3.5.4 Material Properties

3.5.4.1 Concrete

Drilled concrete cores were extracted from all the girders after testing and tested for their compressive strength. The cylinders were drilled using a core drill and diamond-impregnated drill bit. Concrete cores were obtained in accordance with ASTM C42/ C42M [39] and ACI 214.4R-03 [40], were capped in accordance with ASTM C617 [41], and tested in accordance with ASTM C39/ C39M [42]. However, the dimensions of the cylindrical concrete core specimens were 2 in. diameter by 4 in. long, which does not conform with ASTM C39/ C39M [42] or ACI 214.4R-03 [40]. The cores were limited to

the thickness of the flanges of the girders, which was 5 in. Table A.1 (Appendix A) summarizes the test results of the compressive strength of the cores taken from each girder. The core tests resulted in an average compressive strength of 10.2 ksi for 25 cores. The results indicate that the measured compressive strengths of the girders are well above their specified value of 5 ksi.

3.5.4.2 Prestressing strands

Prestressing strands were extracted from specified girders after testing and tested for their tensile ultimate strength at the SCDOT office of materials and research. Uniaxial tensile tests were conducted on 30 in. long specimens. Strands selected for testing were either the lowest strand or the second lowest strand (if possible). A total of eight prestressing strands were collected with various levels of corrosion and section loss. Prior to testing, the severity of strand deterioration was visually inspected. Four levels of corrosion deterioration were considered in the assessment based on the conditions of the strands. These levels were (1) no corrosion, (2) light corrosion, (3) pitting, and (4) heavy pitting, as shown in Figure 3.12. There was no observed wire loss (complete degradation of individual strand wires) or fracture (localized fracture of individual wires). The deterioration levels are also referred to as Deterioration Indices (DI) in this paper. The purpose of classifying strand conditions was to categorize strand strength results to better compare their measured tensile strength. Table A.4 (Appendix A) summarizes the test results of the ultimate tensile strength of the prestressing strands. Figure A.3 displays the strands extracted from the girders. However, only the strands extracted from girders U2, U3, U4, and U5 were tested for their ultimate strength during the early phases of the testing program. The data provided by the SCDOT materials lab recorded the failure loads. It is evident that the ultimate tensile stress for strands with DI 0 or 1 exceeds the specified

ultimate tensile stress of 250 ksi. The average ultimate tensile stress for strands with DI 0 or 1 was 288 ksi.

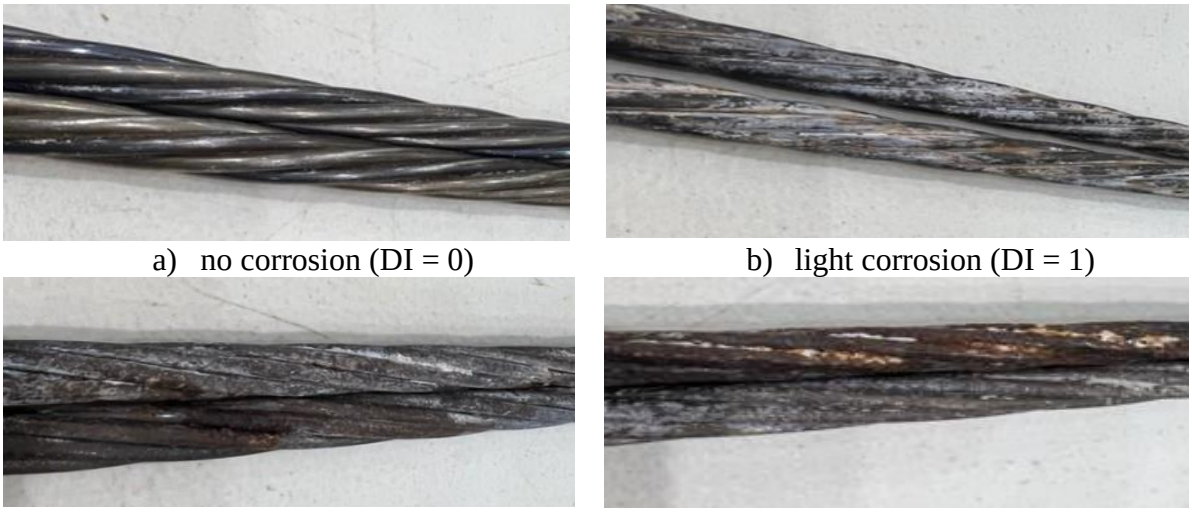

a) no corrosion (DI = 0) b) light corrosion (DI = 1)

c) Pitting (DI = 2) d) Heavy Pitting (DI = 3)

Figure 3.12 Various strand deterioration conditions

3.6 Visual Inspection

Deterioration types and condition states for bridge components have been defined in the AASHTO Manual for Bridge Element Inspection (MBEI) [43] and the Specifications for the National Bridge Inventory (SNBI) inspection criteria [44]. The latter provides a 10-scale condition rating for bridge components from "0" to "9" in which "9" refers to excellent condition, whereas "0" refers to the worst condition. Table 3.5 presents the equivalent member structural condition based on the condition rating.

Table 3.5 Approximate conversion in selecting $\emptyset_c$ [7]

Superstructure Condition Rating (NBI)	Equivalent Member Structural Condition	Condition factor ($\emptyset_c$)
6 or higher	Good or Satisfactory (CS1)	1
5	Fair (CS2)	0.95
4 or lower	Poor (CS3 and CS4)	0.85

Prior to testing, a visual inspection was conducted on the girders to assess their condition. The girder's condition was categorized based on the SNBI inspection criteria. The girders sustained deterioration throughout their service life. Spalling, cracking, and

section loss were observed for most of the girders which led to several feet of an exposed strand(s). In addition, some girders contained visibly corroded strand(s). These types of deterioration for each girder can be seen in Figure 3.13.

Each girder was assigned a condition rating ranging from 0 to 9, based on the observed deterioration. An equivalent member structural condition and a condition factor were assigned to each girder, based on the inspection condition rating. Table 3.6 summarizes the condition rating for each girder.

a) U1 specimen (NBI 4); left) wide crack near midspan, right) large spalling near midspan.

b) U2 specimen (NBI 6); left) small spalling near midspan, right) large spalling at midspan.

c) U3 specimen (NBI 3); left) major defect, right) wide crack near midspan.

d) U4 specimen (NBI 3); left) major defect at midspan, right) moderate defect near the quarter span.

e) U5 specimen (NBI 2); left) moderate defect near midspan, right) major defect, severely compromised.

f) U6 specimen (NBI 7); left) flange spalling at quarter span, right) flange spalling at the end.

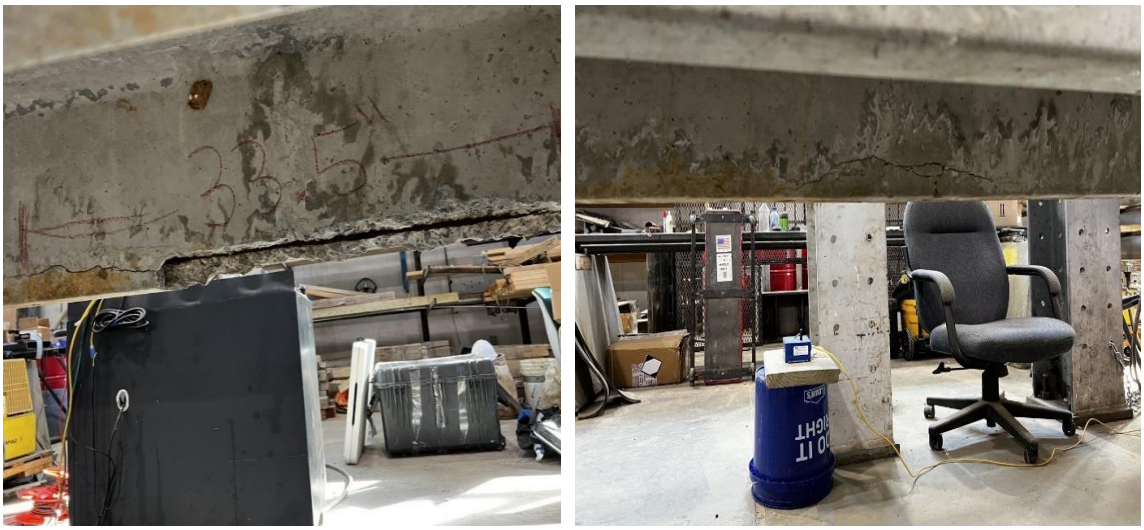

g) SE specimen (NBI 4); left) exposed strand, major defect, right) wide crack near midspan

h) SEB specimen (NBI 7); left) large spalling near midspan, right) small spalling near midspan

i) SB specimen (NBI 7); left) flange spalling near midspan, right) minor defect near midspan.

Figure 3.13 Existing deterioration of the girders

Table 3.6 Condition rating of each girder

Specimen	Visual Inspection	NBI condition rating	Equivalent Structural Condition	Condition factor ($\emptyset_c$)
U1	-Widespread wide cracks at or near the soffit of legs with rust stains -Some leg spalling -Some flange spalling and isolated diaphragm spalling -Widespread moderate defects; strength is affected	4	Poor	0.85
U2	-Widespread flange spalling -Some leg spalling	6	Good	1

U3	-Isolated moderate leg spalling defect -Some leg spalling -Several feet of exposed strand with corrosion at two distinct locations -Isolated wide crack on the soffit of the leg	3	Poor	0.85
U4	-Widespread flange spalling -Several feet of exposed strand with corrosion at multiple locations. -Some wide cracks on the exterior sides of the legs	3	Poor	0.85
U5	-Isolated wide crack -Several feet of exposed strand with corrosion at multiple locations -Rust stains and spalling of concrete along 75% of one leg soffit	2	Poor	0.85
U6	-Some flange spalling -Isolated spalling on the interior of the leg	7	Good	1
SE	-Some leg spalling -Several feet of exposed strand with corrosion at one location	4	Poor	0.85
SEB	-Some evidence of spalling in two locations	7	Good	1
SB	-Some flange and leg spalling in two locations	7	Good	1

3.7 Results and discussion

3.7.1 Flexural behavior of unstrengthened girders

The moments and midspan vertical displacements of the unstrengthened girders are shown in Figure 3.14. The moment in the figure includes the moment from dead weight (including wearing surface if applicable) and the moment from the applied load. Three stages can characterize the general shape of the moment versus displacement plots. First, pre-cracking with a linear moment-deflection response. Second, non-linear phase with no obvious yield point. Third, a significant post-yielding phase up to the maximum load. Flexural failure of the girders was characterized by prestressing strand yield followed by

rupture of the bottom strand or simultaneous rupture of strands at the midspan region, as shown in Figure 3.15.

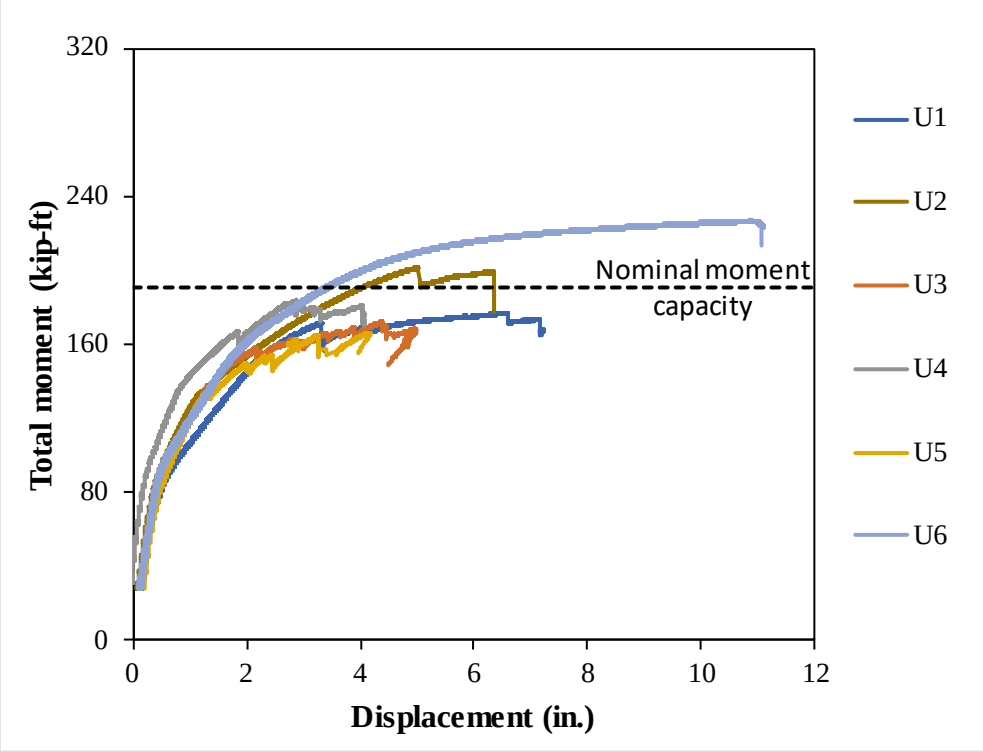

Figure 3.14 Moment versus midspan displacement for the unstrengthened girders

a) U1 specimen

b) U2 specimen

c) U3 specimen

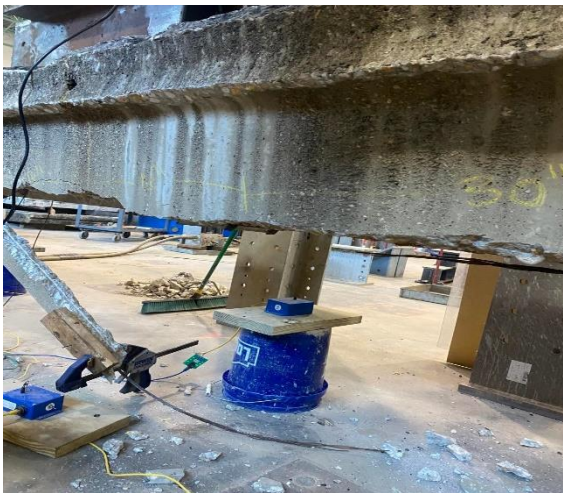

d) U4 specimen

e) U5 specimen

f) U6 specimen

Figure 3.15 Failure modes of the unstrengthened girders.

Table 3.7 summarizes the test results of the unstrengthened girders. The measured moment capacity of the girders was compared to the nominal moment capacity. The nominal moment capacity was calculated in accordance with AASHTO LRFD Bridge Design Specifications [2] based on specified details from SCDOT drawings. The calculations for the nominal capacity of the unstrengthened girders are provided in Appendix B. The dotted line in Figure 3.14 demonstrates a nominal moment capacity of 191 kip-ft.

The results of the tests show that the measured moment capacities of specimens U1, U3, U4, and U5 with a condition rating below 4 (Poor) were 177 kip-ft, 172 kip-ft, 184

kip-ft, and 166 kip-ft, respectively. The measured moment capacities were lower than the nominal moment capacity (191 kip-ft), indicating that the capacities of the girders have been affected by the deterioration observed prior to testing. However, the measured moment capacities of specimens U2 and U6 with a condition rating higher than 6 (Good) were 202 kip-ft and 227 kip-ft, which were higher than the nominal moment capacity (191 kip-ft). This can be attributed to the higher than specified material properties for both strands and concrete. The midspan displacements for the girders at failure were 6.6 in., 5.0 in., 4.4 in., 2.9 in., 3.3 in., and 11 in. for specimen U1, U2, U3, U4, U5, and U6, respectively. It is worth noting that the girder (U6) that failed by simultaneous strand rupture had a higher displacement and measured moment capacity at failure than the other girders.

Table 3.7 Summary of test results of unstrengthened girders

Specimen	Calculated Moment Capacity (Kip-ft)	Measured Moment Capacity (kip-ft)	Measured/Calculated ratio	Displacement (in.)	Condition rating prior to testing	Failure mode
U1	191	177	0.93	6.6	Poor	*
U2	191	202	1.06	5.0	Good	*
U3	191	172	0.90	4.4	Poor	*
U4	191	184	0.96	2.9	Poor	*
U5	191	166	0.87	3.3	Poor	*
U6	191	227	1.20	11.0	Good	*

Notes:
**Yielding of prestressing strand(s) and then rupture.*

3.7.2 Flexural behavior of strengthened girders

The moments and midspan vertical displacements of the strengthened girders are shown in Figure 3.16. The moment in the figure includes the moment from dead weight and the moment from the applied load. Two stages can characterize the general shape of the moment versus displacement plots. The first stage is pre-cracking with a linear moment-displacement response. Second, is a non-linear phase with no obvious yield point until failure. The failure mode of the SE specimen consisted of the full debonding of AA

channels along the length of the girder, as shown in Figure 3.17a. However, the failure mode of the SEB specimen consisted of the end bolt rupture followed by AA channel debonding, as shown in Figure 3.17b. In addition, the failure mode of the SB specimen was concrete splitting at the end bolts, as shown in Figure 3.17c.

The girder strengthened with AA channels bonded and bolted (SEB) has a higher measured moment capacity than the girder strengthened with AA channels bonded only without end bolts (SE). However, it can be seen from Figure 3.16 that the moment-displacement responses follow the same behavior, with SEB having a higher measured moment at failure. This may be attributed to the impact of end-bolting the AA channels. The end bolts prevented the AA channels from debonding, which had a significant impact on the moment capacity and ductility. As a result, the SEB girder continued to carry the load until the end bolts ruptured, whereas the SE girder failed by premature debonding. Furthermore, the SB girder has a higher measured moment capacity than SE and SEB girders. This can be attributed to the fact that bolting the AA channels without epoxy eliminated premature debonding failure.

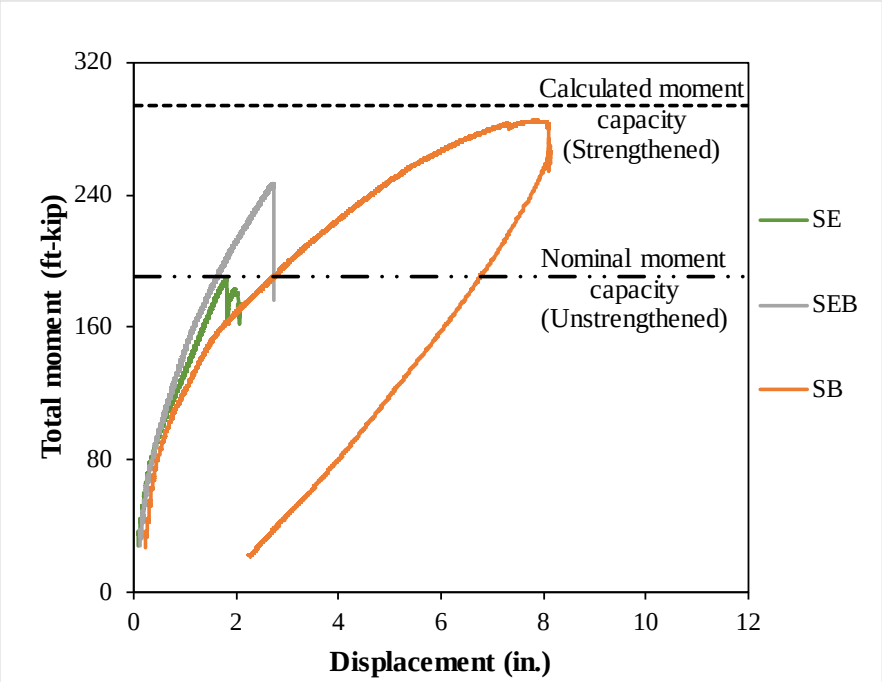

Figure 3.16 Moment versus midspan displacement for the strengthened girders

a) Debonding of the AA channels for specimen SE

b) End bolt rupture for Specimen SEB

c) Concrete splitting at end bolt for Specimen SB.

Figure 3.17 Failure modes for the strengthened girders

Table 3.8 summarizes the test results of the strengthened girders. The measured moment capacities for SE, SEB, and SB were 190 kip-ft, 246 kip-ft, and 285 kip-ft, respectively. The displacement represents the midspan displacement at the full debonding of the AA channels, end bolt rupture, and failure of concrete at the bolts in the case of SE, SEB, and SB, respectively. The midspan displacements for specimens SE, SEB, and SB were 1.8 in., 2.7 in., and 8.0 in, respectively. The nominal moment capacity of the strengthened girders was calculated in accordance with AASHTO LRFD Bridge Design Specifications [2] based on specified details from SCDOT drawings and incorporating the AA channels. The failure mode assumed was the yielding of the AA channels at the

ultimate strain of 0.003 in./in. of concrete. A perfect bond was assumed between AA channels and the concrete substrate, in the case of using epoxy (SE and SEB). The steel bolts were designed to allow the AA channels to yield first (SB). The calculations for the nominal capacity of the strengthened girders are provided in Appendix B. A nominal moment capacity for the strengthened girders of 294 kip-ft is attained, which represents a 54% increase compared to the unstrengthened nominal capacity (191 kip-ft). However, the measured moment capacities were different from the nominal moment capacity. The SE measured moment capacity was 190 kip-ft, which can be attributed to the existing deterioration of the girder and premature debonding of the AA channels. On the other hand, the SEB measured moment capacity was 246 kip-ft, and the failure was attributed to end bolt rupture. The recorded strain at the midspan of the AA channels at failure was 0.003 in./in., which is lower than the specified yield strain (0.004 in./in.), as shown in Figure B.2 in Appendix B. The SB measured moment capacity was 285 kip-ft, and the failure was attributed to the failure of the concrete at the end bolt. The recorded strain at the midspan of the AA channels at failure was 0.0025 in./in., which is lower than the specified yield strain (0.004 in./in.), as shown in Figure B.3 in Appendix B. The aluminum channels did not yield in both cases due to the premature failure that occurred. However, the measured moment capacity for the SB girder is 97% of the calculated moment capacity.

Table 3.8 Summary of test results of strengthened girders.

Specimen	Calculated Moment Capacity (kip-ft)	Measured Moment Capacity (kip-ft)	Measured/Calculated ratio	Displacement (in.)	Condition rating prior to testing	Failure mode
SE	294	190.0	0.65	1.8	Poor	Debonding of AA channels
SEB	294	246.0	0.84	2.7	Good	End bolt rupture followed

SB	294	285.0	0.97	8.0	Good	by debonding Concrete splitting at end bolt

3.8 Summary and comparison

To compare the girders, the girders were grouped based on the condition rating assigned before testing. Five girders were assigned a condition rating below 4 (Poor): U1, U3, U4, U5, and SB, whereas four girders were assigned a condition rating higher than 6 (Good): U2, U6, SEB, and SB. Figure 3.18 and Table 3.9 summarize the comparison between the girders.

The moment-displacement responses of girders with a condition rating below 4 (Poor) are presented in Figure 3.18a. The strengthened girder (SE) demonstrated a higher measured moment capacity compared to the unstrengthened girders (U1, U3, U4, and U5). The average measured moment capacity of the unstrengthened girders with a condition rating below 4 (Poor) was 175 kip-ft. The strengthened girder (SE) measured moment capacity was 9% greater than the average. Additionally, the midspan displacement at failure for the SE girder was 58% less than the average of unstrengthened girders (U1, U3, U4, and U5). The average midspan displacement for the unstrengthened girders (Poor) was 4.3 in. The strengthening approach increased the moment capacity but had an adverse effect on the ductility due to premature debonding which prohibited the required behavior (Yielding of the AA channels).

Figure 3.18b depicts the moment-displacement response of the girders with a condition rating of 6 or higher (Good). The unstrengthened girders exhibited different behaviors at failure, where the displacement and the failure mode varied. It is worth noting that U6 failed by rupture of the prestressing strands simultaneously, in contrast with U2

which failed by rupture of the bottom strands only. The average measured moment capacity and displacement for the unstrengthened girders (U2 and U6) at failure were 214 kip-ft and 8 in., respectively. The strengthened girder (SEB) displayed a 15% higher measured moment capacity and a 66% lower midspan displacement at failure compared to the average of unstrengthened girders (U2 and U6). Once more, the reduced ductility can be attributed to the fact that the end bolt ruptured prior to the AA channels yielding. In addition, the strengthened girder (SB) exhibited a 33% higher measured moment capacity compared to the average of unstrengthened girders (U2 and U6). The measured midspan displacement was equal to the average of the unstrengthened girders (U2 and U6). The strengthening approach increased the moment capacity and provided similar ductility compared to the average of unstrengthened girders (U2 and U6).

The measured moment capacity of the SE specimen was 190 kip-ft, equivalent to the nominal moment capacity (191 kip-ft). In addition, the measured moment capacities of the SEB and SB girders were 246 kip-ft and 285 kip-ft representing an increase of 29% and 49 % compared to the nominal moment capacity (191 kip-ft). The calculations for the rating factors utilizing the LFR and LRFR methods for the girders with the measured moment capacities are provided in Appendix B. It is observed that the rating factors after strengthening the girder (SB) is more than one. This implies that there is potential to eliminate any load posting requirements for the bridge.

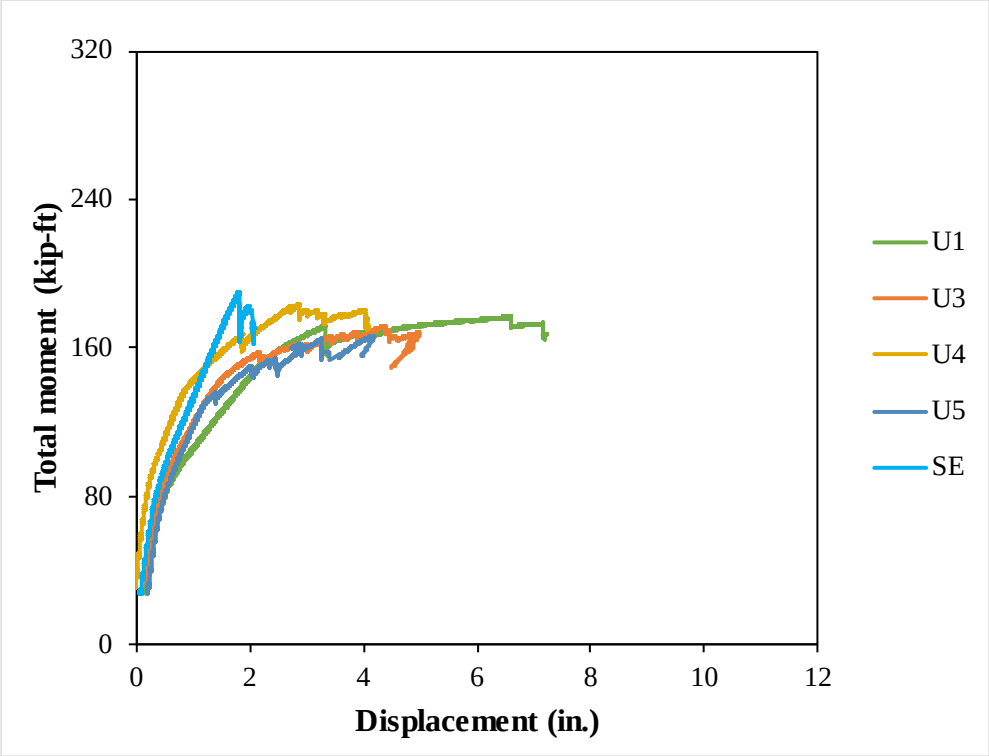

a) Girders with condition factor lower than 4 (Poor)

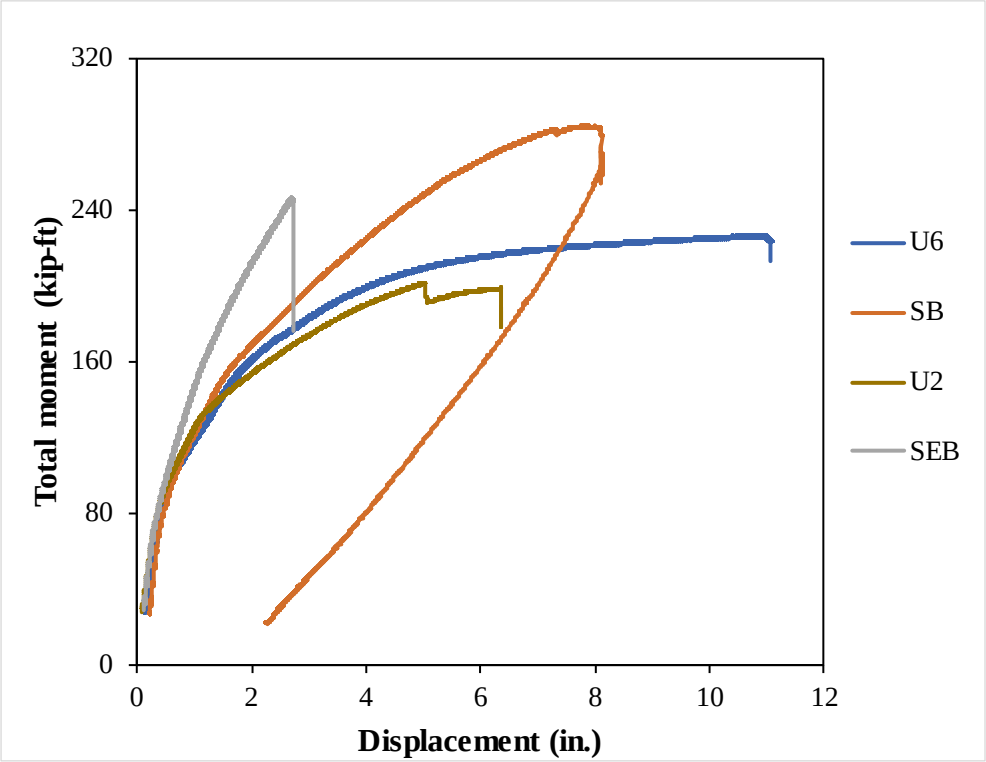

b) Girders with condition factor higher than 6 (Good)

Figure 3.18 Moment versus midspan displacement for the girders

Table 3.9 Comparison of the test results

Group	Specimen	Strengthening (Yes/No)	Measured Moment Capacity (kip-ft)	% Increase in Moment Capacity	Displacement (in.)
Girders with a condition rating factor below 4 (Poor)	U1	No	177	Na	6.6
	U3	No	172	Na	4.4
	U4	No	184	Na	2.9
	U5	No	166	Na	3.3
	SE	Yes	190	8.7*	1.8
Girders with a condition rating factor 6 or higher (Good)	U2	No	202	Na	5.0
	U6	No	227	Na	11.0
	SEB	Yes	246	15**	2.7
	SB	Yes	285	33**	8.0

Notes:
**The average measured moment capacity of girders with a condition rating factor below 4 is 175 kip-ft.*
*** The average measured moment capacity of girders with a condition rating factor 6 or higher is 214 kip-ft.*
Na refers to not applicable

3.9 Conclusions

This study aimed to explore strengthening methods for enhancing the performance of prestressed concrete channel girders. To achieve this, nine decommissioned girders were subjected to flexural tests to failure. Prior to the testing, the girders were visually inspected to identify any existing deterioration that might result in reduced moment capacity. Six unstrengthened girders were tested to failure to assess their flexural behavior and serve as a benchmark to compare with the strengthened girders. Additionally, this paper presents an experimental framework that investigates the feasibility and efficacy of utilizing AA channels as an externally bonded or bolted strengthening method. Based on the experimental findings, the following conclusions can be drawn:

1. The measured moment capacities of the girders varied based on the condition rating of each girder, which was determined by the extent of existing deterioration observed through visual inspection. The girders with a condition rating above 6 (good) exhibited measured moment capacities higher than the nominal moment capacity. This can be attributed to higher than specified material properties for both strands and concrete. Additionally, the measured moment capacities of the girder specimens with a condition rating below 4 (Poor) were less than the nominal moment capacity. This can be attributed to the deterioration observed prior to testing.
2. Externally bonding AA channels with epoxy with or without anchorage may serve as strengthening techniques for bridge girders. The strengthened girders exhibited an increase in measured moment capacity of 9% and 15% for SE and SEB, respectively, compared to the unstrengthened girders. However, premature failure occurred due to the debonding of AA channels and end bolt rupture for SE and SEB, respectively. Further investigation is needed to assess the debonding failure for aluminum alloys attached with epoxy before actual field implementation.
3. Externally anchoring AA channels with bolts was a more convenient method in terms of practicality, ease, and higher increase in the moment capacity. The strengthened girder (SB) exhibited an increase in the measured moment capacity of 33% compared to the unstrengthened girders. In addition, a suitable protective coating should be applied to the steel threaded bolts for field applications.
4. The design method in the AASHTO code can be used to accurately estimate the theoretical moment capacity for the strengthened girder (SB). This is demonstrated

by the results obtained from the calculations, which provided a good estimate with a difference of 3% between the calculated and the measured moment capacity.

Chapter 4

Condition Assessment of Prestressed Concrete Channel Bridge Girders Using Acoustic Emission and Data-Driven Methods [2]

[2]Elbatanouny, E., Ai, L., Henderson, A., & Ziehl, P. (2023). Condition Assessment of Prestressed Concrete Channel Bridge Girders Using Acoustic Emission and Data-Driven Methods. To be submitted to Structures

4.1 Abstract

Numerous bridges in the United States are aging and have experienced various levels of deterioration. Bridge inspections serve a crucial role in guaranteeing the safety and functionality of a bridge during its service life. Visual inspection is used in the United States by bridge owners to evaluate the condition, however, it can be subjective, time-consuming, and labor-intensive. To address these challenges, an alternative solution involves the development and implementation of a structural health monitoring (SHM) system. An SHM system can provide a better evaluation of the condition of the bridges. Nondestructive approaches such as acoustic emission (AE) have been utilized in monitoring bridge degradation. AE was chosen over other methods because it is extremely sensitive to the initiation and propagation of damage in materials. This study proposes a data-driven condition assessment for in-service bridges using acoustic emission. The study aims to utilize AE parameters to assess the condition of the girders and to determine the condition factor used in the load rating of the bridges. Six prestressed concrete channel bridge girders, which were originally used in 30-ft span bridges constructed in the 1960s, were subjected to flexural tests at the University of South Carolina (USC). Acoustic emission (AE) was used to monitor the girders during the tests. The girders were visually inspected prior to testing and each girder was assigned a condition rating based on the Specifications for the National Bridge Inventory (SNBI). Intensity analysis charts were developed based on the collected AE data. The charts may detect if the girders are operating within the specified design criteria and are calibrated to theoretical cracking load and findings of cumulative signal strength analysis. In addition, the charts may assess the

deterioration regardless of the initial girder condition, which can be utilized to determine the condition factor of the girders for load rating purposes.

Keywords: Prestressed Concrete Channel Girders; Bridges; Visual Inspection; Acoustic Emission; Intensity Analysis; Structural Health Monitoring.

4.2 Introduction

Over the past decades, the growing population has led to an increase in both traffic volumes and the weight of trucks required to facilitate the transportation of goods and services. Concurrently, the infrastructure has aged and been exposed to environmental conditions, which has contributed to its deterioration [45], [46]. Therefore, it is imperative to prioritize the structural assessment and rating of bridges.

Bridge load rating is the process of determining the safe load-carrying capacity of a bridge using analytical methods, experimental methods, or a combination of both. Bridges are evaluated to ensure that they have an adequate reserve structural capacity to meet the anticipated live load requirements, with a safety margin [16]. Bridge load rating procedures are specified by AASHTO in the Manual for bridge evaluation [7].

Bridge inspections serve a crucial role in guaranteeing the safety and functionality of a bridge during its service life [47], [48]. The primary purpose of these inspections is to evaluate the current condition of bridges and to detect any existing deterioration. Hence, a condition factor reflecting the bridge's existing condition can be determined. This factor is used to revise the capacity of bridge members and to execute load rating assessments [7].

Visual inspection is primarily used in the United States by bridge owners to evaluate the condition, however, this method is not well suited for detecting concealed defects or those located in areas that are not easily accessible [6]. In addition, visual

inspections are conducted periodically, typically every 2 years [7]. The condition of the bridges may experience alterations during this period. However, in some cases, bridge inspectors are sent to the structure on an increased frequency, resulting in a more time-consuming and labor-intensive process [8]. Furthermore, the efficiency of bridge inspection procedures and the precision of the data collected can be subjective to the expertise of the inspector [9]–[11].

To overcome these challenges, an alternative approach is to develop and install a structural health monitoring (SHM) system. When well-designed and properly implemented, such an SHM system can effectively replace the frequency of repetitive manual inspections, often resulting in cost savings. By identifying critical structural parameters for assessing a structure's performance, sensors can be installed on the bridge and continuously monitor its condition. This not only provides a more objective set of performance measurements but also allows for more frequent data collection, enabling precise and convenient tracking of historical trends. Furthermore, it offers immediate warning to the owner if specific structural thresholds are exceeded. Engineers can monitor current and historical trends from a centralized location, reducing the necessity for unscheduled on-site inspections, unless the collected data suggests otherwise. In addition, it provides site-specific data to know the condition of bridges for purposes of maintenance funding prioritization.

Nondestructive approaches such as acoustic emission (AE) have been employed in monitoring bridge degradation [12], [13]. Several studies have proven the ability of AE to monitor crack initiation and progression in both reinforced and prestressed concrete members [49], [50]. AE was chosen over other methods due to its high sensitivity to detect

stress waves resulting from material changes, such as the formation of cracks [14]. Furthermore, being a passive non-destructive testing method, AE is a feasible candidate for structural health monitoring. Most in-service bridges have experienced various levels of deterioration. The ability of AE to assess deterioration in members with different conditions should be investigated. In addition, there is a lack of investigations employed for the determination of the condition factor for load rating assessments using the collected AE data.

This study proposes a data-driven condition assessment for prestressed concrete bridge girders using acoustic emission. Intensity analysis charts were developed to assess the condition of the girders. In addition, the charts were used to determine the condition factor of the girders to aid in the load rating procedures. Upon validation, this method may serve as a potential approach to provide an objective condition assessment of the bridges based on the collected AE data.

4.3 Acoustic emission

AE is the technique that detects and measures transient elastic waves generated by the sudden release of energy from localized sources within materials, such as cracking or deformation [14]. AE signals are captured through piezoelectric sensors positioned on the surface of the concrete. A "hit" is the recording of an individual signal, identified by parameters such as amplitude, duration, rise time, energy, and signal strength. AE can detect and locate various types of defects by analyzing the measured parameters [49], [51]. Various approaches were developed and implemented to assess deterioration in reinforced and prestressed concrete structures. The intensity analysis method has been utilized to quantify deterioration in structural elements [13], [52], [53]. Moreover, the cumulative

signal strength (CSS) parameter has been employed to detect crack growth and propagation [12], [13], [52]. In this study, signal strength, the measured area of the rectified AE signal with units proportional to volt seconds (pVs), is utilized to establish AE evaluation criteria.

4.3.1 Intensity Analysis

Intensity analysis is a method developed to characterize damage in structural elements. This type of analysis has proven effective for FRP pressure vessels [53], reinforced concrete[54], and prestressed concrete [21], [22], [55]. Intensity analysis is performed by calculating severity and historic index from signal strength. Severity, S_r, is computed as the average for the fifty events having the highest signal strength. This parameter can be constantly updated as new signals are recorded. A rapid increase in severity is typically associated with the onset or detection of structural damage [56]. Historic index, H(t), estimates changes in the slope of the recorded signal strength by comparing the signal strength of the recent hits with the cumulative signal strength of all hits. The historic index can mathematically locate and quantify the rises in the cumulative signal strength and hence give an assessment of the damage. Equations 4.1.a and 4.1.b calculate the historic index and severity, respectively [21], [22], [53]–[55]. The intensity of AE data is obtained by plotting the maximum severity-historic index calculated during each loading phase. Events associated with a higher degree of damage or significance will plot towards the top right corner of the chart.

$$S_r = \frac{1}{50} \sum_{i=1}^{i=50} S_{oi} \quad (4.1.a)$$

$$H(t) = \frac{N}{N-K} \frac{\sum_{i=K+1}^{N} S_{oi}}{\sum_{i=1}^{N} S_{oi}} \quad (4.1.b)$$

Where N = number of hits up to a specific time (t); S_{oi}= signal strength of the ith event; and K = empirically derived factor that varies with the number of hits. One value of K that has been suggested is as follows [12], [13], [49], [57]: (1) not applicable if $N \leq 50$; (2) $N - 30$ if $51 \leq N \leq 200$; (3) $0.85N$ if $201 \leq N \leq 500$; and (4) $N - 75$ if $N \geq 501$.

4.4 Experimental procedure

4.4.1 Test specimens

Six girders having the same geometry and reinforcement details were tested in the laboratory at the University of South Carolina (USC). All girders were originally utilized in 30-ft. span bridges constructed during the 1950's and 1960's. Following their approximately 30 – 40 year service life, the girders were stored in SCDOT facilities. The dimensions and reinforcement details of the girders are depicted in Figure 4.1 and were based on SCDOT's existing drawings. According to these drawings, the typical longitudinal reinforcement consisted of five No. 3 bars spaced evenly along the width of the flange and ten 3/8 in. prestressing strands vertically spaced 1.5 in. on center. The top four strands were prestressed with 13,450 lb. during release, whereas the bottom strands were prestressed with 14,000 lb. The prestressing strands are draped downward at the midspan, except for the bottom strand. In the transverse direction, the girders were reinforced with No. 4 bars and No. 4 stirrups spaced at 12 in. on center. Furthermore, the specified compressive strength of the concrete was 5,000 psi, while the yield strength of the deformed steel bars was 40,000 psi. Additionally, the specified ultimate strength of the prestressing strands was 250,000 psi.

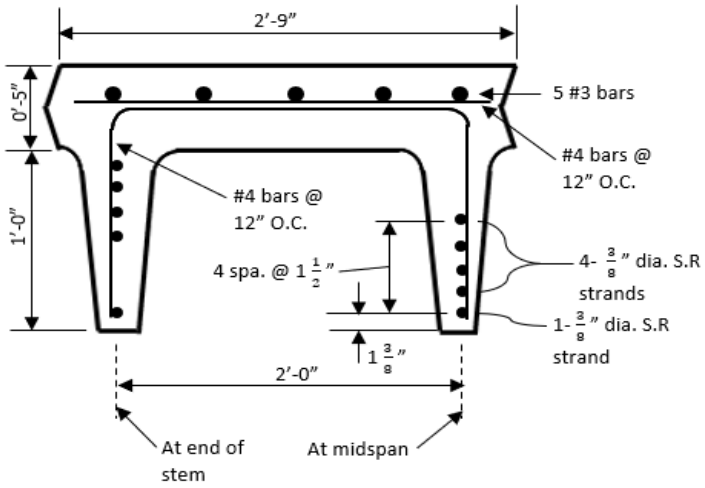

Figure 4.1 Dimensions and reinforcement details of the girders

4.4.2 Test setup

A total of six girders were subjected to a four-point bending test in the laboratory. Figure 4.2 shows schematics of the test setup. The girders were simply supported on two concrete blocks that were made to test full-scale bridge girders. The girders were placed over nine inchwide neoprene bearing pads above the supports to minimize friction when applying the load. The span length of the girders from the centerline of bearings is 27 ft., with a 1.5 ft. overhang at each end. Two structural steel members support the spreader beam, each resting on two neoprene bearing pads to establish four contact points. These contact points are designed to rest directly over the girder legs and create a four-point bending test setup.

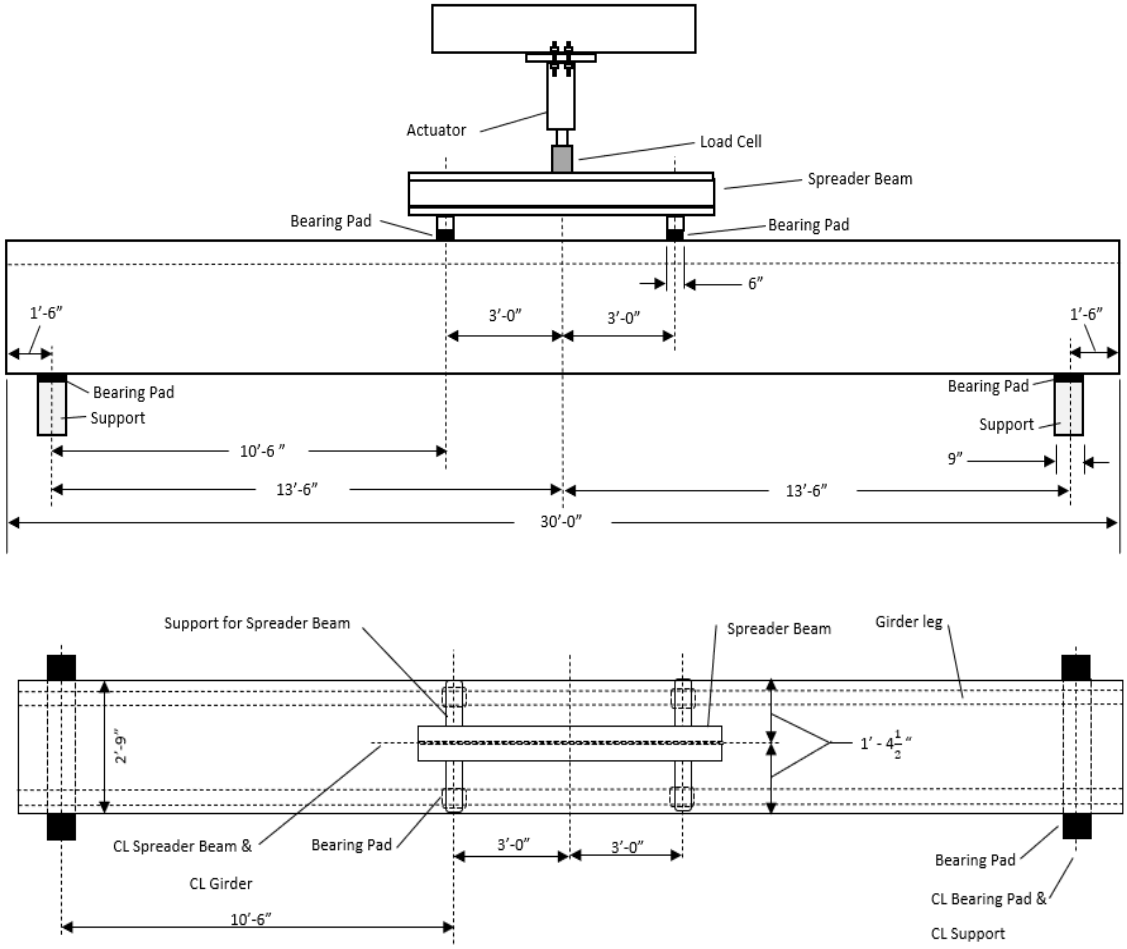

Figure 4.2 Elevation (top) and plan view (bottom) of girders test setup

The load was applied using a hydraulic actuator. A calibrated load cell and pressure gauge were used to monitor the load values during the test. The capacity of the load cell was 250 kip. String potentiometers were utilized to measure vertical displacement at the mid-spans and quarter-spans of the girders. A data acquisition system with 32 channels recorded the data continuously during loading.

AE data was collected using the Sensor Highway II data acquisition system along with eight sensors. Two types of AE sensors were used; four were WDI (broadband) and four were R6i (resonance), with an operating frequency range between 100-900 kHz and 40-100 kHz, respectively. The surfaces of the specimens were first cleaned, then the

sensors were attached using double-bubble epoxy. An array of eight AE sensors were mounted on each specimen. The sensors were placed to detect AE activity and were connected to the data acquisition system. Figure 4.3 shows the AE sensors configuration. In accordance with ASTM E1316[14], pencil lead breaks were conducted to determine the wave speed and attenuation associated with each sensor. The test threshold was set to 50 dB for all channels during testing. This value was chosen to minimize background noise while maintaining enough sensitivity to detect and record AE activity. Photos of the test setup are depicted in Figure 4.4.

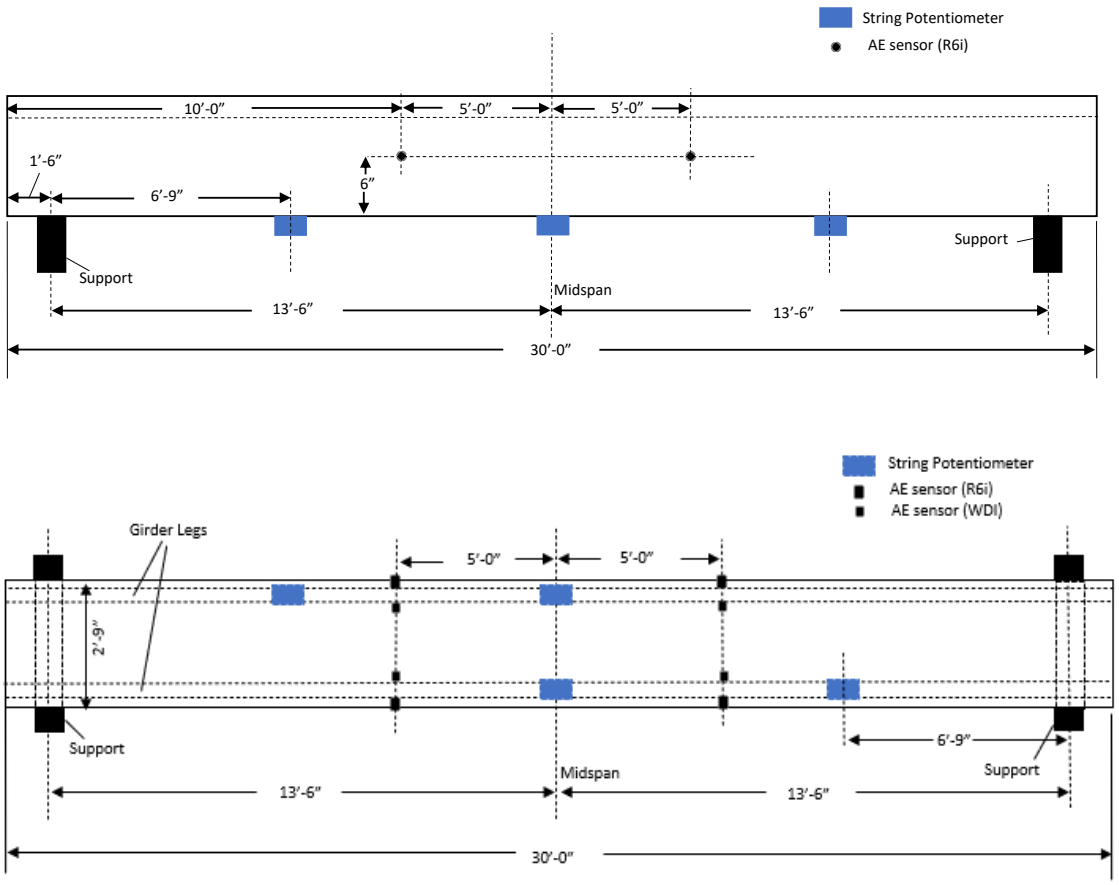

Figure 4.3 Elevation (top) and plan (bottom) instrumentation layout

Figure 4.4 Photos of the test setup of the girders

4.4.3 Loading Protocol

Specimens were loaded in increasing magnitude load cycles. All specimens were subjected to five load cycles. Figure 4.5 shows the load cycles versus time. The girders were originally designed to meet the H15-44 loading criteria. However, the current standards have shifted to HL-93 criteria, which involve the utilization of an HS-20 design truck and a design lane load of 0.64 kip/ft. The moments induced by both H15-44 and HL-93 loading criteria were calculated and then converted into applied loads, considering the four-point test setup. Only one line of wheels was considered in the calculation. This is due to the limitation that only one line of the wheel will fit on a single girder at any given time. A live load distribution factor of 0.5 was assumed, which is a conservative estimate based on the worst-case scenario from a previous study. Furthermore, an impact factor of 33% was applied to both the H15-44 and HL-93 analyses. The theoretical cracking load was calculated utilizing specified material properties and dimensions based on SCDOT drawings. Figure 4.5 displays three distinct lines for each load level.

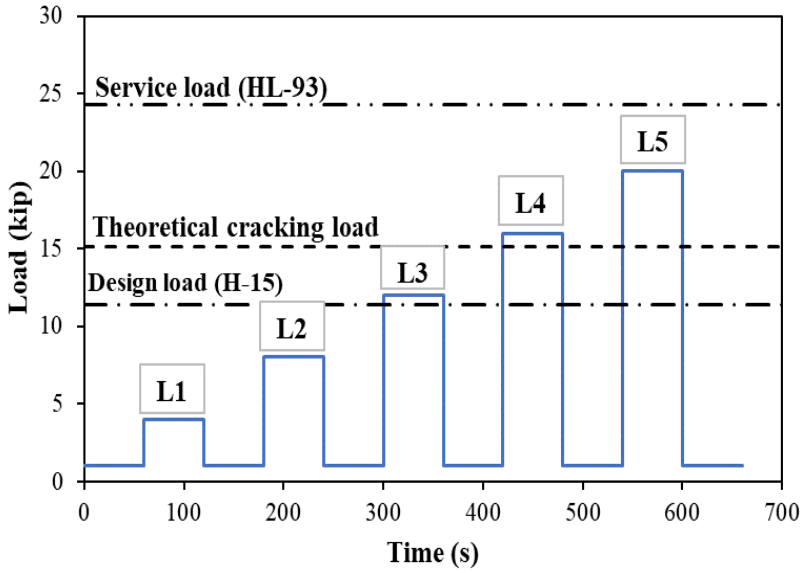

Figure 4.5 Load vs time

4.5 Visual Inspection

Condition states and types of deterioration have been established in both the AASHTO Manual for Bridge Element Inspection (MBEI) [43] and the Specifications for the National Bridge Inventory (SNBI) inspection criteria [44]. The latter provides a 10-scale condition rating for bridge components from "0" to "9" in which "0" refers to the worst condition, whereas "9" refers to the excellent condition. Table 4.1 displays the equivalent member structural condition based on the condition information recorded in the form of NBI condition ratings [7].

Table 4.1 Approximate conversion in selecting $\emptyset_c$ [7]

Superstructure Condition Rating (NBI)	Equivalent Member Structural Condition	Condition factor ($\emptyset_c$)
6 or higher	Good or Satisfactory (CS1)	1
5	Fair (CS2)	0.95
4 or lower	Poor (CS3 and CS4)	0.85

Before conducting the tests, a comprehensive inspection was carried out on all the girders to identify any existing deterioration. Deterioration was mapped and logged for each girder. The girders sustained deterioration throughout their service life. This

deterioration manifested in forms such as spalling, cracking, and section loss, which were prevalent in most of the girders. Furthermore, some girders had visibly corroded strands. These several types of deterioration are illustrated in Figure 4.6.

Each girder received a condition rating ranging from 0 to 9, which was determined based on the observed deterioration. A condition factor and an equivalent structural condition were given to each girder, considering the inspection condition rating. Table 4.2 provides a summary of the condition ratings assigned to each girder.

a) U1 specimen (NBI 4); left) wide crack near midspan, right) large spalling near midspan.

b) U2 specimen (NBI 6); left) small spalling near midspan, right) large spalling at midspan.


c) U3 specimen (NBI 3); left) major defect, right) wide crack near midspan.

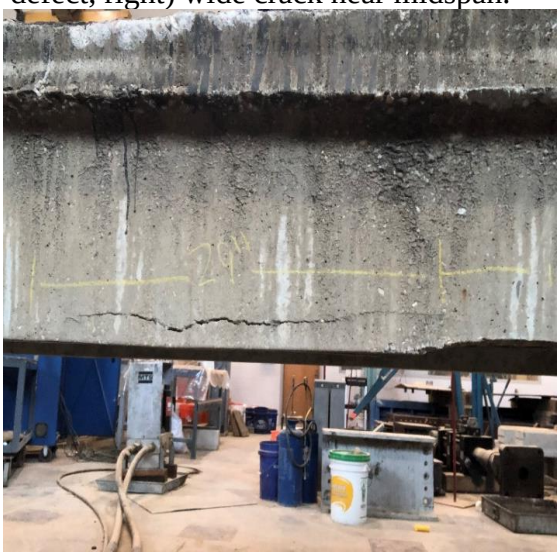

d) U4 specimen (NBI 3); left) major defect at midspan, right) wide crack near the quarter span.


e) U5 specimen (NBI 2); left) wide crack near midspan, right) major defect, exposed strand.

f) U6 specimen (NBI 7); left) flange spalling at quarter span, right) flange spalling at the end.

Figure 4.6 Existing deterioration for the girders

Table 4.2 Summary of condition state of each girder

Specimen	Visual Inspection	NBI condition rating	Equivalent Structural Condition	Condition factor ($\emptyset_c$)
U1	-Wide crack at or near the soffit of legs with rust stains -Some leg spalling -Some flange spalling and isolated diaphragm spalling. -Widespread moderate defects; strength is affected	4	Poor	0.85
U2	-Widespread flange spalling -Some leg spalling -Isolated moderate leg spalling defect	6	Good	1.00
U3	-Some leg spalling -Several feet of exposed strand with corrosion at two distinct locations -Wide crack on the soffit of the leg	3	Poor	0.85
U4	-Widespread flange spalling -Several feet of exposed strand with corrosion at multiple locations. - Wide cracks on exterior sides of legs	3	Poor	0.85
U5	-Isolated wide crack -Several feet of exposed strand with corrosion at multiple locations	2	Poor	0.85

U6	-Rust stains and spalling of concrete along 75% of one leg soffit -Some flange spalling -Isolated spalling on the interior of the leg	7	Good	1.00

4.6 Results and discussion

4.6.1 Detection and assessment of active crack growth using cumulative signal strength.

The girders were grouped based on the condition rating assigned prior to testing. Four girders were assigned a condition rating below 4 (Poor): U1, U3, U4, and U5, whereas two girders were assigned a condition rating higher than 6 (Good): U2 and U6. The detection of cracking, either visible or nonvisible, is associated with AE signals having high strength and sharp changes in the slope of the cumulative signal strength (CSS) curve [22], [55]. Figure 4.7 shows the CSS and load curves with respect to time for girders in good condition (U2 and U6). No sharp changes in the slope of the CSS curve were observed when loading was below the theoretical cracking load. However, as the load exceeded the theoretical cracking load, abrupt changes in the slope of the CSS curve were observed in the AE data, potentially indicating the presence of crack initiation and extension. The actual onset of AE occurred immediately after the load exceeded the theoretical cracking load, indicated by the first rise in the CSS data.

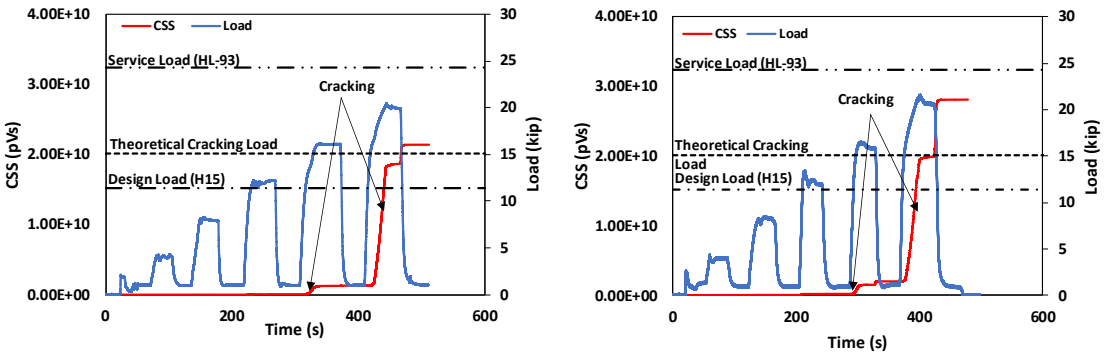

Figure 4.7 CSS and Load curves versus time for girders in good condition

Figure 4.8 shows the CSS and load curves with respect to time for girders in poor condition (U1, U3, U4, and U5). Sharp changes in the CSS curve were observed before reaching the theoretical cracking load. This can be due to the presence of existing cracks. Under loading, AE can be generated due to existing cracks expansion and propagation. Furthermore, the findings of the CSS curves align with the visual inspection where cracks were observed for these girders. The rise in the CSS curve after exceeding the cracking load represents a combination of the initiation of new cracks and the propagation of existing cracks. It is worth noting that for girder U3 the CSS value at the end of load cycle five was equal to 9 x 10^{10} pVs.

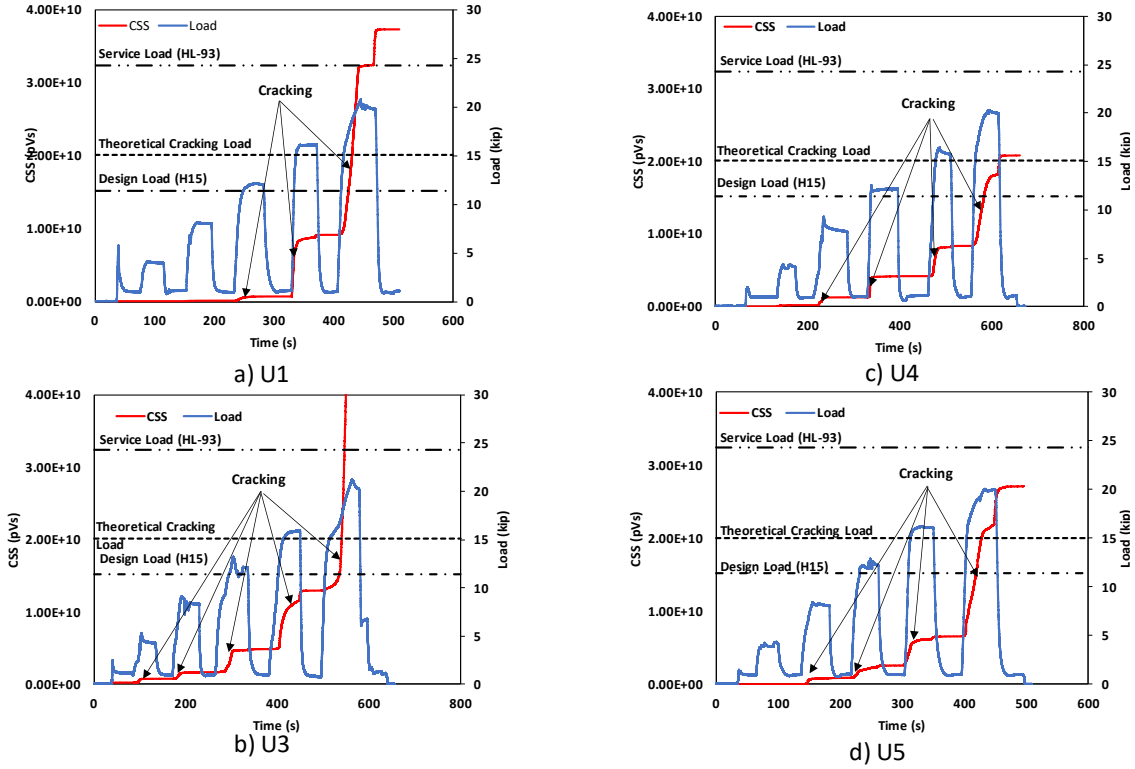

Figure 4.8 CSS and Load curves versus time for girders in poor condition

4.6.2 Intensity Analysis

Intensity Analysis was conducted on all the girders utilizing Equations 4.1.a and 4.1.b. The analysis was performed using AE data collected during the loading phases of tests only. The AE data collected during the unloading phases was excluded from the analysis, as the focus was on the direct effects of loading, particularly the initiation of cracks. The analysis was conducted employing data collected by all sensors.

The data points for intensity analysis were computed as the maximum historic index and maximum severity recorded during each load step. The intensity analysis chart for the girders in good condition is shown in Figure 4.9. Data points in this chart are presented with respect to the theoretical cracking load; therefore, four different labels are used to show data before and after the theoretical cracking load in the two girders in good condition. For instance, the closed circle is for data points before the theoretical cracking load in girder U6 while the opened circle is for after the theoretical cracking load for the same girder. In accordance with the design criteria for Class U prestressed members, which do not allow cracking, the initiation of cracks was used to determine failure. It is worth noting that the CSS curves for the girders in good condition did not show any signs of cracking in the load cycles before reaching the theoretical cracking load. As depicted in Figure 4.9, the intensity analysis distinguishes between data points calculated before and after reaching the theoretical cracking load. Leveraging the information of the two girders in good condition (U2 and U6), the area in the intensity analysis chart where the girders are within the design criteria (did not crack) was determined.

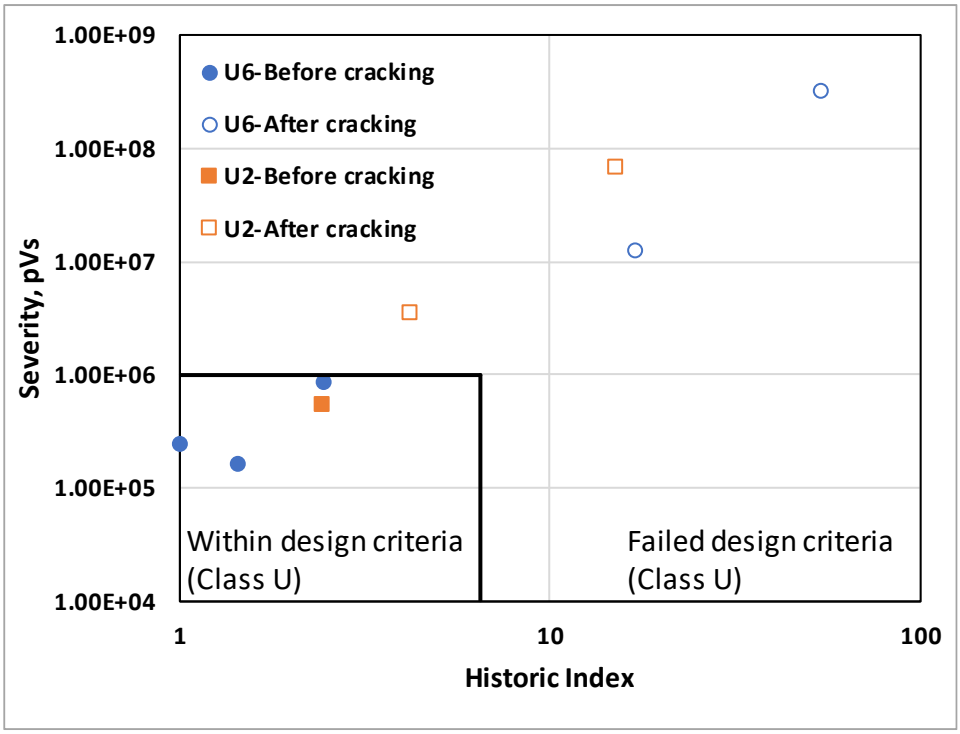

Figure 4.9 Intensity analysis chart (girders in good condition)

The intensity analysis chart developed on the girders in good condition was used to assess the deterioration of the girders in poor condition. An intensity analysis chart for girders in poor condition is shown in Figure 4.10. Similarly, data points in this chart are presented with respect to the theoretical cracking load; therefore, eight different labels are used to show data before and after the theoretical cracking load in the four girders in poor condition. The results show that the girders in poor condition fail the design criteria at lower loads than the theoretical cracking load. It was noticed that all the data points for all the girders in poor condition are plotted in the failed design criteria area; this indicates that the girders have already deteriorated, which is true based on the visual inspection. The results show that the intensity analysis can discriminate between the girders' initial conditions. In addition, the charts consider the existing deterioration in the girders.

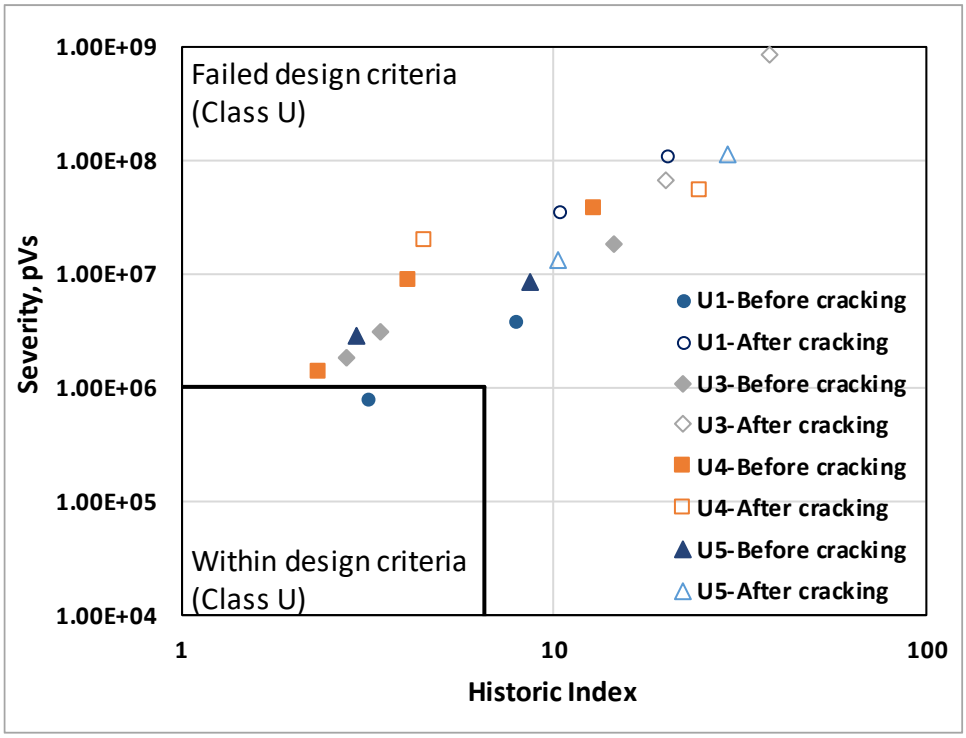

Figure 4.10 Intensity analysis chart (girders in poor condition)

The girders in poor condition, which were assigned a condition factor ($\emptyset_c$) of 0.85 from visual inspection, have a higher historic index and severity at lower loads below the theoretical cracking load, compared to the girders in good condition. The intensity grading criteria were developed based on the girders in good condition, which were assigned a condition factor ($\emptyset_c$) of one from visual inspection. The concept is to relate the condition factor of the girders regarding crack extension and propagation. The proposed criteria for each condition state: good condition corresponds to "insignificant cracks with no propagation," whereas poor condition corresponds to "identified cracks that are propagating." The intensity analysis charts can be used to determine the condition factor ($\emptyset_c$) of the girders used in load rating procedures. If the girders do not meet the design criteria before reaching the required theoretical cracking load, this can be used to update the condition factor ($\emptyset_c$) of the girders for load rating purposes.

4.7 Conclusions

This study summarizes an effort to use non-destructive evaluation techniques, particularly AE, to evaluate the condition state of prestressed concrete channel bridge girders. Six prestressed concrete channel bridge girders, which were originally used in 30-ft span bridges constructed in the 1960s, were subjected to flexural tests at the University of South Carolina (USC). Acoustic emission was used to monitor the girders during the tests. The girders were visually inspected prior to testing and each girder was assigned a condition rating based on the SNBI condition rating descriptions. The main conclusions of the paper are summarized as follows:

1. Cumulative signal strength (CSS) can be used as an assessment method to develop the Intensity Analysis design criteria for girders in good condition.
2. Intensity analysis developed condition assessment charts may assess the deterioration in the girders in good condition. This can be utilized to determine whether the girders are operating in accordance with the design criteria.
3. The charts may also quantify the existing deterioration regardless of the initial condition as seen in the results for the girders in poor condition. In the event that the girders do not meet the design criteria before reaching the required load, this information can be used to update the condition factor ($\emptyset_c$) of the girders for load rating purposes.

Many of the conclusions and results from this research can potentially be directly applied to structural health monitoring of prestressed skinny-leg girder bridges upon validation. Further studies should focus on developing intensity grading criteria for these

structures based on field testing. The test data from both field testing and laboratory work will provide a solid basis to begin developing these criteria.

Chapter 5

An Automated Load Determination System for Bridges based on Acoustic Emission and Machine Learning Techniques[3]

[3]Elbatanouny, E., Ai, L., Henderson, A., Laxman, K. C., & Ziehl, P. (2023). An Automated Load Determination System for Bridges based on Acoustic Emission and Machine Learning Techniques. Submitted to Construction and Building Materials.

5.1 Abstract

Many bridges in the United States are aging and approaching the end of their design life. Most of these bridges were designed using standards from the 1950s that are now obsolete. Over the years, vehicles have become heavier than they were in the past, which has resulted in an overloading problem. Hence, an assessment of the bridges' current condition, as well as an evaluation of safe load capacities, are required. With these measures taken, updated vehicle weight restrictions for these structures can be implemented. Nondestructive approaches such as acoustic emission (AE) have been widely used in monitoring bridge degradation, recently stimulated by developments in sensor technology and data analysis methodologies. The innovation of this paper lies in presenting a potential approach for predicting the vehicle loads on prestressed concrete girder bridges from the collected AE data while monitoring the damage. Upon validation, this method may serve as an alternative or to supplement the conventional method using weigh-in-motion (WIM) sensors. To achieve this goal, three improved machine learning algorithms based on artificial neural networks (ANN), AdaBoost, and random forest were adopted to analyze the AE data. An ensemble training strategy was employed to eliminate the imbalance issue while training machine learning models. The AE data was collected by conducting a flexural test on a full-scale prestressed concrete girder. In this study, load determination is considered a classification problem. The loading procedure was divided into load steps and the AE signals were classified to their corresponding load steps. The results show that the improved random forest algorithm outperformed the improved ANN and AdaBoost algorithms in classifying AE hits to their corresponding load steps.

Keywords: Prestressed concrete girder, Acoustic emission, Structural health monitoring, Artificial neural network, AdaBoost, Random Forest

5.2 Introduction

Bridges are an integral part of our aging infrastructure throughout the United States and many other parts of the world. South Carolina relies significantly on its numerous bridges for community connectivity, trade, and transportation. The state ranks 26th in the nation in bridge inventory, with more than 9,000 bridges. Most bridges were designed utilizing the H-10 or H-15 loading standards, while the current loading standard, HL-93, is much greater [1], [2]. The South Carolina Department of Transportation (SCDOT) manages approximately 90% of all bridges. On average, the bridges are approximately 40 years old, approaching the 50-year service level, with 6.8% being load posted, 11% being structurally deficient, and 0.33% being reported closed [3]. This is a direct outcome of bridge deterioration and overloading due to long service life and increased vehicle loads.

Bridges are inspected regularly to evaluate the condition of their components. Additionally, they are evaluated to ensure that they possess adequate reserve structural capacity to accommodate the anticipated live load demands, with a safety margin. In cases where the reserve structural capacity is insufficient to support the anticipated live load demands, measures such as load posting, rehabilitation, or closure of the bridge may be necessary to guarantee public safety. As a result, load rating is a crucial asset management tool employed by bridge owners to determine the margin between the anticipated live load demands and the reserve structural capacity of the bridge [16].

Bridge loads are subject to a great deal of uncertainty, primarily due to live loads. One effective way to decrease uncertainty is by obtaining site-specific traffic data to assess

live loads [15]. Hence, weigh-in-motion (WIM) systems are installed at multiple locations to measure vehicle loads passing through bridges. The most widely utilized commercially available WIM sensors are piezoelectric, load cell, and bending plate sensors. However, WIM systems with load cells have large cross sections, bending plate sensors are cumbersome to install, and piezoelectric sensors can only be used to collect traffic data and cannot measure weight [58], [59]. In addition, the WIM sensors need to be embedded in the pavement, necessitating lane closure for a week or more, which might be problematic for certain bridges. As a result, it is crucial to investigate compact, efficient, and lightweight sensors for measuring vehicle loads that can be rapidly and easily deployed on bridges.

Various sensors have been utilized in the structural health monitoring of structures as sensor technology has advanced [60]–[62]. For instance, Acoustic Emission (AE) sensors are widely utilized due to their ease of use, high damage sensitivity, and ability to monitor the response of structures regularly [63], [64]. With an array of piezoelectric sensors, AE detects the elastic waves generated by crack formation and growth. Structural damage can be detected and localized by AE emissions before it becomes visible at the surface of an element [65]. AE parameters were analyzed to assess structural damage, including crack detection, crack location, crack type, and corrosion [66], [67]. Measuring the vehicle loads while concurrently monitoring the bridge will be a great advantage as it saves time and money through its easy installation.

Researchers analyzed AE data using various methods and parameters [68]–[71]. Statistical analyses for the AE parameters were utilized to evaluate and monitor the condition of bridge components. The validity of damage assessment of prestressed concrete

I-beams using conventional AE parameter-based methodology was examined by Zeng et al. [72]. A four-point bending test was conducted on a full-scale I-section prestressed concrete beam. To assess the response of the beam in terms of damage formation, the variance in AE signal activity throughout incremental loading cycles was analyzed. In addition, Worley et al. [73] investigated the potential of AE sensing techniques for crack detection and localization in prefabricated prestressed concrete girders. The results indicated that AE sensing could be applied as a quality control procedure for prefabricated bridge elements.

Although many AE parameters are gathered, statistical analysis depends on a single parameter or correlation plots of two parameters. Hence, some information on the signals may be lost, resulting in a failure to make a strategic decision and lower productivity [74]. Several AE parameters should be considered simultaneously to overcome this limitation [75], [76]. Several machine learning algorithms, such as artificial neural network (ANN), AdaBoost, and random forest, were adopted to interpret multiple AE parameters concurrently. Machine learning is a method of supervised intelligent data processing [77]. It can analyze the data pattern and make a judgment by learning the features derived from the data [78].

Nair et al. [79] monitored the damage modes in CFRP-strengthened concrete structures. The main sources of AE activities were identified based on visual observation and damage mechanism expectation. AE data was clustered using the unsupervised k-means technique. Each cluster was associated with one or more damage mechanisms. The ANN models, support vector machines (SVM), and multilayer perceptron (MLP) algorithms were then trained using the classified AE data. Finally, the trained models were

applied to identify the damage in similar specimens. The results pointed out the high performance of classification rates for both algorithms. Ai et al. [80] developed an automated impact detection system for aircraft components utilizing AE and machine learning algorithms. The authors employed ANN and AdaBoost algorithms. The results show that AdaBoost performed better than ANN in localizing the impact. Ai et al. [81] conducted a study to localize cracking on dry cask storage system canisters. The authors employed three machine learning algorithms (ANN, random forest, and stacked autoencoders) to analyze the AE data. The results revealed that the random forest method outperformed the ANN algorithm, with an accuracy of 91.5% for the random forest and 80% for the ANN. These studies demonstrate the capacity of machine learning algorithms in the field of AE monitoring.

Recently, K C et al. [23] investigated the potential of utilizing AE to predict vehicle loads on bridges. Two precast flat slabs were tested under a four-point bending test. The authors employed the ANN algorithm by simultaneously analyzing 13 AE parameters. The results revealed the feasibility of ANN in classifying the AE hits to their corresponding vehicle loads with acceptable accuracy. However, in this study, the classification was done on two load steps with a step size of ten kip, and only the ANN algorithm was implemented. Moreover, this study is limited to precast RC flat slab bridges. Using AE to predict the vehicle loads on other typical bridges, such as girder bridges, was not studied.

The current study explores an improved load determination method for girder bridges based on previous work [23]. A laboratory experiment was performed on a prestressed concrete girder to simulate vehicle loads. AE data was collected and analyzed from four load steps with a step size of four kip. In addition, various machine learning

algorithms, ANN, AdaBoost, and random forest, were investigated. The main contribution of this paper is to develop an optimized method for predicting vehicle loads that pass over girder bridges from the collected AE data. Information on traffic loads can help transportation networks operate more efficiently and cost-effectively [82].

The remaining sections of this paper are arranged as follows. First, the experimental setup is presented in Section 5.3. Next, the data preprocessing and methodology are presented in Section 5.4. Section 5.5 details the results and discussion. Finally, section 5.6 provides a summary of the conclusions and recommendations.

5.3 Experimental Setup

5.3.1 Test Specimen

A flexural test was conducted at the University of South Carolina (USC) on a prestressed concrete girder. The girder was originally employed in a 30-ft span bridge built in the 1960s, which was later removed after 30 years of service and stored in an SCDOT facility. Figure 5.1 presents the dimensions and the reinforcement details of the girder. Based on SCDOT drawings, reinforcement details of the girder consist of five No. 3 bars and ten 3/8 in. prestressing strands longitudinally. Prestressing strands are draped downward at the midspan except for the bottom strand, as depicted in Figure 5.1. At release, the bottom strand was prestressed with 14,000 lb. for each leg, while the top four strands were prestressed with 13,450 lb. In addition, transverse reinforcement consists of No. 4 bars spaced at 12 in. on center and No. 4 stirrups spaced at 12 in. on center. The specified compressive strength of concrete and the yield strength of the deformed steel bars were 5,000 psi and 40,000 psi, respectively. The ultimate strength of the prestressing strands was 250,000 psi.

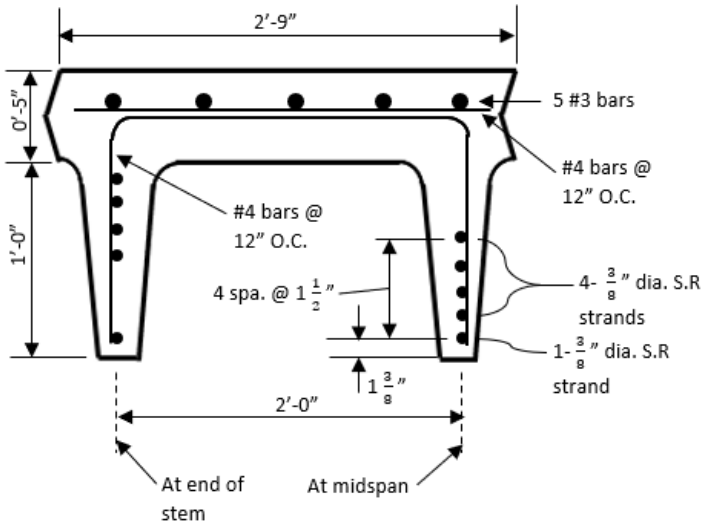

Figure 5.1 Dimensions and reinforcement details of girder

5.3.2 Test Setup

An experimental test was conducted to simulate the effect of a vehicle passing over the bridge girders. One 30-foot long, simply supported girder was subjected to a four-point bending test [83] in the lab at the University of South Carolina (USC). Fig. (2) shows schematics of the test setup. The girder was placed over nine inchwide neoprene bearing pads above the supports to lessen friction during the application of the load. Two structural steel members support the spreader beam, each resting on two neoprene bearing pads to establish four contact points. These contact points are designed to rest directly over the girder legs and create a four-point bending test setup, as shown in Figure 5.2. The span of the girder is 27 feet.

String potentiometers were used to measure vertical displacement at the quarter-spans and mid-spans of the girders. The load was applied using a hydraulic actuator. A calibrated load cell and pressure gauge were used to monitor the load values during the test. The capacity of the load cell was 250 kip. A data acquisition system with 32 channels

recorded the data continuously during loading. Figure 5.3 presents photos from the test setup.

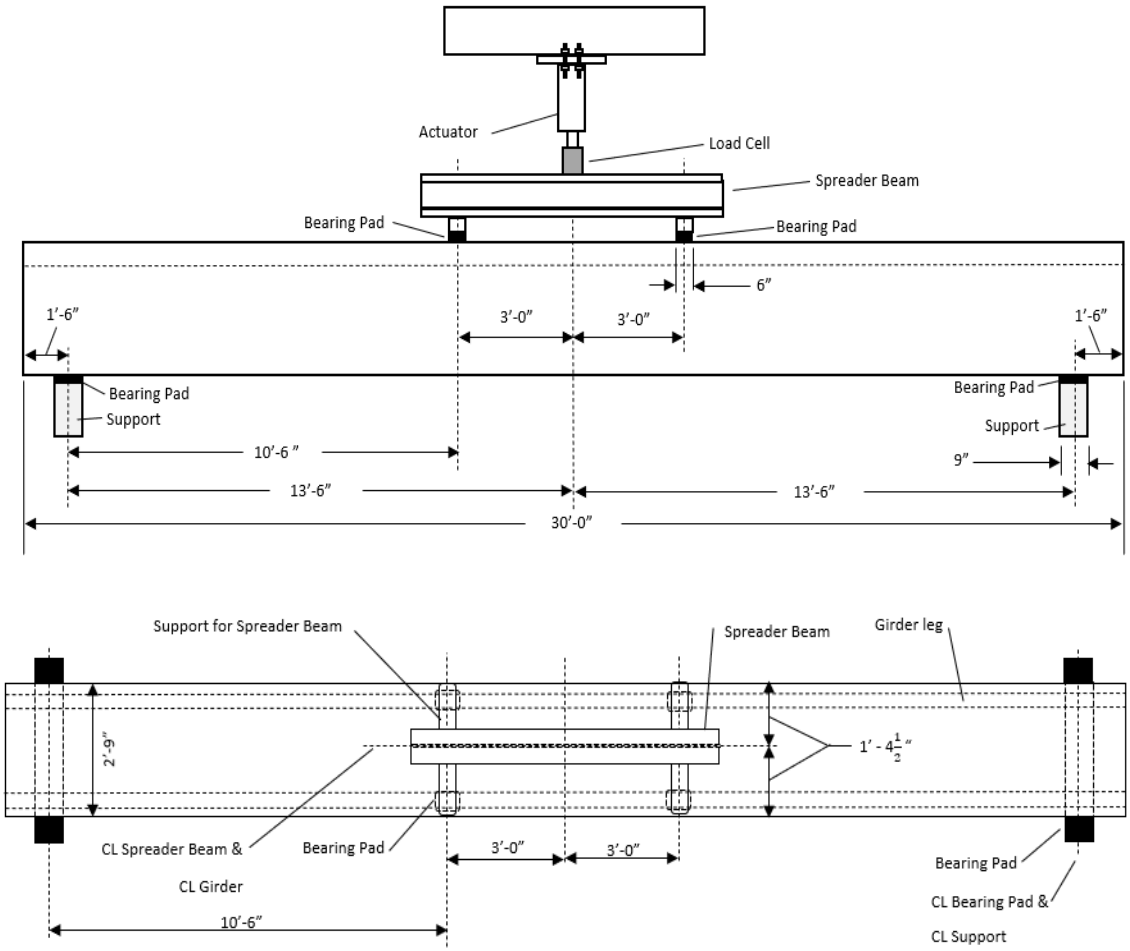

Figure 5.2 Test setup of the girder

Figure 5.3 Photos of the test setup of the girder

Loading on the girder was stepwise cyclic to simulate the vehicle wheel loads passing over the bridge girders. The girder was initially loaded to 1 kip. Next, the load was raised to 4 kip, maintained there for 60 s, and then dropped back to 1 kip (referred to as load step 1, L1). Next, the load was raised to 8 kip, maintained there for 60 s, and then dropped back to 1 kip (referred to as load step 2, L2). The girder was then loaded to 12 kip, maintained there for 60 s, and then dropped back to 1 kip (referred to as load step 3, L3). Next, the load was raised to 16 kip, maintained there for 60 s, and then dropped back to 1 kip (referred to as load step 4, L4). The girder was then loaded to 20 kip, maintained there for 60 s, and then dropped back to 1 kip (referred to as load step 5, L5). In this study, load steps 1 through 5 were designed to mimic the expected range of vehicle loads these girders may encounter throughout their lifespan. Figure 5.4 illustrates the load versus time graph for the test.

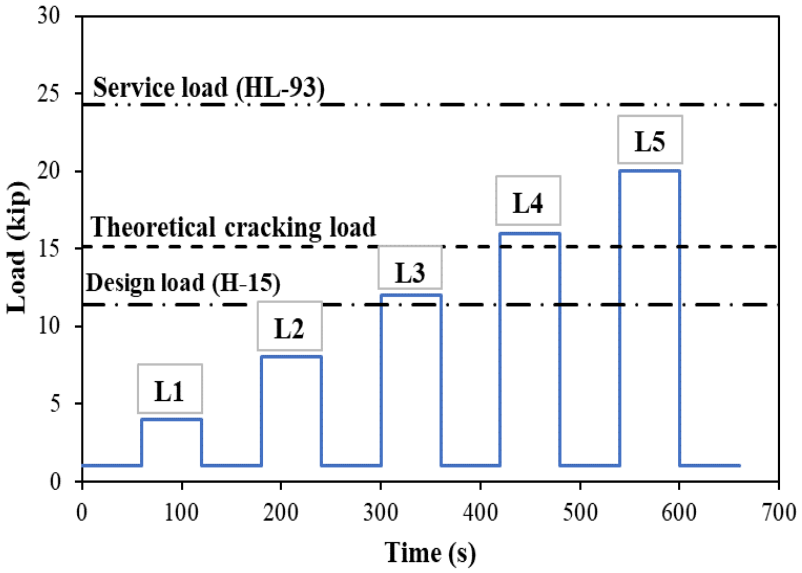

Figure 5.4 Load vs Time

5.3.3 Acoustic emission

The transient elastic waves within a material induced by the quick release of localized strain energy are known as Acoustic Emission (AE) [14]. Load determination was performed with the AE sensing system, which uses piezoelectric sensors coupled to the test specimen. AE sensors detect high-frequency stress waves created by a quick release of energy, such as a crack growth event. A "hit" is the recording of an individual signal, characterized by parameters such as amplitude, duration, rise time, energy, average frequency, and signal strength as shown in Figure 5.5. The collected AE parameters are extracted to understand the patterns better and develop filters to minimize the noise in the data set.

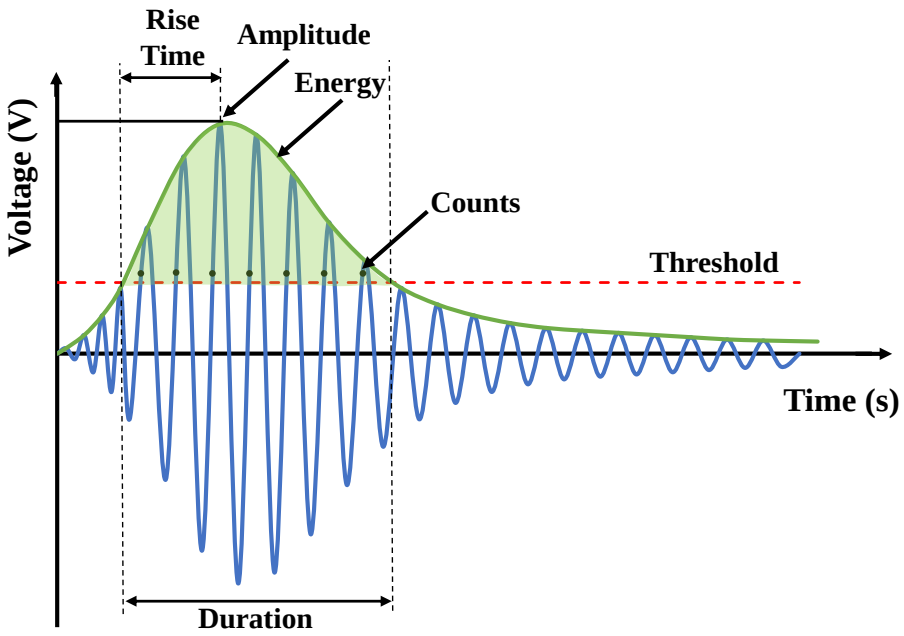

Figure 5.5 Schematic of acoustic emission parameters [84]

AE data was collected using the Sensor Highway II data acquisition system and four resonant sensors (type R6i). An R6i sensor has an operating frequency range of 40 to 100 kHz. AE sensors were installed on the specimen. The surface of the specimen was first cleaned, then the sensors were attached using double-bubble epoxy. An array of 4 AE sensors were mounted on the specimen. The sensors were placed strategically to detect AE activity and were linked to the data acquisition system. Figure 5.6 shows the AE sensors configuration. In accordance with ASTM E1316[14], pencil lead breaks were utilized to calculate the wave speed and attenuation associated with each sensor. The test threshold was set to 45 dB for all channels during testing. This value was chosen to reduce background noise while providing enough sensitivity to detect and record AE activity.

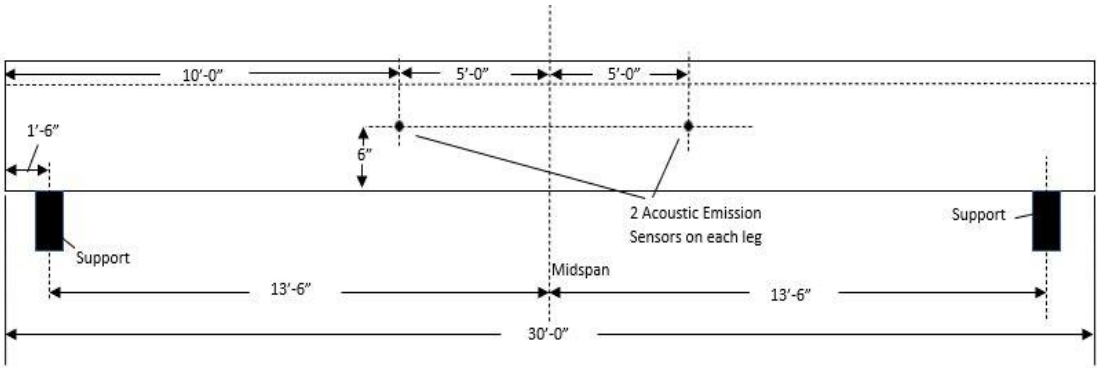

Figure 5.6 AE sensors configuration

5.4 Data Processing and Methodology

5.4.1 Data Filtering

Before data analysis, it is critical to filter AE data to exclude any data irrelevant to the structure's response (noise). In laboratory conditions, mechanical and electrical noise is minimal[85]. In this test, wave reflections and friction between the loading apparatus and the specimens were the primary sources of irrelevant data. The latter was reduced by employing neoprene pads between the supports and the girders. In addition, front-end filters were employed to minimize reflections by setting peak definition time (PDT), hit definition time (HDT), and hit lockout time (HLT) values of 200 μs, 400 μs, and 800 μs, respectively. A description of terminology related to AE can be found in ASTM E1316 [14].

Two post-processing filters were implemented to reduce the collected data after testing. The first filter is an amplitude filter that excludes hits with an amplitude below a specified threshold, which was determined at 50 dB based on the characteristics of the AE signals. The second filter, typically known as a D-A filter or Swansong II filter [86], is based on duration and amplitude limits. A similar filtration procedure was adopted for prestressed concrete beams in [84], [85], [87]. Table 5.1 lists the limitations of the second filter.

Table 5.1 Limitations of the second filter [85]

Filter Type	Rejection limits		Rejection limits		Rejection limits	
	Amplitude dB	Duration μs	Amplitude dB	Duration μs	Amplitude dB	Duration μs
Duration-Amplitude	44-46	>800	54-56	>2,500	70-75	>7,500
	46-48	>1,000	56-58	>3,000	75-80	>9,000
	48-50	>1,200	58-60	>3,500	90-100	>10,000
	50-52	>1,500	60-65	>4,500		
	52-54	>2,000	65-70	>6,500		

5.4.2 Framework

AE hits were collected during the flexural test for further analysis. Table 5.2 presents the AE parameters and their definitions that were employed in this study. Three machine learning algorithms are used in this study to classify a group of AE hits to their corresponding load steps based on their corresponding AE parameters. The rationale behind this method is that the variances among the 14 AE parameters would enable the machine learning algorithm to classify the data points. In field applications, the AE data collected from a vehicle passing over a bridge will be a group of AE hits, not a single AE hit. Hence, the overall goal was to classify a group of AE hits to their corresponding load step.

Table 5.2 AE signal parameters

Number	AE parameters	Definitions
1	Amplitude (dB)	The maximum amplitude at the peak of the wave
2	Count	The number of threshold crossings
3	Rise time (μs)	The time interval between the first threshold crossing and the maximum amplitude
4	Duration (μs)	The time between the first and last threshold crossing of the signal
5	Root mean square (RMS) (V)	The effective voltage with a characteristic time T_{RMS} for average ranging from 10 to 1000 ms
6	Average signal level (ASL) (V)	The effective voltage with a characteristic time T_{ASL} for average ranging from 10 to 1000 ms

7	Energy (10^{-14} V^2s)	The measure of the electrical energy measured for an AE signal
8	Absolute energy	The absolute measure of the electrical energy measured for an AE signal
9	Reverberation frequency (kHz)	Frequency after the peak
10	Initial frequency (kHz)	Frequency before the peak
11	Signal strength	A parameter to evaluate the AE source strength
12	Counts to peak (PCNTS)	The number of threshold crossings from the first threshold crossing to the peak
13	Peak frequency (P-FRQ) (Hz)	Frequency of maximum signal contribution
14	Frequency centroid (C-FRQ) (Hz)	A parameter to characterize the overall frequency content of an AE signal

After the filtering process, the total data collected from the test was 30,274 hits. The girder was loaded stepwise cyclic (five load steps: L1, L2, L3, L4, and L5). The number of AE hits collected during the load step L1 (referred to as L1 hereafter) was 241. The number of AE hits collected from L2, L3, L4, and L5 were 1395, 5337, 8140, and 15161, respectively. The classification was only performed on the AE hits collected from load steps L2, L3, L4, and L5 due to the lack of data gathered from L1. Figure 5.7 depicts the AE hits and their corresponding load step for the test.

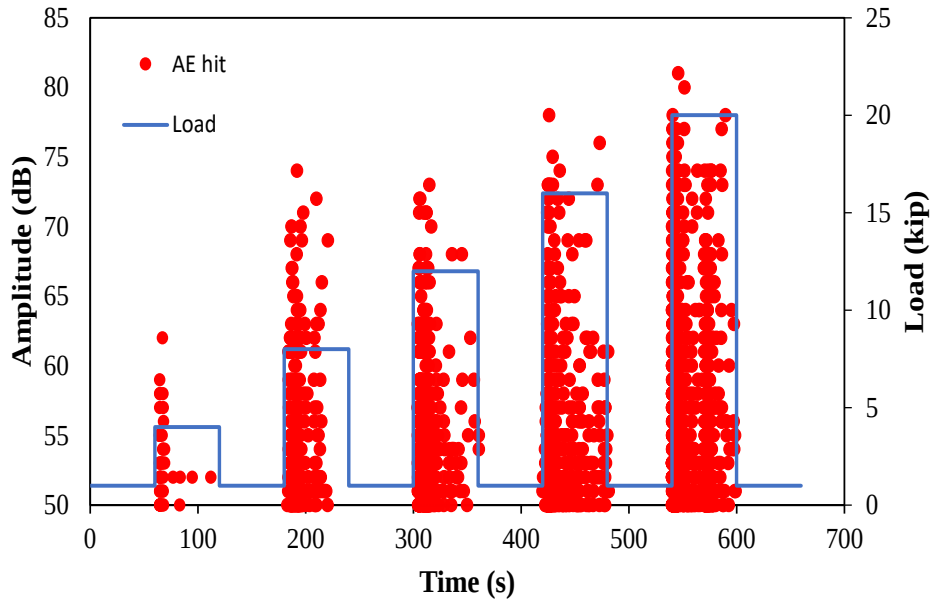

Figure 5.7 Amplitude and load vs time for the test

The machine learning model goes through three phases of classification: training, validation, and testing. Most of the AE hits in the total dataset from the test belonged to L5, which led to an imbalance issue in the machine learning model as reported in the findings of K C et al. [23]. To address the imbalance issue, an equal amount of data for each load step was fed into the machine learning model. It was determined that the ratio of the number of hits belonging to L3, L4, and L5 to L2 was 4 to 1, 6 to 1, and 12 to 1, respectively. The machine learning model was then fed with the total data from L2 and a random dataset from each L3, L4, and L5. To even out the data, a total of 288 data combinations ($C_4^1 \times C_6^1 \times C_{12}^1$) were composed to balance the data. Using these combinations as training data, 288 different models were trained and validated. This procedure is referred to as balanced training (BT). A group of AE hits consisting of 200 hits from each load step (L2, L3, L4, and L5) was collected prior to training and validation. The testing data collected was used to test these models, and each model made a

classification vote. The majority rule applied to the votes of the model. Figure 5.8 shows the process of the framework.

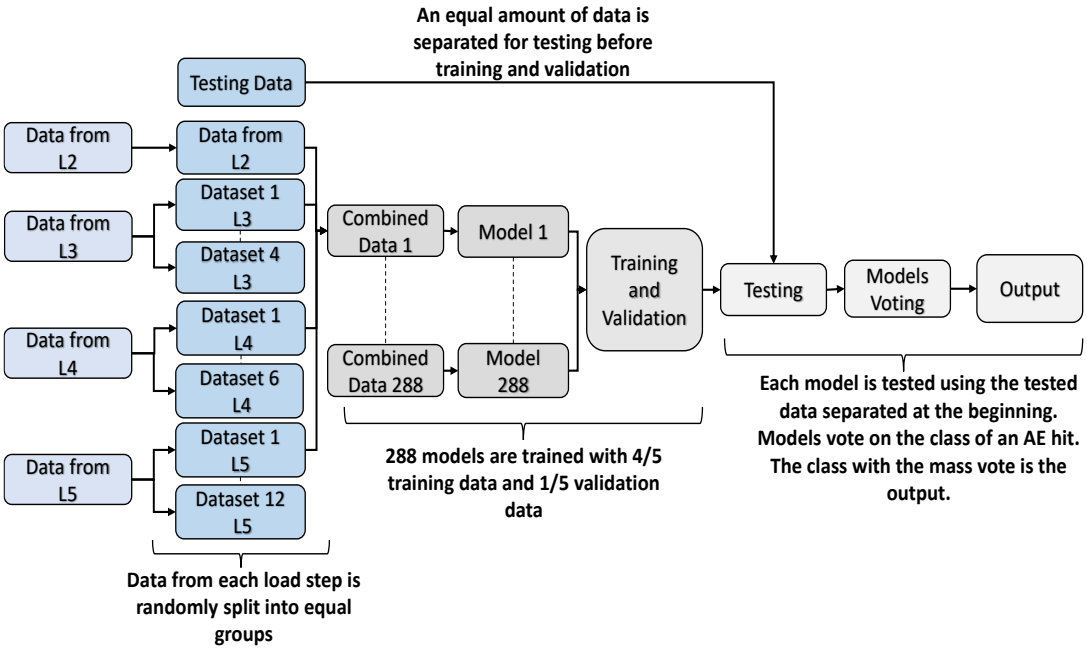

Figure 5.8 Balanced training (BT) and testing for the machine learning models

It should be noted that if an AE hit is entered into the BT model shown in Figure 8, the predicted result is the load step to which this single AE hit belongs. However, the AE hits collected from the vehicle loads will be a group of AE hits, as presented in Figure 5.9, not a single AE hit. If all AE hits are entered into the BT model, a set of predicted loads will be obtained. Therefore, a decision-making process was developed in this application to finally determine the load step. As shown in Figure 5.9, the AE hits generated by the load step were assigned to the trained BT machine learning model. Then, the output was converted into the probabilities that this load belongs to the steps. The final determination was made based on the maximum probability.

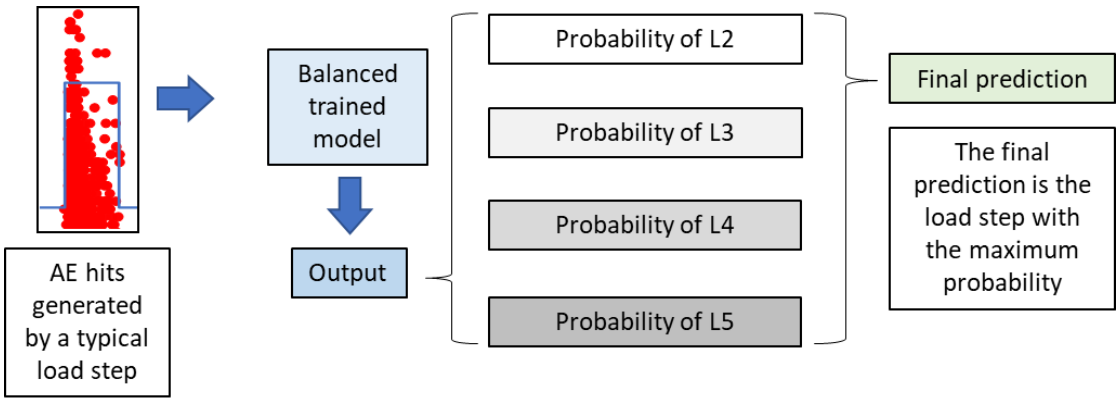

Figure 5.9 Decision-making process

The Artificial Neural Networks (ANN), AdaBoost, and random forest algorithms improved by the BT strategy were used in this study to classify the AE hits to their corresponding vehicle loads based on their corresponding AE parameters.

5.4.2.1 Artificial Neural Network (ANN)

The neural network used in this study is a backpropagation artificial neural network (BP-ANN), which is one of the most widely used ANN techniques [88]. It is comprised of an input layer, a series of hidden layers, and an output layer [89]. Each layer has several processing elements defined as neurons. Furthermore, each neuron is linked with every other neuron in the neighboring layers [90]. The number of neurons in the input and output layers correlates to the input variables and the output dimension [91].

Figure 5.10 depicts a typical three-layer artificial neural network comprised of layers i, j, and k. The number of neurons is a for layer i, b for layer j, and c for layer k. The weights between neurons in neighboring layers are denoted by W(ij) and W(kj). The values of a and c are related to the problem for solving, whereas the network designer determines b.

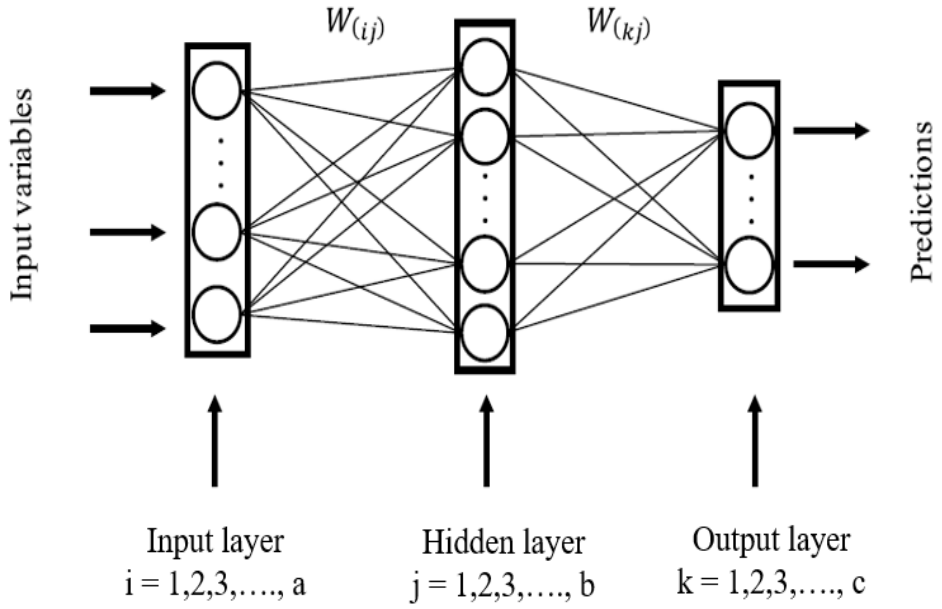

Figure 5.10 Three-layer artificial neural network

A BP network is calculated using feedforward and error-backward computations. In feedforward computations, the input layer neurons receive the processed data, and Eq. (1) calculates the weighted sum corresponding to each neuron in the subsequent layer.

$$net_{(i)} = \sum_{j=1}^{n} W_{(ij)} \cdot O_{(j)} \quad (1)$$

Where net is the net input of the i-th neuron, $W_{(ij)}$ is the weight, and $O_{(j)}$ is the output of the neuron.

The weighted sum is submitted to the activation function, which may be linear, nonlinear, or a unit step function, to determine the output of the i-th neuron. The S-type activation function is represented in Eq. (2), which is typically used to explain the nonlinearity of the system. The result obtained by the output layer will be employed to generate an error. Error E is calculated as shown in Eq. (3).

$$O_{(i)} = f\left[net_{(i)}\right] = \frac{1}{1+e^{-net_{(i)}}} \quad (2)$$

$$E = \frac{1}{2} \sum_{j=1}^{l} [d_{(k)} - O_{(k)}]^2 \quad (3)$$

Where, $d_{(k)}$ is the label value. $O_{(k)}$ is the prediction value in the k-th neuron of the output layer.

The error of the output layer will be backpropagated to the previous adjacent layer using the gradient descent method and lastly propagated to the input layer to produce more accurate results. Eq. (4) yields the value of the weight change. All connection weights are initially assigned random values and subsequently changed based on the outcomes of the BP training process. Figure 5.11 depicts the mechanism of a backpropagation network.

$$\Delta W_{(kj)} = -\alpha \frac{\partial \mathrm{E}}{\partial \mathrm{W}_{(\mathrm{kj})}} \quad (4)$$

Where α is the learning rate that adjusts the amplitude of the weight change.

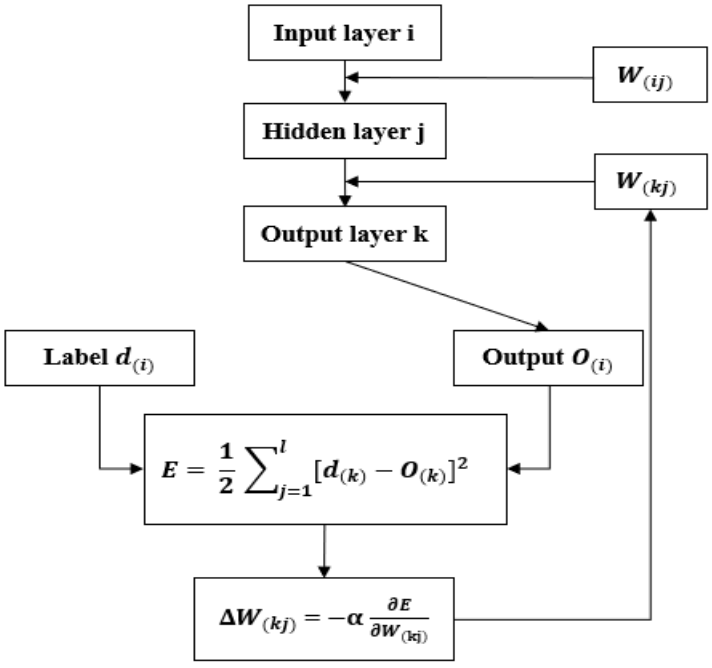

Figure 5.11 Mechanism of a backpropagation network

5.4.2.2 AdaBoost

The Boosting algorithm is an integrated learning method that can improve multiple weak learning models[92]. "Adaptive Boosting" is referred to as AdaBoost. In contrast to the random forest, the weak learning model utilized in the AdaBoost algorithm is usually

just a decision node and two leaf nodes referred to as a decision stump (referred to as a stump hereafter). The stump can only use one variable to decide. AdaBoost is adaptive in that succeeding stumps are weighted in favor of instances misclassified by prior stumps. Each stump inside the AdaBoost obtains a function through multiple iterations. At the end of the iterations, each stump is assigned a weight. The final classification is voted from the results of all the stumps, considering the weight. In other words, some stumps get more say in the classification than others [93].

An initial weight set (W) is assigned to the AdaBoost model: W = (W_1, W_2, …, W_N). Every element in the weight set has the same initial weight of 1/N. Assuming the AdaBoost model has k stumps. Eq. (5) can calculate the kth stump, and the updated coefficient of the weight can be obtained by Eq. (6).

$$\varepsilon_k = \sum_{i=1}^{N} W_{ki}, T_k(X_i) \neq y_i \quad (5)$$

$$\alpha_k = \frac{1}{2} \ln \left(\frac{1-\varepsilon_k}{\varepsilon_k}\right) \quad (6)$$

The updated weight W_{k+1} for the next stump T_{k+1} can be provided by Eq. (7) and Eq. (8):

$$W(correct)_{k+1i} = \frac{W_{ki}}{Z_k} e^{-\alpha_k} \quad (7)$$

$$W(wrong)_{k+1i} = \frac{W_{ki}}{Z_k} e^{\alpha_k} \quad (8)$$

$$Z_k = \text{sum}\ (W_k) \quad (9)$$

Where W(correct) refers to the weight assigned to the input data correctly classified by the last stump and W (wrong) refers to the weight assigned to the input data incorrectly classified by the last stump. Z_k is the normalization factor. The architecture of the AdaBoost algorithm is shown in Figure 5.12.

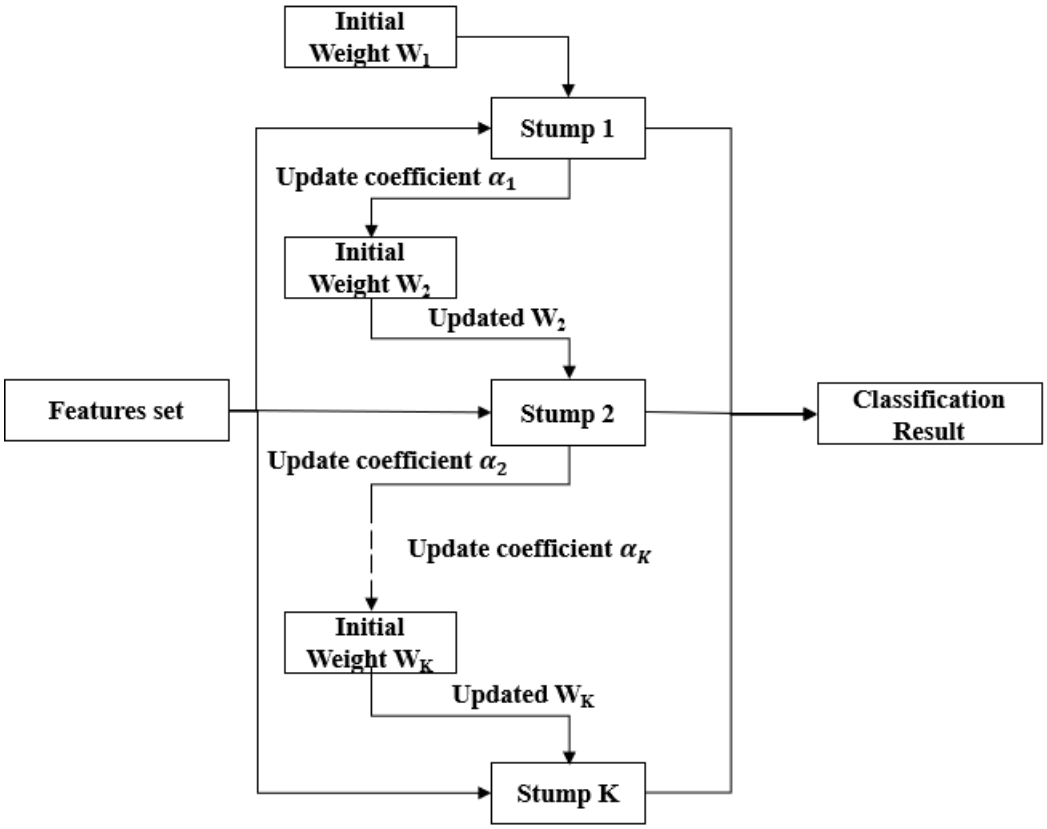

Figure 5.12 The architecture of the AdaBoost algorithm

5.4.2.3 Random Forest

Random forest is an ensemble learning algorithm, a bagging algorithm [94]. Multiple weak learning models are employed in this algorithm. To determine the outcome of the overall model, the outcomes of the weak learning models are voted on or averaged [95]. The model with a prediction accuracy marginally better than a random guess is referred to as a weak learning model. The decision tree is the weak (basic) learning model employed in the random forest.

The decision tree classifies the dataset based on multiple features. There are two kinds of nodes: decision nodes and leaf nodes. The former contains a condition to split the data, and the latter helps us to define the class. At each node of the tree, the decision node of the following layer is branched based on the performance of the features. The sampling

categories incorporated in the decision nodes will gradually become consistent with layer-by-layer branching, and the leaf node is the decision tree classification result.

Bagging is the combination of bootstrapping and aggregation. Utilizing the bootstrapping method, a predefined number of samples from the training with replacements are obtained. Bootstrapping ensures that the same data is not used for each tree, so it helps the model to be less sensitive to the original training data. As a result, a sample set is created for each basic learning model. Because of the replacement sampling, specific samples may be drawn again, while others may not. Finally, the final classification result is voted or averaged from the results of all the basic models, which is called aggregation.

The random forest algorithm is a combination of a decision tree and bagging. The decision tree, combined with bagging efficiently, reduces the variance of a single decision tree. This process results in a random forest, as shown in Figure 5.13. The Gini impurity of the node is employed as the branching criteria in this study for generating the decision tree. The Gini impurity of a node refers to the probability that the sample was incorrectly classified and is obtained by Eq. (10). If the Gini impurity is less than a predetermined threshold (typically zero), it indicates that the samples belong to the same class. Otherwise, the sample is split into two parts, N1 and N2, as given in Eq. (11), and then assigned to two sub-nodes.

$$Gini\ (N) = 1 - \sum_{i=1}^{k} P\left(i/t\right) \quad (10)$$

Where $P\left(i/t\right)$ is the probability of category i at node t.

$$Gini\ (N, F) = \frac{N1}{N} Gini\ (N1) + \frac{N2}{N} Gini\ (N2) \quad (11)$$

The random forest model can determine and assess the significance of features through the feature division process while classifying [81].The method is shown in Eqs. (12) and (13).

$$I_t(F) = Gini|(N) - Gini(N,F) \quad (12)$$

$$S(F) = \sum_t I_t(F) \quad (13)$$

Where $I_t(F)$ refers to the decrease of the Gini impurity before and after node t is split into two sub-nodes according to feature F. The absolute importance of feature $S(F)$ can be defined as the sum of $I_t(F)$ at all nodes split by feature F.

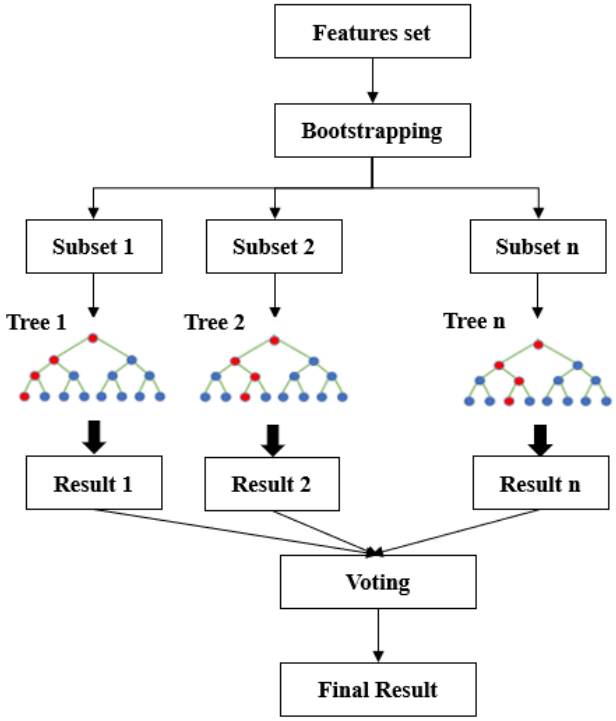

Figure 5.13 The architecture of the random forest

5.5 Results and Discussion

Three improved machine-learning models were developed to classify a group of AE hits using 14 parameters extracted from the Sensor Highway II system. The collected

AE data for a vehicle passing through a bridge in field applications will consist of a group of AE hits, rather than a single AE hit. Hence, the overall goal was to classify a group of AE hits to their corresponding load step.

5.5.1 Performance of BT-ANN

The ANN model was fed with data from the test, which included 30,233 AE hits. AE hits were divided into four data sets, with their corresponding parameters, and labeled as L2, L3, L4, and L5. As input, these data sets were fed into the BT-ANN (balanced training ANN). Prior to training and validation, a randomly selected group of AE hits (200 hits) was taken from each data set for testing. To resolve the imbalance issue, a balanced training data set was developed where 288 different models were trained using even data from each load step. The ANN randomly selected 4/5 of the data for training and 1/5 of the data for validation. Then the models were tested, and each model voted. Most of the votes determined the classification of the AE hits.

The AE hits gathered from the vehicle loads will be a group of AE hits rather than a single AE hit. Therefore, the classification aimed to identify the corresponding load step for each group of AE hits (200 hits). First, a group of AE hits (200 hits) was classified into their corresponding load step based on the maximum number of AE hits assigned to each load step.

Figure 5.14 presents the outputs of the BT-ANN model and the decision-making process when the AE data generated by the vehicle loads are input to the model. For the data caused by L2, the number of AE hits correctly classified to L2 was 94, whereas 46, 21, and 39 were incorrectly classified to L3, L4, and L5, respectively. Since the largest number of hits were classified as L2 for this group of AE hits (200), it can be considered

that the probability of the number of AE hits generated by L2 is the largest. Hence, this group of AE hits was classified correctly into L2.

For the data generated by L3, the number of AE hits accurately assigned to L3 was 85, while 29, 28, and 58 were inaccurately assigned to L2, L4, and L5, respectively. The probability of those AE hits being generated by L3 is the largest in this grouping. Therefore, this group of AE hits (200) was classified accurately into L3. According to the above rules, the AE data generated by L4 is incorrectly classified as L3. The data from L5 is correctly classified as L5. The results show that, except for misclassifying L4 as L3, the BT-ANN model correctly classifies each group of AE hits to its corresponding load step.

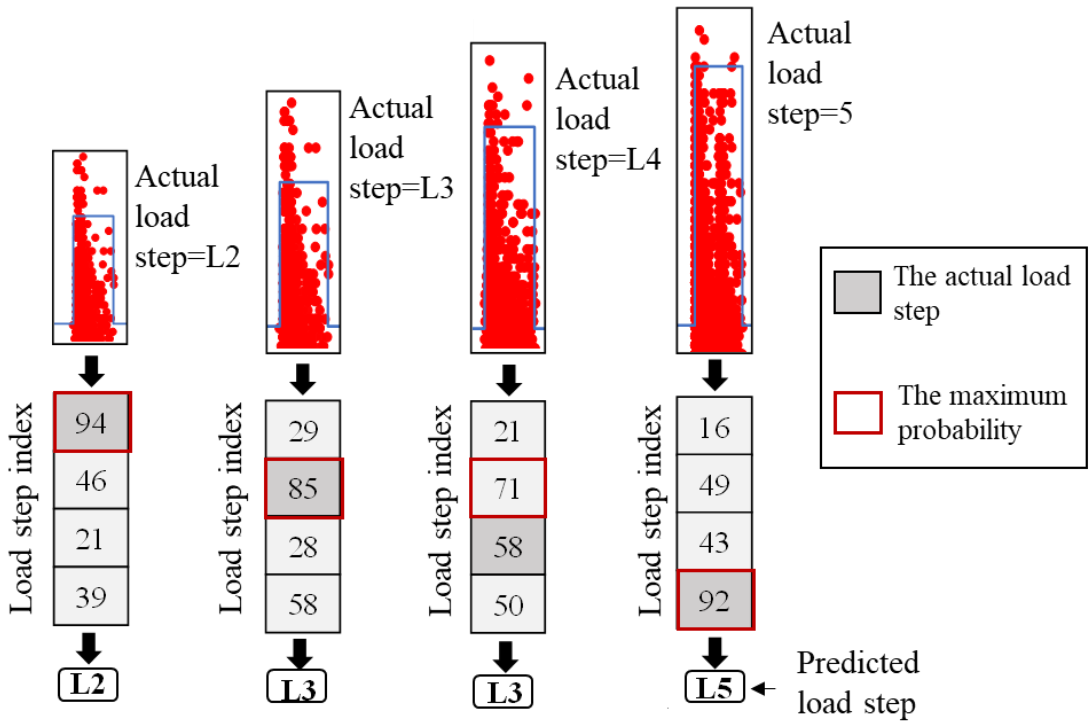

Figure 5.14 Output of BT-ANN

In addition, a scenario was developed to eliminate the randomness in the data selection and determine the model's overall accuracy. One hundred groups of AE hits were randomly selected, and the data was tested on the trained model (BT-ANN). This scenario

was named GTANN (Group Testing on ANN). The final classification (Figure 5.17a) presents the number of groups of AE hits that were assigned to their corresponding load step.

5.5.2 Performance of BT-AdaBoost

Similarly, the AdaBoost model was fed with data from the test. AE hits were separated into four data sets and labeled as L2, L3, L4, and L5. These data sets were the input for the BT-AdaBoost (balanced training AdaBoost). Before training and validation, a group of AE hits (200 hits) was randomly selected from each data set for testing. Even data from each load step was used to train 288 different models to address the imbalance issue. The AdaBoost model randomly selected 4/5 and 1/5 of the data for training and validation, respectively. Next, the models were tested, and each model cast a vote. AE hits were classified based on the majority of the votes.

Following the procedure mentioned in section 5.5.1, the first step was to allocate a group of 200 AE hits to their associated load step based on the maximum number of AE hits allotted to each load step. Figure 5.15 shows the outputs of the BT-AdaBoost model and the decision-making process when the AE caused by the vehicle loads is input to the model. For the data generated by L2, the number of AE hits correctly assigned to L2 was 92, while 19, 43, and 46 were incorrectly assigned to L3, L4, and L5, respectively. The majority of the AE hits were assigned to L2, showing the highest probability that this group of AE hits was correctly correlated to L2. Following the above rules, the AE data caused by L3 and L4 were incorrectly assigned to L5. The data from L5 was correctly assigned to L5. The results indicate that the BT-AdaBoost model correctly classified the group of AE hits belonging to L2 and L5 to their corresponding load step. However, the group of AE hits belonging to L3 and L4 were misclassified to L5.

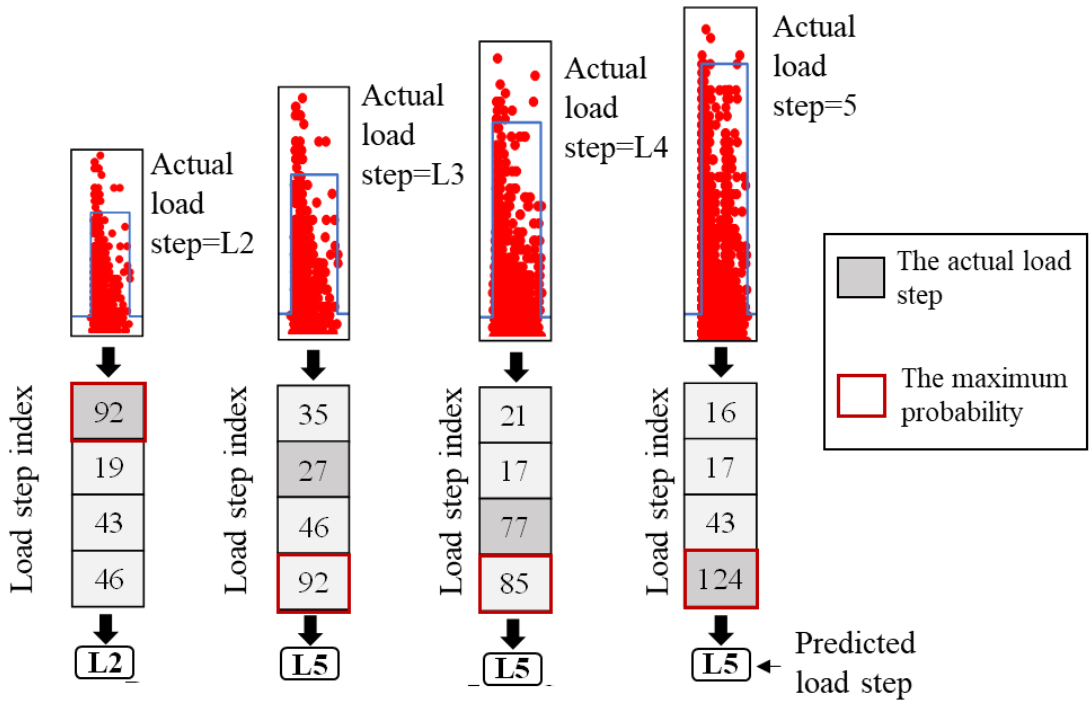

Figure 5.15 Output of BT-AdaBoost

Moreover, a scenario was created to reduce the randomization in data selection and assess the overall reliability of the model. One hundred random samples of group AE hits were chosen, and the data was evaluated on the trained model (BT-AdaBoost). This scenario was called GTAdaBoost (Group Testing on AdaBoost). Figure 5.17b shows the final classification of these groups of AE hits that were allocated to their respective load step.

5.5.3 Performance of BT-RF

A random forest model was developed to compare the results of ANN and AdaBoost models. The data from the test was fed to the BT-RF (balanced training random forest). AE hits were split into four data sets and labeled as L2, L3, L4, and L5. A group of AE hits (200 hits) was randomly selected from each data set for testing prior to training and validation. An equal amount of data from each load step was utilized for training 288

different models to solve the imbalance issue. The random forest model used 4/5 of the data for training and 1/5 for validation. Next, the models were tested, and each model voted on the class of AE hits. The majority of the votes rule was applied to obtain the final classification.

First, a group of AE hits (200 hits) was assigned to their corresponding load step according to the maximum number of hits classified to each load step. Figure 5.16 displays the results of the BT-RF and the decision-making process when the AE data produced by the applied loads are input into the model. For the data produced by L2, the number of AE hits accurately classified to L2 was 112, whereas 48, 21, and 19 were misclassified to L3, L4, and L5, respectively. Since the maximum number of AE hits was allocated to L2 for this group of AE hits, the probability of those AE hits being allocated to L2 is the highest. Thus, this group of AE hits was accurately classified as L2. Following the same decision-making process, the AE data generated by L3, L4, and L5 were correctly classified into L3, L4, and L5, respectively. The results show that the BT-RF model correctly classified each group of AE hits to their corresponding load step.

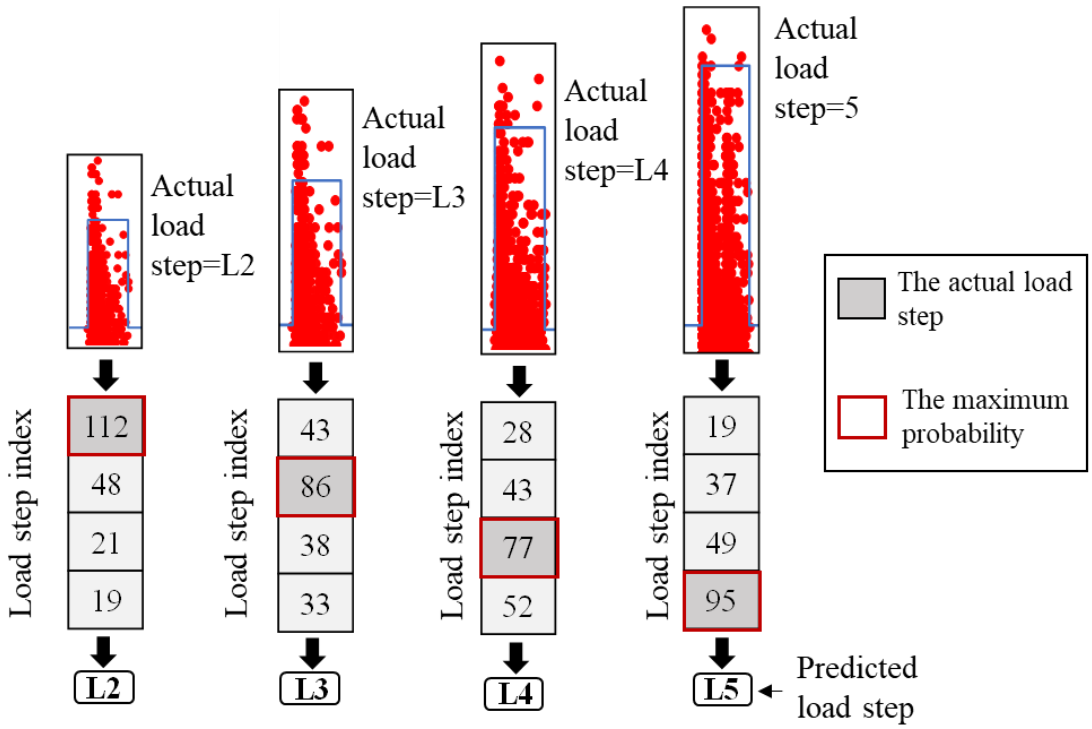

Figure 5.16 Output of BT-random forest

Furthermore, a scenario was designed to decrease randomness in data selection and evaluate the overall credibility of the model. One hundred groups of AE hits were randomly selected, and the data was assessed on the trained model (BT-RF). This scenario was named GTRF (Group Testing on random forest). The final classification in Figure 5.17c depicts how many of these 100 groups of AE hits were assigned to their related load step.

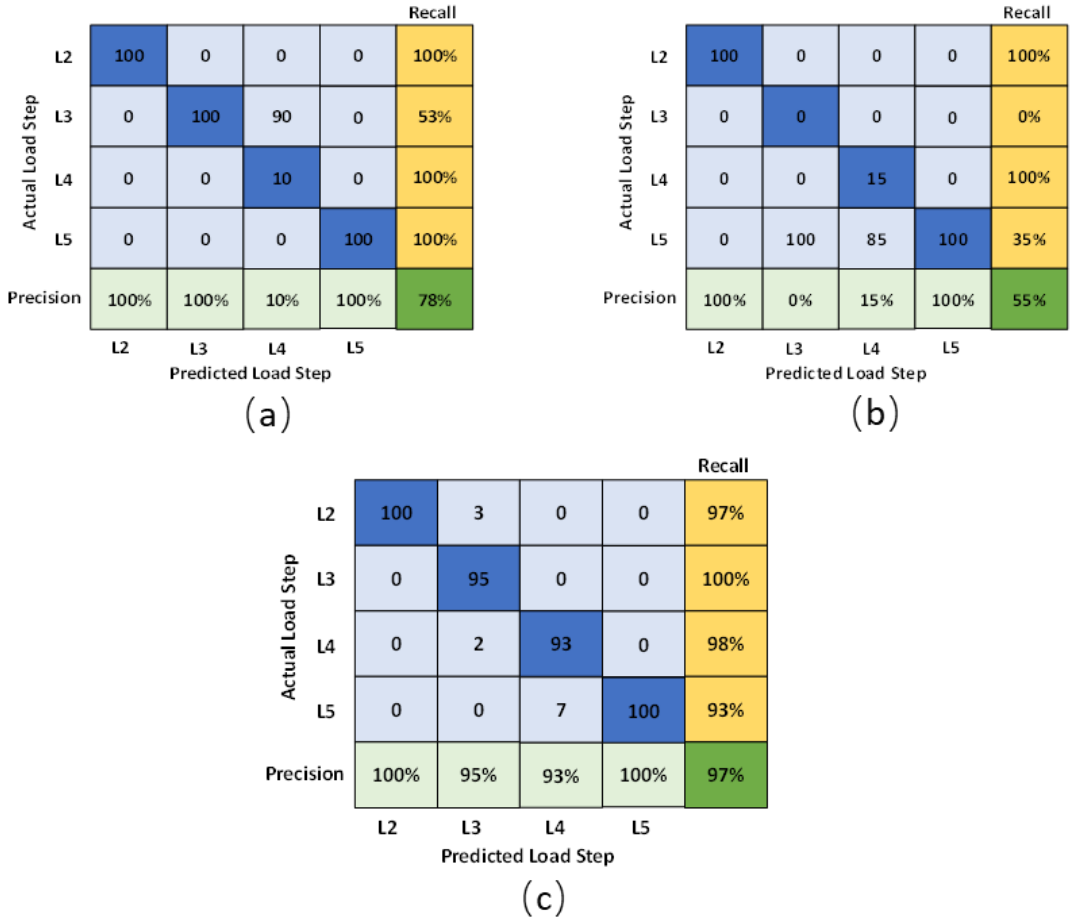

Figure 5.17 The confusion matrixes of (a) GTANN; (b) GTAdaBoost; (c) GTRF

4.5.4 Comparison and discussion

A scenario was designed to assess the accuracy of the three improved machine learning models that were developed to classify a group of AE hits according to their respective load steps. The accuracy value is given by Eq. (14). The accuracies of the classification using three different machine learning algorithms are presented in Table 5.3. The approach using random forest (GT-RF) provides the highest accuracy of 97%, whereas the accuracies by the ANN approach (GT-ANN) and the AdaBoost approach (GT-AdaBoost) are 78% and 55%, respectively.

$$Accuracy = \frac{Number\ of\ correctly\ classified\ groups\ of\ AE\ hits\ in\ the\ test}{Total\ number\ of\ groups\ of\ AE\ hits\ in\ the\ test} \quad (14)$$

Table 5.3 Accuracies of the three algorithms

Machine learning algorithm	Accuracy
GT-ANN	78%
GT-AdaBoost	55%
GT-RF	97%

In addition to accuracy, the performance of the model can be evaluated by calculating the precision, recall, and F1 score of each class [96], [97]. The values of the precision and the recall are obtained by Eqs. (15) and (16), respectively. An F1 score is defined as the harmonic mean of precision and recall [96]. It can be calculated by Eq. (17).

$$Precision = \frac{Number\ of\ correctly\ classified\ groups\ of\ AE\ hits\ in\ the\ load\ step}{Total\ number\ of\ actual\ groups\ of\ AE\ hits\ in\ the\ load\ step} \quad (15)$$

$$Recall = \frac{Number\ of\ correctly\ classified\ groups\ AE\ hits\ in\ the\ load\ step}{Total\ number\ of\ groups\ of\ AE\ hits\ predicted\ in\ the\ load\ step} \quad (16)$$

$$F1\ score = \frac{2\ x\ Precision\ x\ Recall}{Precision + Recall} \quad (17)$$

For the GT-ANN, the precisions of the four load steps are respectively 100%, 100%, 10%, and 100% from L2 to L5. While the recalls are respectively 100%, 100%, 53%, and 100% from L2 to L5. The F1 scores of the four load steps are respectively 100%, 69%, 18%, and 100% from L2 to L5. Moreover, the precisions of the four load steps, L2 to L5, for the GT-AdaBoost are 100%, 0%, 15%, and 100%, respectively. The recalls are respectively 100%, 0%, 100%, and 35% from L2 to L5. The F1 scores are respectively 100%, 0%, 26%, and 58% from L2 to L5. The precision, recall, and F1 score for each load step was calculated for the GT-RF. Precisions of the four load steps are respectively 100%, 95%, 93%, and 100%. Recalls of the four load steps are respectively 97%, 100%, 98%, and 93%. F1 scores of the four load steps are 98.5%, 97.4%, 95.4%, and 96.4%, respectively. Figure 5.18 presents the evaluation of each load step for the three machine learning algorithms.

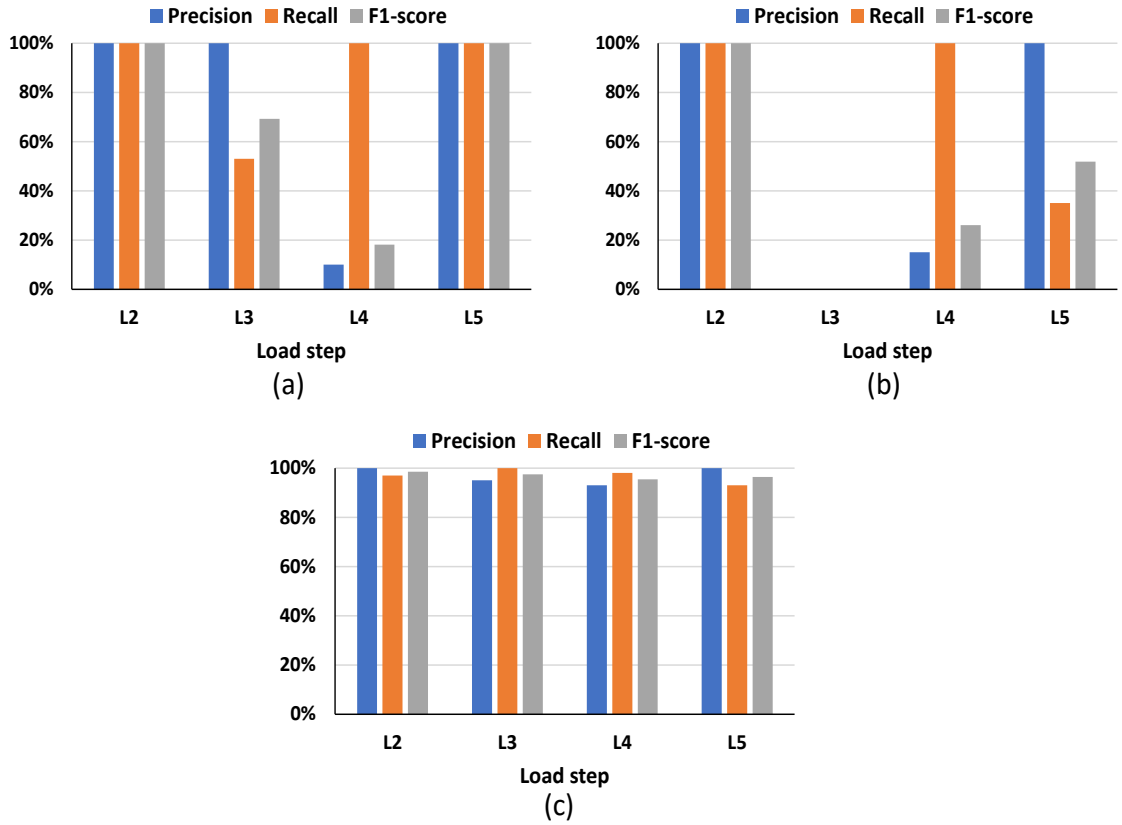

Figure 5.18 Evaluation of load steps (a) GT-ANN; (b) GT-AdaBoost; (c) GT-RF

The F1 scores obtained by the three different machine algorithms are shown in Figure 5.19. It can be observed that the F1 scores of four load steps attained by the ANN and AdaBoost show a wide variety. However, the F1 scores obtained by the random forest are stable. In addition, the F1 scores of random forest are higher than ANN and AdaBoost. Hence, the random forest has the best performance for classifying the AE hits in each load step.

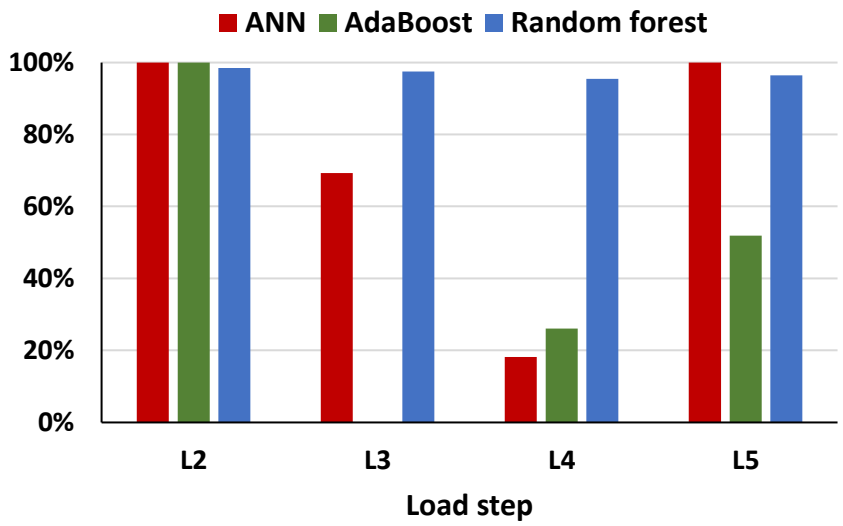

Figure 5.19 Comparison of F1 scores

The performance of the random forest algorithm was better than the ANN and AdaBoost algorithms in classifying the AE hits to their corresponding load steps. One possible explanation could be related to how each machine-learning model deals with outliers. In machine learning, outliers are data points that differ from most of the data points in a data set. Fourteen AE parameters were fed to the machine learning models to classify the data points.

AdaBoost is an ensemble learning method designed to enhance the performance of multiple weak learning models, referred to as decision stumps. During the AdaBoost process, each stump is trained over multiple iterations, resulting in a weighted function. At the end of these iterations, each stump receives a weight. The final classification is determined by a vote from all the stumps, considering their respective weights. AdaBoost can be impacted by outliers. This is due to outliers receiving higher weights in the iterative process, having a more significant impact on the final model. Similarly, ANN can be affected by outliers, potentially leading to poor performance. Outliers can mislead the model during training, causing it to overfit the training data. The model may try to fit the

outliers, resulting in inaccurate weight updates. This will result in poor performance when subjected to the testing data.

On the other hand, random forest is an ensemble learning algorithm, specifically a bagging algorithm. It leverages multiple weak learning models, which are decision trees, to make predictions. The strength of this algorithm lies in the way it determines its final prediction: by averaging the outcomes of these decision trees. This approach helps mitigate the risk associated with individual trees making errors. In addition, random forests consider only a subset of features when constructing each decision tree, which effectively lessens the influence of outliers, resulting in a better classification outcome. This can be demonstrated by the performance of the three machine learning algorithms employed in this study. The robustness of the random forest model in classifying the AE data collected from other girders is presented in Appendix C.

5.6 Conclusions and recommendations

AE data was collected from a flexural test of a prestressed concrete girder. This paper considered three improved machine learning approaches to classify AE hits to their corresponding load steps (theoretical vehicle loads). ANN, AdaBoost, and random forest were used, and their performance was compared. The main conclusions of the paper are summarized as follows:

1. Balanced training for the training data is essential to resolve the imbalance issue when unequal data sets are fed to the machine learning model. Since the machine learning model can be biased in the classification to the largest data set.
2. The performance of the BT-RF algorithm was better than the BT-ANN and BT-AdaBoost algorithms in classifying the AE hits to their corresponding load steps.

The BT-RF had an overall accuracy of 97%, whereas the BT-ANN and BT-AdaBoost models had an accuracy of 78% and 55%, respectively.

3. AE in conjunction with improved random forest may potentially be used to determine the vehicle loads on bridge girders. The F1-scores indicated that the performance of random forest is the best among the three algorithms.

This study is limited to one 30-foot-long prestressed reinforced concrete girder. Since AE sensors depend on the surface properties to which they are attached, more research must be done on other typical structures. In addition, this study is limited to the application of a static load, whereas the vehicle loads are dynamic. Hence, future studies should focus on analyzing AE data acquired from the effects of dynamic loads.

Chapter 6

Summary and Conclusions

6.1 Summary

One specific superstructure type, prestressed skinny-leg girders, was addressed in this study. SCDOT manages several structurally deficient and load-posted prestressed skinny-leg channel girder bridges. The primary goal of this study is to address a particular challenge related to reducing load restrictions on these bridges. In many cases, repairing and strengthening the sections with deficiencies presents a cost-effective and structurally efficient solution. In addition, SCDOT is currently in the process of load rating its inventory of bridges. The load rating is based on the existing structural conditions, as well as the load and traffic conditions. Therefore, there is a need for non-destructive evaluation methods that can evaluate the condition of in-service bridges, provide site-specific traffic data, and perform continuous monitoring in case the bridge conditions change.

In the first study, nine girders obtained from decommissioned bridges in South Carolina were tested under monotonic loading to failure. The test program consisted of six unstrengthened girders, one strengthened with bonded aluminum channels (SE), one strengthened with bonded and bolted aluminum channels (SEB), and one strengthened with bolted aluminum channels (SB). Before testing, a visual inspection of the girders was conducted to identify any existing deterioration, and each girder was given a condition rating based on the SNBI inspection criteria. The results of the tests were presented to evaluate the efficacy of the strengthening methods in enhancing the moment capacity of the girders. In addition, a correlation was established between the moment capacity and the condition rating to evaluate the impact of existing deterioration.

In the second study, six prestressed concrete channel bridge girders, which were originally used in 30-ft span bridges constructed in the 1960s, were subjected to flexural

tests. AE was used to monitor the girders during the tests. The girders were visually inspected prior to testing and each girder was assigned a condition rating based on the SNBI inspection criteria. Intensity analysis charts were developed based on the collected AE data. The charts were utilized to determine the condition factor ($\emptyset_c$) of the girders for load rating applications.

In the third study, AE data was collected from a flexural test of a prestressed concrete girder. Three improved machine learning algorithms based on artificial neural networks (ANN), AdaBoost, and random forest were adopted to classify AE hits to their corresponding load steps (theoretical vehicle loads). In this study, load determination is considered a classification problem. The loading procedure was divided into load steps and the AE signals were classified to their corresponding load steps. The three models were tested, and their performance was compared.

6.2 Conclusions of each study

6.2.1 Full-Scale Experimental Investigation of Prestressed Concrete Channel Bridge Girders Strengthened with Aluminum Alloy Channels

This study aimed to explore strengthening methods for enhancing the performance of prestressed concrete channel girders. To achieve this, nine decommissioned girders were subjected to flexural tests to failure. Prior to the testing, the girders were visually inspected to identify any existing deterioration that might result in reduced moment capacity. Six unstrengthened girders were tested to failure to assess their flexural behavior and serve as a benchmark to compare with the strengthened girders. Additionally, this paper presented an experimental framework that investigated the feasibility and efficacy of utilizing AA

channels as an externally bonded or bolted strengthening method. Based on the experimental findings, the following conclusions can be drawn:

- The measured moment capacities of the girders varied based on the condition rating of each girder, which was determined by the extent of existing deterioration observed through visual inspection. The girders with a condition rating above 6 (good) exhibited measured moment capacities higher than the nominal moment capacity, and the measured moment capacities of girders with a condition rating below 4 (Poor). Additionally, the measured moment capacities of the girder specimens with a condition rating below 4 (Poor) were less than the nominal moment capacity.
- Externally bonding AA channels with epoxy with or without anchorage may serve as strengthening techniques for bridge girders. The strengthened girders exhibited an increase in measured moment capacity of 9% and 15% for SE and SEB, respectively, compared to the unstrengthened girders. However, premature failure occurred due to debonding of AA channels and end bolt rupture for SE and SEB, respectively. Further investigation is needed to assess the debonding failure for aluminum alloys attached with epoxy before actual field implementation.
- Externally anchoring AA channels with bolts was a more convenient method in terms of practicality, easiness, and higher increase in the moment capacity. The strengthened girder (SB) exhibited an increase in measured moment capacity of 33% compared to the unstrengthened girders. In addition, a suitable protective coating should be applied to the steel threaded bolts for field applications.
- The design method in the AASHTO code can be used to accurately estimate the

theoretical moment capacity for the strengthened girder (SB) demonstrated by the results obtained from the calculations which provided a good estimate with a difference of 3% between the calculated and the measured moment capacity.

6.2.2 Condition Assessment of Prestressed Concrete Channel Bridge Girders Using Acoustic Emission and Data-Driven Methods

This study summarizes an effort to use non-destructive evaluation techniques, particularly AE, to evaluate the condition state of prestressed concrete channel bridge girders. Six prestressed concrete channel bridge girders, which were originally used in 30-ft span bridges constructed in the 1960s, were subjected to flexural tests at the University of South Carolina (USC). Acoustic emission was used to monitor the girders during the tests. The girders were visually inspected prior to testing and each girder was assigned a condition rating based on the SNBI condition rating descriptions. The main conclusions of this study are summarized as follows:

- Cumulative signal strength (CSS) can be used as an assessment method to develop the Intensity Analysis design criteria for girders in good condition.
- Intensity analysis developed condition assessment charts may assess the deterioration in the girders in good condition. This can be utilized to determine whether the girders are operating in accordance with the design criteria.
- The charts may also quantify the existing deterioration regardless of the initial condition as seen in the results for the girders in poor condition. In the event that the girders do not meet the design criteria before reaching the required load, this information can be used to update the condition factor ($\emptyset_c$) of the girders for load rating purposes.

6.2.3 An Automated Load Determination System for Bridges Based on Acoustic Emission and Machine Learning Techniques

AE data was collected from a flexural test of a prestressed concrete girder. This paper considered three improved machine learning approaches to classify AE hits to their corresponding load steps (theoretical vehicle loads). ANN, AdaBoost, and random forest were used, and their performance was compared. The main conclusions of the study are summarized as follows:

- Balanced training for the training data is essential to resolve the imbalance issue when unequal data sets are fed to the machine learning model. Since the machine learning model can be biased in the classification to the largest data set.
- The performance of the BT-RF algorithm was better than the BT-ANN and BT-AdaBoost algorithms in classifying the AE hits to their corresponding load steps. The BT-RF had an overall accuracy of 97%, whereas the BT-ANN and BT-AdaBoost models had an accuracy of 78% and 55%, respectively.
- AE in conjunction with improved random forest may potentially be used to determine the vehicle loads on bridge girders. The F1-scores indicated that the performance of random forest is the best among the three algorithms.

6.3 General conclusions

The results of this study align with the established objectives and can be summarized as follows:

- Three strengthening methods were investigated in this study. Externally anchoring AA channels with bolts was a more convenient method in terms of practicality, ease, and higher increase in the moment capacity. The strengthened girder (SB)

exhibited an increase in the measured moment capacity of 33% compared to the unstrengthened girders.

- AE may be used as an SHM technique to evaluate the condition of in-service bridges. Intensity analysis developed condition assessment charts may be used to assess the deterioration in the girders and to determine the condition factor ($\emptyset_c$) of the girders for load rating purposes.
- AE in conjunction with an optimized random forest machine learning model may potentially be used to determine the vehicle loads on prestressed concrete channel bridge girders.

6.4 Recommendations and Future Work

In the first study, the goal was to investigate methods to strengthen the prestressed skinny-leg girder bridges. An experimental framework is presented that investigates the feasibility and efficacy of utilizing AA channels as an externally bonded or bolted strengthening method. Nevertheless, further investigation is needed to assess the debonding failure for aluminum alloys attached with epoxy before actual field implementation. Future studies may be conducted to evaluate the performance of the strengthening methods using bolted aluminum alloy channels on poor condition girders. In addition, a suitable protective coating should be applied to the steel threaded rods for field applications. Improving the reliability of the results could be achieved by conducting more tests on the available girders. Based on the findings of the flexural tests, it is recommended to conduct further assessments on bridges that seem to be in good condition. This additional evaluation is crucial to determine whether these bridges should be posted for load. This recommendation is based on the observation that the measured moment capacity of the

girders in good condition exceeded the calculated moment capacity using plan specified properties.

In the second study, AE was used to perform condition assessment of the prestressed skinny-leg girders during a flexural test in the laboratory. Many of the conclusions and results from this research may potentially be directly applied to structural health monitoring of prestressed skinny-leg girder bridges upon validation. The limits established for the developed AE quantification charts are empirical, necessitating further investigations before employing these methods. Future studies should focus on developing intensity grading criteria for these structures based on field testing. The test data from both field testing and laboratory work will provide a solid basis in understanding field conditions in terms of noise level and required filtering techniques. Moreover, these limits should be verified and established for other typical structures.

In the third study, the objective was to develop a potential approach to predict the vehicle loads that pass over prestressed concrete bridge girders from the collected AE data utilizing a machine learning model. Since AE sensors depend on the surface properties to which they are attached, more research must be done on other typical structures. In addition, this study is limited to the application of a static load, whereas the vehicle loads are dynamic. Hence, future studies should focus on analyzing AE data acquired from the effects of dynamic loads. Based on the findings of the robustness of the model when applied on another girder as detailed in Appendix C, enhancing the performance of the random forest model can be achieved by expanding the training dataset with more diverse and broader data. Future research may explore transfer learning methods for classifying AE data even without historical AE signals for training. Finite element models may be

developed to simulate the stress wave propagation and generate numerical AE signals. These signals could then be utilized to provide the models with a broader and more comprehensive training dataset.

References

[1] G. Hearn, *State Bridge Load Posting Processes and Practices*. Washington, D.C.: Transportation Research Board, 2014. doi: 10.17226/22412.

[2] "Aashto, *AASHTO LRFD Bridge Design Specifications*. 2020.

[3] I. Org/South-Carolina, "SOUTH CAROLINA SECTION OF THE AMERICAN SOCIETY OF CIVIL ENGINEERS", Accessed: Jan. 02, 2023. [Online]. Available: www.infrastructurereportcard.org/south-carolina.

[4] R. S. Gunter, "TigerPrints Structural Evaluation of SCDOT Prestressed Channel Bridges," 2016. [Online]. Available: https://tigerprints.clemson.edu/all_theses

[5] T. Tigerprints and W. Eubanks, "Effect of Transverse Post-Tensioning on Moment Distribution Effect of Transverse Post-Tensioning on Moment Distribution Between Channel Girders Between Channel Girders," 2023. [Online]. Available: https://tigerprints.clemson.edu/all_theses

[6] "Hadzor, T. J., Barnes, R. W., Ziehl, P. H., Xu, J., & Schindler, A. K. (2011). Development of acoustic emission evaluation method for repaired prestressed concrete bridge girders (No. FHWA/ALDOT 930-601-1). Auburn University. Highway Research Center.".

[7] AASHTO. 2018. The manual for bridge evaluation. 3rd ed. Washington, DC: AASHTO.

[8] S. C. Lovejoy, "Acoustic emission testing of beams to simulate SHM of vintage reinforced concrete deck girder highway Bridges," *Struct Health Monit*, vol. 7, no. 4, pp. 329–346, 2008, doi: 10.1177/1475921708090567.

[9] T. Nishikawa, J. Yoshida, T. Sugiyama, and Y. Fujino, "Concrete Crack Detection by Multiple Sequential Image Filtering," *Computer-Aided Civil and Infrastructure Engineering*, vol. 27, no. 1, pp. 29–47, 2012, doi: 10.1111/j.1467-8667.2011.00716.x.

[10] W. Wang and C. Su, "Semi-supervised semantic segmentation network for surface crack detection," *Autom Constr*, vol. 128, 2021, doi: 10.1016/j.autcon.2021.103786.

[11] J. I. Dietrich, M. A. Inkala, and V. J. Männistö, "Bridge inspection quality management," *Transp Res Rec*, no. 1933, 2005, doi: 10.1177/0361198105193300101.

[12] R. Anay, A. Lane, D. V. Jáuregui, B. D. Weldon, V. Soltangharaei, and P. Ziehl, "On-Site Acoustic-Emission Monitoring for a Prestressed Concrete BT-54 AASHTO Girder Bridge," *Journal of Performance of Constructed Facilities*, vol. 34, no. 3, Jun. 2020, doi: 10.1061/(asce)cf.1943-5509.0001440.

[13] R. Anay *et al.*, "On-Site Acoustic-Emission Monitoring for Assessment of a Prestressed Concrete Double-Tee-Beam Bridge without Plans," 2015, doi: 10.1061/(ASCE)CF.1943.

[14] ASTM E1316-16a. (2016). Standard Terminology for Nondestructive Examinations.

[15] N. Uddin, H. Zhao, C. Waldron, L. Dong, and A. Greer, "Weigh-in-Motion (WIM) Data for Site-Specific LRFR Bridge Load Rating," 2011.

[16] R. Hou, S. Jeong, J. P. Lynch, M. M. Ettouney, and K. H. Law, "Data-driven analytical load rating method of bridges using integrated bridge structural response and weigh-in-motion truck data," *Mech Syst Signal Process*, vol. 163, Jan. 2022, doi: 10.1016/j.ymssp.2021.108128.

[17] A. Z. Henderson, "Scholar Commons Scholar Commons Load Rating Evaluation of Deteriorated Prestressed Channel Load Rating Evaluation of Deteriorated Prestressed Channel Girders." [Online]. Available: https://scholarcommons.sc.edu/etd

[18] H. A. Rasheed, J. Abdalla, R. Hawileh, and A. K. Al-Tamimi, "Flexural behavior of reinforced concrete beams strengthened with externally bonded Aluminum Alloy plates," *Eng Struct*, vol. 147, pp. 473–485, Sep. 2017, doi: 10.1016/j.engstruct.2017.05.067.

[19] O. R. Abuodeh, J. A. Abdalla, and R. A. Hawileh, "Flexural strengthening of RC beams using aluminum alloy plates with mechanically-fastened anchorage systems: An experimental investigation," *Eng Struct*, vol. 234, May 2021, doi: 10.1016/j.engstruct.2021.111969.

[20] Z. Zhang, Y. ting Liu, L. zhi Li, and Z. dao Lu, "The use of bolted side aluminum alloy plates for flexural capacity of reinforced concrete beams: An experimental investigation," *Structures*, vol. 42, pp. 417–433, Aug. 2022, doi: 10.1016/j.istruc.2022.05.082.

[21] M. K. Elbatanouny, P. H. Ziehl, A. Larosche, J. Mangual, F. Matta, and A. Nanni, "Acoustic emission monitoring for assessment of prestressed concrete beams," *Constr Build Mater*, vol. 58, pp. 46–53, May 2014, doi: 10.1016/j.conbuildmat.2014.01.100.

[22] R. Anay *et al.*, "On-Site Acoustic-Emission Monitoring for Assessment of a Prestressed Concrete Double-Tee-Beam Bridge without Plans," 2015, doi: 10.1061/(ASCE)CF.1943.

[23] L. K C *et al.*, “Determination of vehicle loads on bridges by acoustic emission and an improved ensemble artificial neural network,” *Constr Build Mater*, vol. 364, Jan. 2023, doi: 10.1016/j.conbuildmat.2022.129844.

[24] “NBI. (2021). National Bridge Inventory. Federal Highway Administration. https://www.fhwa.dot.gov/bridge/nbi/ascii2021.cfm. Accessed 2023”.

[25] J. Aidoo, K. A. Harries, and M. F. Petrou, “Full-Scale Experimental Investigation of Repair of Reinforced Concrete Interstate Bridge Using CFRP Materials”, doi: 10.1061/ASCE1084-0702200611:3350.

[26] S. Aykac, I. Kalkan, B. Aykac, S. Karahan, and S. Kayar, “Strengthening and Repair of Reinforced Concrete Beams Using External Steel Plates,” *Journal of Structural Engineering*, vol. 139, no. 6, pp. 929–939, Jun. 2013, doi: 10.1061/(asce)st.1943-541x.0000714.

[27] Eberline, D. K., Klaiber, F. W., & Dunker, K. (1988). Bridge strengthening with epoxy-bonded steel plates. Transportation Research Record, 1180, 7-11.

[28] Yang, D., Merrill, B. D., & Bradberry, T. E. (2011). Texas’ use of CFRP to repair concrete bridges. Special Publication, 277, 39-57.

[29] E. Ozbek, ∗ Meryem Bocek, and S. Aykac, “Strengthening of RC Beams with Solid Steel Plates,” 2016.

[30] S. Huovinen, “ACTION OF GLUED STEEL PLATES IN STRENGTHENING OF STRUCTURES,” 1996.

[31] B. M. Phares, T. J. Wipf, F. W. Klaiber, A. Abu-Hawash, and Y.-S. Lee, “Strengthening of Steel Girder Bridges Using FRP,” 2003.

[32] D. Yang, B. D. Merrill, and T. E. Bradberry, “Texas’ Use of CFRP to Repair Concrete Bridges.”

[33] J. L. Kasan, A. M. Asce, K. A. Harries, M. Asce, ; Richard Miller, and R. J. Brinkman, “Repair of Prestressed-Concrete Girders Combining Internal Strand Splicing and Externally Bonded CFRP Techniques,” 2014, doi: 10.1061/(ASCE)BE.1943.

[34] W.-W. Wang, J.-G. Dai, and K. A. Harries, “Performance Evaluation of RC Beams Strengthened with an Externally Bonded FRP System under Simulated Vehicle Loads,” *Journal of Bridge Engineering*, vol. 18, no. 1, pp. 76–82, Jan. 2013, doi: 10.1061/(asce)be.1943-5592.0000324.

[35] G. Spadea, F. Bencardino, F. Sorrenti, and R. N. Swamy, “Structural effectiveness of FRP materials in strengthening RC beams,” *Eng Struct*, vol. 99, pp. 631–641, Sep. 2015, doi: 10.1016/j.engstruct.2015.05.021.

[36] J. A. Abdalla, A. R. Abu-Obeidah, and R. A. Hawileh, “Use of aluminum alloy plates as externally bonded shear reinforcement for R/C beams,” in *Procedia Structural Integrity*, Elsevier B.V., 2019, pp. 403–410. doi: 10.1016/j.prostr.2019.08.053.

[37] J. A. Abdalla, A. S. Abu-Obeidah, R. A. Hawileh, and H. A. Rasheed, “Shear strengthening of reinforced concrete beams using externally-bonded aluminum alloy plates: An experimental study,” *Constr Build Mater*, vol. 128, pp. 24–37, Dec. 2016, doi: 10.1016/j.conbuildmat.2016.10.071.

[38] Sika Product Data Sheet. SikaDur®-30. Sika Construction Chemicals; 2020.

[39] ASTM, Standard Method of Test for obtaining and testing drilled cores and sawed beams of concrete, Standard Specifications for Transportation Materials and Methods of Sampling and Testing. 23 (2018).

[40] J.E. Cook, D.J. Akers, W.L. Barringer, F.M. Bartlett, J.L. Brown, A. Graf, J. Parnes, Guide for Obtaining Cores and Interpreting Compressive Strength Results, Society. (2003).

[41] ASTM C617/C617M 12, Standard Practice for Capping Cylindrical Concrete Specimens, ASTM International. 98 (2012).

[42] ASTM C39–21, Standard Test Method for Compressive Strength of Cylindrical Concrete Specimens 1, ASTM Standard Book. i (2021).”.

[43] M. M. Farrar and B. Newton, ‘The AASHTO Manual for Bridge Element Inspection,’ Aspire, 2014.

[44] Federal Highway Administration. (2022). Specifications for the National Bridge Inventory.

[45] T. Omar and M. L. Nehdi, “Condition assessment of reinforced concrete bridges: Current practice and research challenges,” *Infrastructures (Basel)*, vol. 3, no. 3, 2018, doi: 10.3390/infrastructures3030036.

[46] S. Yehia, O. Abudayyeh, S. Nabulsi, and I. Abdelqader, “Detection of Common Defects in Concrete Bridge Decks Using Nondestructive Evaluation Techniques,” *Journal of Bridge Engineering*, vol. 12, no. 2, 2007, doi: 10.1061/(asce)1084-0702(2007)12:2(215).

[47] S. Abdelkhalek and T. Zayed, “Comprehensive Inspection System for Concrete Bridge Deck Application: Current Situation and Future Needs,” *Journal of Performance of Constructed Facilities*, vol. 34, no. 5, 2020, doi: 10.1061/(asce)cf.1943-5509.0001484.

[48] A. M. Abdallah, R. A. Atadero, and M. E. Ozbek, “A State-of-the-Art Review of Bridge Inspection Planning: Current Situation and Future Needs,” *Journal of*

Bridge Engineering, vol. 27, no. 2, 2022, doi: 10.1061/(asce)be.1943-5592.0001812.

[49] M. K. ElBatanouny, A. Larosche, P. Mazzoleni, P. H. Ziehl, F. Matta, and E. Zappa, "Identification of Cracking Mechanisms in Scaled FRP Reinforced Concrete Beams using Acoustic Emission," *Exp Mech*, vol. 54, no. 1, pp. 69–82, Jan. 2014, doi: 10.1007/s11340-012-9692-3.

[50] "Xu, J. G. (2008). Nondestructive evaluation of prestressed concrete structures by means of acoustic emissions monitoring (Doctoral dissertation).".

[51] S. E. Hamdi, A. Le Duff, L. Simon, G. Plantier, A. Sourice, and M. Feuilloy, "Acoustic emission pattern recognition approach based on Hilbert-Huang transform for structural health monitoring in polymer-composite materials," *Applied Acoustics*, vol. 74, no. 5, pp. 746–757, 2013, doi: 10.1016/j.apacoust.2012.11.018.

[52] M. K. El Batanouny, A. Larosche, P. H. Ziehl, and L. Yu, "WIRELESS ACOUSTIC EMISSION MONITORING OF IN SITU DECOMMISSIONING FOR NUCLEAR STRUCTURES."

[53] T. J. Fowler, "The MONPAC system," 1989. [Online]. Available: https://www.researchgate.net/publication/275960110

[54] K. Ono, "Diagnostics of Reinforced Concrete Bridges by Acoustic Emission," 2002. [Online]. Available: https://www.researchgate.net/publication/237207030

[55] R. Anay, A. Lane, D. V. Jáuregui, B. D. Weldon, V. Soltangharaei, and P. Ziehl, "On-Site Acoustic-Emission Monitoring for a Prestressed Concrete BT-54 AASHTO Girder Bridge," *Journal of Performance of Constructed Facilities*, vol. 34, no. 3, Jun. 2020, doi: 10.1061/(asce)cf.1943-5509.0001440.

[56] R. S. Gostautas, A. M. Asce, G. Ramirez, M. Asce, R. J. Peterman, and D. Meggers, "Acoustic Emission Monitoring and Analysis of Glass Fiber-Reinforced Composites Bridge Decks", doi: 10.1061/ASCE1084-0702200510:6713.

[57] A. Nair and C. S. Cai, "Acoustic emission monitoring of bridges: Review and case studies," *Eng Struct*, vol. 32, no. 6, pp. 1704–1714, Jun. 2010, doi: 10.1016/j.engstruct.2010.02.020.

[58] A. I. Dontu, P. D. Barsanescu, L. Andrusca, and N. A. Danila, "Weigh-in-motion sensors and traffic monitoring systems - Sate of the art and development trends," in *IOP Conference Series: Materials Science and Engineering*, IOP Publishing Ltd, Dec. 2020. doi: 10.1088/1757-899X/997/1/012113.

[59] M. Mihaila, P. Barsanescu, and C. Moraras, "Weigh-in-Motion Sensors and Traffic Monitoring Systems. State of the Art and Perspectives," *Bulletin of the*

Polytechnic Institute of Iași. Machine constructions Section, vol. 68, no. 1, pp. 125–146, Mar. 2022, doi: 10.2478/bipcm-2022-0010.

[60] J. Zhu *et al.*, "Online Monitoring System for Concrete Structures Affected by Alkali-Silica Reaction," 2021.

[61] X. Tan, Y. Bao, Q. Zhang, H. Nassif, and G. Chen, "Strain transfer effect in distributed fiber optic sensors under an arbitrary field," *Autom Constr*, vol. 124, Apr. 2021, doi: 10.1016/j.autcon.2021.103597.

[62] X. Tan, P. Guo, X. Zou, and Y. Bao, "Buckling detection and shape reconstruction using strain distributions measured from a distributed fiber optic sensor," *Measurement (Lond)*, vol. 200, Aug. 2022, doi: 10.1016/j.measurement.2022.111625.

[63] P. H. Ziehl, "Applications of acoustic emission evaluation for civil infrastructure," in *Nondestructive Characterization for Composite Materials, Aerospace Engineering, Civil Infrastructure, and Homeland Security 2008*, SPIE, Mar. 2008, p. 69340I. doi: 10.1117/12.779069.

[64] M. K. Elbatanouny, P. H. Ziehl, A. Larosche, J. Mangual, F. Matta, and A. Nanni, "Acoustic emission monitoring for assessment of prestressed concrete beams," *Constr Build Mater*, vol. 58, pp. 46–53, May 2014, doi: 10.1016/j.conbuildmat.2014.01.100.

[65] E. Vandecruys, C. Martens, C. Van Steen, H. Nasser, G. Lombaert, and E. Verstrynge, "Preliminary results on acoustic emission and vibration-based monitoring of locally corroded reinforced concrete beams." [Online]. Available: http://www.ndt.net/?id=27258

[66] R. Worley *et al.*, "Acoustic Emission Sensing for Crack Monitoring in Prefabricated and Prestressed Reinforced Concrete Bridge Girders," 2019, doi: 10.1061/(ASCE)BE.1943.

[67] M. K. ElBatanouny, J. Mangual, P. H. Ziehl, and F. Matta, "Early Corrosion Detection in Prestressed Concrete Girders Using Acoustic Emission," *Journal of Materials in Civil Engineering*, vol. 26, no. 3, pp. 504–511, Mar. 2014, doi: 10.1061/(asce)mt.1943-5533.0000845.

[68] X. Zhou, W. Shan, J. Liu, and J. Li, "Fracture characterization of composite slabs with different connections based on acoustic emission parameters," *Struct Control Health Monit*, vol. 28, no. 4, Apr. 2021, doi: 10.1002/stc.2703.

[69] D. G. Aggelis, S. Verbruggen, E. Tsangouri, T. Tysmans, and D. van Hemelrijck, "Characterization of mechanical performance of concrete beams with external reinforcement by acoustic emission and digital image correlation," *Constr Build Mater*, vol. 47, pp. 1037–1045, 2013, doi: 10.1016/j.conbuildmat.2013.06.005.

[70] N. A. A. S. Bahari *et al.*, “Crack classification in concrete beams using AE parameters,” in *IOP Conference Series: Materials Science and Engineering*, Institute of Physics Publishing, Dec. 2017. doi: 10.1088/1757-899X/271/1/012090.

[71] “ElBatanouny, M. K. (2012). Implementation of acoustic emission as a non-destructive evaluation method for concrete structures (Doctoral dissertation, University of South Carolina).”.

[72] H. Zeng, J. A. Hartell, and M. Soliman, “Damage evaluation of prestressed beams under cyclic loading based on acoustic emission monitoring,” *Constr Build Mater*, vol. 255, Sep. 2020, doi: 10.1016/j.conbuildmat.2020.119235.

[73] R. Worley *et al.*, “Acoustic Emission Sensing for Crack Monitoring in Prefabricated and Prestressed Reinforced Concrete Bridge Girders,” 2019, doi: 10.1061/(ASCE)BE.1943.

[74] G. Ma and Q. Du, “Structural health evaluation of the prestressed concrete using advanced acoustic emission (AE) parameters,” *Constr Build Mater*, vol. 250, Jul. 2020, doi: 10.1016/j.conbuildmat.2020.118860.

[75] V. Soltangharaei, R. Anay, L. Assi, M. Bayat, J. R. Rose, and P. Ziehl, “Analyzing acoustic emission data to identify cracking modes in cement paste using an artificial neural network,” *Constr Build Mater*, vol. 267, Jan. 2021, doi: 10.1016/j.conbuildmat.2020.121047.

[76] K. M. Holford *et al.*, “A new methodology for automating acoustic emission detection of metallic fatigue fractures in highly demanding aerospace environments: An overview,” *Progress in Aerospace Sciences*, vol. 90. Elsevier Ltd, pp. 1–11, Apr. 01, 2017. doi: 10.1016/j.paerosci.2016.11.003.

[77] Jordan, M. I., & Mitchell, T. M. (2015). Machine learning: Trends, perspectives, and prospects. Science, 349(6245), 255-260.

[78] Wang, H., Lei, Z., Zhang, X., Zhou, B., & Peng, J. (2016). Machine learning basics. Deep Learn, 98-164.

[79] A. Nair, C. S. Cai, and X. Kong, “Using Acoustic Emission to Monitor Failure Modes in CFRP-Strengthened Concrete Structures,” *J Aerosp Eng*, vol. 33, no. 1, Jan. 2020, doi: 10.1061/(asce)as.1943-5525.0001106.

[80] A. Li, V. Soltangharaei, P. Ziehl, and M. Van Tooren, “A Smart Impact Detection System for Thermoplastic Aircraft Components based on Acoustic Emission and AdaBoost Algorithm,” 2017.

[81] L. Ai, V. Soltangharaei, M. Bayat, B. Greer, and P. Ziehl, “Source localization on large-scale canisters for used nuclear fuel storage using optimal number of acoustic emission sensors,” *Nuclear Engineering and Design*, vol. 375, Apr. 2021, doi: 10.1016/j.nucengdes.2021.111097.

[82] M. Lydon, S. E. Taylor, D. Robinson, A. Mufti, and E. J. O. Brien, “Recent developments in bridge weigh in motion (B-WIM),” *J Civ Struct Health Monit*, vol. 6, no. 1, pp. 69–81, Feb. 2016, doi: 10.1007/s13349-015-0119-6.

[83] Standard, A. S. T. M. (2017). Standard test method for flexural properties of unreinforced and reinforced plastics and electrical insulating materials by four-point bending, D6272–17. Standard, ASTM.

[84] M. K. Elbatanouny, P. H. Ziehl, A. Larosche, J. Mangual, F. Matta, and A. Nanni, “Acoustic emission monitoring for assessment of prestressed concrete beams,” *Constr Build Mater*, vol. 58, pp. 46–53, May 2014, doi: 10.1016/j.conbuildmat.2014.01.100.

[85] M. K. Elbatanouny, “IMPLEMENTATION OF ACOUSTIC EMISSION AS A NON-DESTRUCTIVE EVALUATION METHOD FOR CONCRETE STRUCTURES.”

[86] B. V Tinkey, T. J. Fowler, and R. E. Klingner, “Nondestructive Testing of Prestressed Bridge Girders with Distributed Damage (FHWA/TX-03/1857-2),” 2002.

[87] R. Anay *et al.*, “On-Site Acoustic-Emission Monitoring for Assessment of a Prestressed Concrete Double-Tee-Beam Bridge without Plans,” 2015, doi: 10.1061/(ASCE)CF.1943.

[88] R. HECHT-NIELSEN, “Theory of the Backpropagation Neural Network,” *Neural Networks for Perception*, pp. 65–93, Jan. 1992, doi: 10.1016/B978-0-12-741252-8.50010-8.

[89] J. Z. Wang, J. J. Wang, Z. G. Zhang, and S. P. Guo, “Forecasting stock indices with back propagation neural network,” *Expert Syst Appl*, vol. 38, no. 11, pp. 14346–14355, Oct. 2011, doi: 10.1016/j.eswa.2011.04.222.

[90] Tsai, C. P., & Lee, T. L. (1999). Back-propagation neural network in tidal-level forecasting. Journal of Waterway, Port, Coastal, and Ocean Engineering, 125(4), 195-202.

[91] R. J. Erb, “Introduction to Backpropagation Neural Network Computation,” *Pharm Res*, vol. 10, no. 2, pp. 165–170, 1993, doi: 10.1023/A:1018966222807.

[92] G. R. ¨ Atsch and K.-R. M. ¨ Uller, “Soft Margins for AdaBoost,” 2001. [Online]. Available: www.first.gmd.de

[93] Schapire, R. E. (2013). Explaining adaboost. In Empirical Inference: Festschrift in Honor of Vladimir N. Vapnik (pp. 37-52). Berlin, Heidelberg: Springer Berlin Heidelberg.

[94] Breiman, L. (2001). Random forests. Machine learning, 45, 5-32.

[95] M. Sandri and P. Zuccolotto, “Variable Selection Using Random Forests,” in *Data Analysis, Classification and the Forward Search*, Springer Berlin Heidelberg, 2007, pp. 263–270. doi: 10.1007/3-540-35978-8_30.

[96] L. Zhong, L. Hu, and H. Zhou, “Deep learning based multi-temporal crop classification,” *Remote Sens Environ*, vol. 221, pp. 430–443, Feb. 2019, doi: 10.1016/j.rse.2018.11.032.

[97] F. Guo, Y. Qian, Y. Wu, Z. Leng, and H. Yu, “Automatic railroad track components inspection using real-time instance segmentation,” *Computer-Aided Civil and Infrastructure Engineering*, vol. 36, no. 3, pp. 362–377, Mar. 2021, doi: 10.1111/mice.12625.

[98] American Concrete Institute. (2021). ACI 562-21."Code Requirements for Assessment, Repair, and Rehabilitation of Existing Concrete Structures".

[99] B. Yan *et al.*, “LOAD TESTING REPORT OF SKINNY LEG CHANNEL BRIDGES ACROSS SOUTH CAROLINA MAJOR CONTRIBUTORS.”

[100] Sika, “Sika® CarboDur® S Carbon fiber laminate for structural strengthening PRODUCT DESCRIPTION,” 2018.

[101] American Concrete Institute. and ACI Committee 440., *Guide for the design and construction of externally bonded FRP systems for strengthening concrete structures*. American Concrete Institute, 2017.

Appendix A - Material Testing Results

A.1 Concrete compression test results:

Drilled concrete cores were extracted from all the girders after testing and tested for their compressive strength. The cylinders were drilled using a core drill and diamond-impregnated drill bit. Concrete cores were obtained in accordance with ASTM C42/ C42M [39] and ACI 214.4R-03 [40], were capped in accordance with ASTM C617 [41], and tested in accordance with ASTM C39/ C39M [42]. However, the dimensions of the cylindrical concrete core specimens were 2 in. diameter by 4 in. long, which does not conform with ASTM C39/ C39M [42] or ACI 214.4R-03 [40]. As the cores were limited to the thickness of the flanges of the girders, which was 5 in. The average compressive strength of the cores was 10,200 psi.

Table A.1 Concrete compression test results

Specimen	Core	Diameter (in.)	Area (in^2)	Ultimate Load (lbs.)	Compressive strength (f_{core}) (psi)	Failure type	Average Compressive strength (f_{core}) (psi)
U1	1	2.090	3.43	32070	9340	3	9900
	2	2.086	3.42	33430	9780	2	
	3	2.084	3.41	35880	10510	2	
U2	1	2.092	3.44	38600	11230	2	10400
	2	2.078	3.39	33600	9910	4	
	3	2.094	3.44	34790	10100	2	
U3	1	2.043	3.28	38650	11790	1	10600
	2	2.041	3.27	37280	11400	2	
	3	2.041	3.27	28260	8640	3	
U4	1	2.043	3.28	34800	10620	1	10600
	2	2.048	3.28	29180	8890	4	
	3	2.043	3.28	40340	12310	1	
U5	1	2.038	3.26	37527	11510	5	10900
	2	2.043	3.27	35640	10880	2	
	3	2.040	3.27	33752	10320	4	
U6	1	2.005	3.16	25960	8220	3	8580
	2	2.013	3.18	28450	8940	2	
SE	1	2.001	3.14	30320	9640	3	10400
	2	2.006	3.16	33530	10600	2	

	3	2.005	3.16	34640	10970	3	
SEB	1	1.998	3.14	30910	9850	3	10200
	2	2.002	3.15	34140	10840	3	
	3	2.005	3.16	31110	9850	2	
SB	1	2.007	3.16	30150	9530	2	9700
	2	2.005	3.16	31120	9850	3	

Notes:
The cores were 2 in. diameter and 4 in. long.
Failure Type: 1) well-formed cones on both ends, 2) well-formed cone with vertical cracks, 3) columnar vertical cracking, 4) diagonal fracture with no cracking, 5) side fracture at top or bottom corners, 6) like type 5 but end of cylinder is pointed. Refer to ASTM C39/ C39M for further clarification.
$\boldsymbol{f_{core}}$ *= Ultimate load / Area*

To determine the equivalent specified strength ($\boldsymbol{f'_{c,eq}}$), equation 6.4.3.1 discussed in ACI 562-21 [98] was used and the results are displayed in Table A.2. The average equivalent specified strength of the girders was 9,100 psi.

Table A.2 Equivalent specified strength results *($f'_{c,eq}$)*

Specimen	Equivalent specified strength ($f'_{c,eq}$)
U1	9,170
U2	9,580
U3	8,770
U4	8,780
U5	10,170
U6	7,480
SE	9,600
SEB	9,300
SB	9,100

Equivalent specified strength ($f'_{c,eq}$) calculations:

$$f_{ceq} = 0.9\, f_c^{-}\, [1 - 1.28\sqrt{\frac{(k_c V)^2}{n} + 0.0015} \quad \text{(A.1)}$$

where:

f_{ceq} = Equivalent specified concrete strength

f_c^{-} = Average core strength after applying modification factors.

k_c = coefficient of variation modification factor

V = coefficient of variation of the core strengths

n = number of cores taken

$$f_c = F_{l/d}\ F_{mc} F_{dia} F_d F_{core} \quad \text{(A.2)}$$

where:

f_c = equivalent in place strength

$F_{l/d}$ = strength correction factor account for the effect of length-to-diameter ratio

F_{mc} = strength correction factor account for the effect of moisture condition of the core

F_{dia} = strength correction factor account for the effect of diameter of the core

F_d = correction factor account for the effect of damage due to drilling

F_{core} = core strength

Table A.3 Calculations of equivalent specified strength ($f'_{c,eq}$)

Specimen	f_{core}(psi)	f_c(psi)	f_c^-(psi)	n	kc	V	$f'_{c,eq}$(psi)
U1	9,340	10,497	11,097	3	1.47	0.06	9,170
	9,780	10,985					
	10,510	11,809					
U2	11,230	12,618	11,698	3	1.47	0.07	9,580
	9,910	11,131					
	10,500	11,344					
U3	11,790	13,247	11,920	3	1.47	0.16	8,770
	11,390	12,803					
	8,640	9,710					
U4	10,620	11,932	11,918	3	1.47	0.16	8,780
	8,890	9,992					
	12,310	13,831					
U5	11,510	12,932	12,250	3	1.47	0.05	10,170
	10,880	12,228					
	10,310	11,591					
U6	8,220	9,233	9,636	2	2.4	0.06	7,480
	8,935	10,039					
SE	9,640	10,830	11,688	3	1.47	0.06	9,600
	10,600	11,914					
	10,970	12,321					
SEB	9,850	11,071	11,327	3	1.47	0.07	9,300
	10,840	12,176					
	9,550	10,730					
SB	9,520	10,702	10,886	2	2.4	0.02	9,100
	9,850	11,070					
*Strength correction factors: $F_{l/d}$=1, F_{mc}=1, F_{dia}=1.06, and F_d= 1.06							

A.2 Prestressing strands ultimate tensile strength test results

Prestressing strands were extracted from specified girders after testing and tested for their tensile ultimate strength at the SCDOT office of materials and research. Uniaxial tensile tests were conducted on 30 in. long specimens. Strands selected for testing were either the lowest strand or second lowest strand (if possible). A total of eight prestressing strands were collected with various levels of corrosion and section loss. Prior to testing, the severity of strand deterioration was visually inspected. Four levels of corrosion deterioration were considered in the assessment based on the conditions of the strands.

Figure A.1 Strands extracted from specimens

Table A.4 Ultimate tensile strength for strands tested.

Girder	Strand location	Ultimate tensile load (P_u)(lbs.)	Ultimate tensile strength*** (ksi)	P_u/ P_{nu}**	Deterioration Index* (DI)	Measured moment capacity (kip-ft)
U2	bottom	23,050	288	1.15	1	202
	one up from bottom	23,100	289	1.16	1	
U3	bottom	14,150	NA	0.71	3	172

	one up from bottom	21,910	274	1.10	1	
U4	bottom	16,760	NA	0.84	2	184
	one up from bottom	23,760	297	1.19	0	
U5	bottom	19,460	NA	0.97	2	166
	one up from bottom	23,800	298	1.19	0	

Notes:
**DI: 0) No corrosion, 1) Light corrosion, 2) Pitting with minor section loss, 3) Heavy Pitting with section loss.*
***$\boldsymbol{P_{nu}}$ is the specified ultimate tensile load based on the specified ultimate tensile strength and the specified area of the prestressing strands. $\boldsymbol{P_{nu}}$= 250,000 * 0.08 = 20,000 lbs.*
**** Ultimate tensile strength = Ultimate load / specified area of prestressing strand*

Appendix B - Calculations

B.1 Nominal moment capacity of the unstrengthened girders based on the specified drawings from SCDOT

Geometrical and reinforcing details (SCDOT drawings):

Concrete:

Specified compressive strength of concrete, f_c' = 5 ksi

Specified compressive strength of concrete at transfer, f_{ci}' = 4 ksi

Channel Properties:

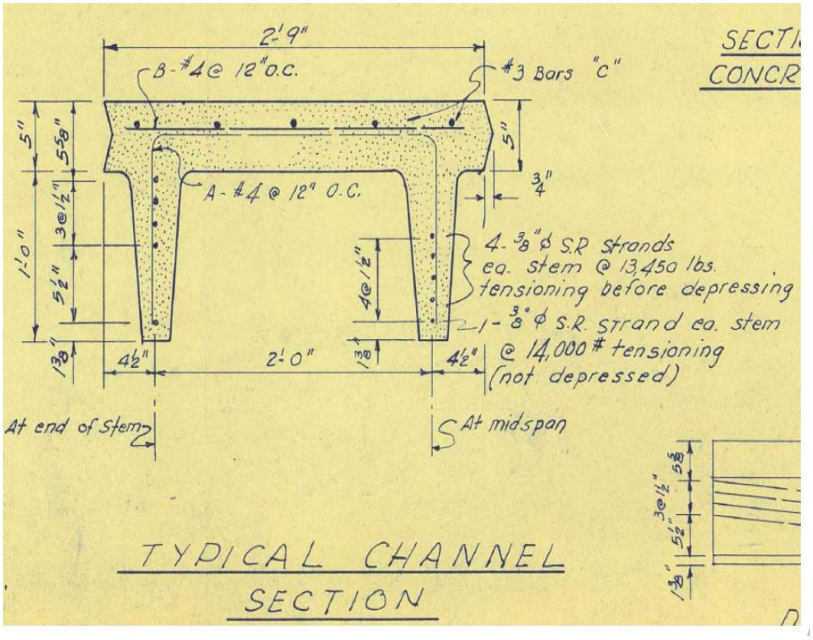

Figure B.1 Typical Channel Cross-Section (SCDOT drawing)

Top flange width, B = 33.0 in.

Flange thickness, t_s = 5.0 in.

Web thickness, t_w = 12.0 in.

Girder thickness, h = 17.0 in.

Bottom web width, b_{wb}= 2.5 in.

Upper web width, b_{wu}= 4.5 in.

Cross-section Area, A_g

A_g = B t_s + 2 ($b_{wb} t_w$) + 4 (0.5 t_w $\frac{b_{wu}-b_{wb}}{2}$)

= 33 x 5 + 2 (2.5 x 12) + 4 (0.5 x 12 x $\frac{4.5-2.5}{2}$) = 249.0 in.^{2}

Distance between centroid of prestressing strands to bottom fiber at midspan, y_{bs} = 4.4 in.

Distance between centroid of prestressing strands to top fiber at midspan, d_{ps} = 12.7 in.

Strands Properties:

Specified area of one strand, A_{Strand} = 0.08 in.^{2}

Number of strands, $n_{strands}$ = 10

Area of prestressing strands, A_{ps} = 10 x 0.08 = 0.8 in.^{2}

Specified ultimate tensile strength of prestressing strands, f_{pu}= 250.0 ksi

Ultimate tensile strength of prestressing strands before transfer, f_{pi}= 0.70 x 250 = 175.0 ksi

Ultimate tensile strength of prestressing strands after transfer, f_{pe}= 0.8 x 175 = 140.0 ksi

Yield strength of prestressing strands, f_{py} = 0.85 x 250 = 212.5 ksi (stress-relieved strands)

Modulus of Elasticity of prestressing strands, E_{ps} = 28500 ksi (stress-relieved strands)

Compression Steel Properties:

Number of bars, n_{bars} = 5

Specified area of one bar (#3), A_s' = 0.11 in.^{2}

Yield strength of bars, f_y' = 40 ksi

Modulus of Elasticity of bars, E_s = 29000 ksi

Cross-Section Properties:

Distance from neutral axis to top fiber, y_{top}

$$y_{top} = \frac{\mathrm{B}\, t_s\left(\frac{t_s}{2}\right) + 2\,(b_{wb}t_w)\left(t_s+\frac{t_w}{2}\right) + 4\left(0.5\, t_w\, \frac{b_{wu}-b_{wb}}{2}\right)\left(t_s+\frac{t_w}{3}\right) + (n_{ps}-1)A_{ps}d_{ps}}{A_g + (n_{ps}-1)A_{ps}}$$

$$= \frac{33 \text{ x } 5 \text{ x } \left(\frac{5}{2}\right) + 2\,(2.5 \text{ x } 12)\left(5+\frac{12}{2}\right) + 4\left(0.5 \text{ x } 12 \text{ x } \frac{4.5-2.5}{2}\right)\left(5+\frac{12}{3}\right) + (6.65-1)(0.8)(12.6)}{249+(6.65-1)(0.8)} = 5.3 \text{ in.}$$

Distance from neutral axis to bottom fiber, y_b

y_b = h - y_{top} = 17 – 5.3 = 11.7 in.

Strands eccentricity at midspan, $e_c = y_b - y_{bs}$ = 11.7 – 4.4 = 7.3 in.

Moment of Inertia, I_g

$$I_g = \frac{\mathrm{B}t_s^3}{12} + \mathrm{B}t_s(y_t - \frac{t_s}{2})^2 + 2\,[\frac{b_{wb}t_w^3}{12} + (b_{wb}t_w)(y_t - t_s - \frac{t_w}{2})^2] + 4\,[\frac{\frac{b_{wu}-b_{wb}}{2}t_w^3}{36} + \left(0.5\, t_w\, \frac{b_{wu}-b_{wb}}{2}\right)(y_t - t_s - \frac{t_w}{3})^2] + (n_{ps}-1)A_{ps}(y_t - d_{ps})^2 = \frac{33\text{x } 5^3}{12} + 33 \text{ x } 5\,(5.3 - \frac{5}{2})^2 + 2\,[\frac{2.5 \text{ x } 12^3}{12} + (2.5)(5.3 - 5 - \frac{12}{2})^2] + 4\,[\frac{\frac{4.5-2.5}{2}x\,12^3}{36} + \left(0.5\,x\,12\,x\,\frac{4.5-2.5}{2}\right)(5.3 - 5 - \frac{12}{3})^2] + (6.65-1)(0.8)(5.3-12.6)^2 = 4824.3 \text{ in.}^4$$

Section modulus for bottom fiber, S_b

$S_b = \frac{I_g}{y_b} = \frac{4824.3}{11.7}$ = 412.6 in.^{3}

Section modulus for top fiber, S_t

$S_t = \frac{I_g}{y_t} = \frac{4824.3}{5.3}$ = 909.0 in.^{3}

Cracking Moment, M_{cr}

Modulus of rupture of concrete, f_r = 7.5 $\sqrt{f_c'}$ = 7.5 $\sqrt{5000}$ = 530.3 psi

$P_{pe} = A_{ps}\, f_{pe}$ = 0.8 x 140 = 112.0 kip

$f_{cpe} = \frac{P_{pe}}{A_g} + \frac{P_{pe}e_c}{S_b} = \frac{112}{249} + \frac{112\,x\,7.3}{412.6}$ = 2.4 ksi

M_{cr} = (f_r + f_{cpe}) S_b = (0.53 + 2.4) x 412.6 x 1/12 = 100.7 kip-ft

AASHTO-define Nominal Strength, M_n

Assumptions:

Plane sections remain plane.

Concrete will not carry tension forces.

Prestressing strands yield.

Concrete crushing occurs at failure and has a usable strain of 0.003 in./in.

K_1 = 2(1.04 - $\frac{f_{py}}{f_{pu}}$) = 2 (1.04 - $\frac{212.5}{250}$) = 0.38

$\beta_1 = 0.85 - (0.05 * \frac{f_c' - 4000}{1000}) = 0.85 - (0.05 * \frac{5000 - 4000}{1000}) = 0.8$

$c = \frac{A_{ps} f_{pu}}{0.85 f_c' \beta_1 B + K_1 A_{ps} \frac{f_{pu}}{d_p}} = \frac{0.8\ x\ 250}{0.85\ x\ 5\ x\ 0.8\ x\ 33 + 0.38\ x\ 0.8\ x \frac{250}{12.6}} = 1.7$ in.

$a = \beta_1\ c$ = 0.8 x 1.7 = 1.4 in.

a = 1.4 in. < t_s = 5 in. "The depth of the equivalent stress block is less than the thickness of the compression flange."

check if compression steel yields.

$\varepsilon_s' = 0.003 \frac{(c - d_s')}{c}$ = 0.003 x $\frac{1.7 - 2.2}{1.7}$ = -8.8 x 10^{-4} in./in.

$\varepsilon_y' = \frac{f_y}{E_s} = \frac{40}{29000}$ = 1.4 x 10^{-3} in./in.

$\varepsilon_s' < \varepsilon_y'$. "Compression steel did not yield."

$f_{ps} = f_{pu} (1 - K_1 \frac{c}{d_p})$ = 250 (1 – 0.38 x $\frac{1.7}{12.6}$) = 238 ksi

$M_n = A_{ps} f_{ps} \left(d_p - \frac{a}{2} \right)$ = 0.8 x 238 (12.7 - $\frac{1.4}{2}$) x 1/12 = 191 kip-ft

B.2 Nominal moment capacity of the strengthened girders based on the specified drawings from SCDOT

Geometrical and reinforcing details:

Two aluminum channels sections (6061 Aluminum Alloy 3 x 0.258 x 1.498 x 300)

Specified yield strength, f_{yA} = 40 ksi

Modulus of Elasticity, E_A = 10000 ksi

Web Height = 3.0 in

Flange Height = 1.5 in

Thickness = 0.3 in

d_{al} (distance between top fiber and c.g. of aluminum channels) = 13.5 in (2" from bottom +1/2 Web Height) (Similar to the test setup)

Area of one aluminum channel, A_{al}= 1.4 in^2

Cross-Section Properties:

Distance from neutral axis to top fiber, y_{top}

$$y_{top} = \frac{\mathrm{B}\, t_s\left(\frac{t_s}{2}\right) + 2\,(b_{wb}t_w)\left(t_s+\frac{t_w}{2}\right) + 4\left(0.5\, t_w\, \frac{b_{wu}-b_{wb}}{2}\right)\left(t_s+\frac{t_w}{3}\right) + (n_{ps}-1)A_{ps}d_{ps} + n_{al}A_{al}d_{al}}{A_g + (n_{ps}-1)A_{ps} + n_{al}A_{al}}$$

$$= \frac{33 \text{ x } 5 \text{ x } \left(\frac{5}{2}\right) + 2\,(2.5 \text{ x } 12)\left(5+\frac{12}{2}\right) + 4\left(0.5 \text{ x } 12 \text{ x } \frac{4.5-2.5}{2}\right)\left(5+\frac{12}{3}\right) + (6.65-1)(0.8)(12.6) + 2.3\, x\, 2\, x\, 1.41\, x\, 13.5}{249 + (6.65-1)(0.8) + 2.3\, x\, 2\, x\, 1.41}$$

y_{top} = 5.5 in.

Distance from neutral axis to bottom fiber, y_b

y_b = h - y_{top} = 17 – 5.5 = 11.5 in.

Strands eccentricity at midspan, $e_c = y_b - y_{bs}$ = 11.5 – 4.4 = 7.1 in.

Moment of Inertia, I_g

$$I_g = \frac{\mathrm{B}t_s^3}{12} + \mathrm{B}t_s(y_t - \frac{t_s}{2})^2 + 2\,[\frac{b_{wb}t_w^3}{12} + (b_{wb}t_w)(y_t - t_s - \frac{t_w}{2})^2] + 4\,[\frac{\frac{b_{wu}-b_{wb}}{2}t_w^3}{36} + \left(0.5\, t_w\, \frac{b_{wu}-b_{wb}}{2}\right)(y_t - t_s - \frac{t_w}{3})^2] + (n_{ps}-1)A_{ps}(y_t - d_{ps})^2 + n_{al}A_{al}(y_t - d_{al})^2 =$$

$$\frac{33\text{x } 5^3}{12} + 33 \text{ x } 5\,(5.5 - \frac{5}{2})^2 + 2\,[\frac{2.5 \text{ x } 12^3}{12} + (2.5)(5.5 - 5 - \frac{12}{2})^2] + 4\,[\frac{\frac{4.5-2.5}{2}\, x\, 12^3}{36} + \left(0.5\, x\, 12\, x\, \frac{4.5-2.5}{2}\right)(5.5 - 5 - \frac{12}{3})^2] + (6.65-1)(0.8)(5.5-12.6)^2 + (2.3)(2\, x\, 1.41)(5.5-13.5)^2 = 5281.5 \text{ in.}^4$$

Section modulus for bottom fiber, S_b

$S_b = \frac{I_g}{y_b} = \frac{5281.5}{11.5}$ = 459.3 in.^{3}

Section modulus for top fiber, S_t

$S_t = \frac{I_g}{y_t} = \frac{5281.5}{5.5}$ = 9060.3 in.^{3}

Cracking Moment, M_{cr}

Modulus of rupture of concrete, f_r = 7.5 $\sqrt{f_c'}$ = 7.5 $\sqrt{5000}$ = 530.3 psi

$P_{pe} = A_{ps}\, f_{pe}$ = 0.8 x 140 = 112.0 kip

$f_{cpe} = \frac{P_{pe}}{A_g} + \frac{P_{pe}e_c}{S_b} = \frac{112}{249} + \frac{112\, x\, 7.1}{459.3}$ = 2.2 ksi

$M_{cr} = (f_r + f_{cpe})\, S_b$ = (0.53 + 2.2) x 459.3 x 1/12 = 103.8 kip-ft

AASHTO-define Nominal Strength, M_n

Assumptions:

Plane sections remain plane.

Perfect bond between aluminum channels and concrete substrate.

Concrete will not carry tension forces.

Aluminum channel sections yield.

Concrete crushing occurs at failure and has a usable strain of 0.003 in./in.

K_1 = 2(1.04 - $\frac{f_{py}}{f_{pu}}$) = 2 (1.04 - $\frac{212.5}{250}$) = 0.38

$\beta_1 = 0.85 - (0.05 * \frac{f'_c - 4000}{1000}) = 0.85 - (0.05 * \frac{5000 - 4000}{1000}) = 0.8$

$c = \frac{A_{ps} f_{pu} + A_s f_y}{0.85 f'_c \beta_1 B + K_1 A_{ps} \frac{f_{pu}}{d_p}} = \frac{0.8\ x\ 250 + 2\ x\ 1.41\ x\ 40}{0.85\ x\ 5\ x\ 0.8\ x\ 33 + 0.38\ x\ 0.8\ x \frac{250}{12.6}} = 2.6$ in.

$a = \beta_1$ c = 0.8 x 2.6 = 2.1 in.

a = 2.1 in. < t_s = 5 in. "The depth of the equivalent stress block is less than the thickness of the compression flange."

check if compression steel yields.

$\varepsilon'_s = 0.003 \frac{(c - d'_s)}{c} = 0.003$ x $\frac{2.6 - 2.2}{2.6} = 5$ x 10^{-4} in./in.

$\varepsilon'_y = \frac{f_y}{E_s} = \frac{40}{29000} = 1.4$ x 10^{-3} in./in.

$\varepsilon'_s < \varepsilon'_y$. "Compression steel did not yield."

check if aluminum channels yield.

$\varepsilon_s = 0.003 \frac{(d_s - c)}{c} = 0.003$ x $\frac{13.5 - 2.6}{2.6} = 0.012$ in./in.

$\varepsilon_y = \frac{f_y}{E_s} = \frac{40}{10000} = 4$ x 10^{-3} in./in.

$\varepsilon_s > \varepsilon_y$ "Aluminum channels yielded."

$f_{ps} = f_{pu} (1 - K_1 \frac{c}{d_p}) = 250 (1 - 0.38$ x $\frac{2.6}{12.6}) = 230$ ksi

$M_n = A_{ps} f_{ps} \left(d_p - \frac{a}{2}\right) + A_s f_y \left(d_s - \frac{a}{2}\right) = 0.8$ x 230 x (12.6 - $\frac{2.1}{2}$) x 1/12 + 2 x 1.41 x 40 (13.5 - $\frac{2.1}{2}$) x 1/12 = 294 kip-ft

% Increase in moment capacity = $\frac{294 - 191}{191}$ x 100 = 54%

Calculation for the bolts

5/8" ASTM A193 Grade B7 Steel threaded rod

$f_{u,bolt} = 125\ ksi$

$shear\ strength\ bolt = 0.563 * fu, bolt = \ 70.3\ ksi$ (AISC C-J3-3)

$d = \frac{5}{8}\ in.$

$Thread\ pitch\ (P) = \frac{length}{n\ \#\ of\ threads} = \frac{1\ in.}{14} = 0.0714\ in.$

$H = P * \frac{\sqrt{3}}{2} = 0.0619\ in.$

$d_{\ minor,bolt} = d_{major,bolt} - \left(2 * \left(\frac{5}{8}\right) * H\right) = 0.548\ in.$

$A_{minor,bolt} = 0.236\ in^2$

$f_{y,channel} = 40\ ksi$

$A_{channel} = 1.41\ in.^2$

To make the channel yield prior to bolt failure, the total force in the channel must be equal to: $F_{channel} = A_{channel}\, f_{y,channel} = 56.4\ kip$

$d = \frac{5}{8}\ in.$

$\#\ bolts = \frac{F_{channel}}{70.3\ ksi * A_{minor,bolt}} = 3.4\ bolts \rightarrow use\ 4\ bolts\ minimum\ in\ each\ shear\ span$

Bearing Stress Check:

$d = \frac{5}{8}\ in.$

$L_{bearing}$ = 3.1 *in.*

Surface Area Bolt in contact with concrete (SA) = $\pi\ d\ L_{bearing}$ = π x $\frac{5}{8}$ x 3.1 = 6.1 in^2

$F_{one,bolt} = \frac{F_{channel}}{4\ bolts} = 14.1\ kips$

$\sigma_{bearing} = \frac{F_{one,bolt}}{SA} = 2.3\ ksi < \emptyset(0.85 f'c) = 0.65\ x\ 0.85\ x\ 5 = 2.76\ ksi$

B.3 Moment capacity (material tested)

A summary of the calculated moment capacities using specified material properties and tested material properties for the girders in good condition is located in Table B.1.

Table B.1 Moment capacity for different material properties

Material Properties	Compressive strength (ksi)	Ultimate tensile strength (ksi)	Calculated moment capacity(M_n) (kip-ft)	M^{*}_{tested}/M_n Specimen U2	M^{**}_{tested}/M_n Specimen U6
Plan Specified	5.0	250	191	1.06	1.2
USC tests	9.1	250	197	1.02	1.16
*Measured moment capacity (M_{tested}) for specimen U2 was 202 kip-ft. ** Measured moment capacity (M_{tested}) for specimen U6 was 227 kip-ft.					

B.4 Load rating of the girders:

The load rating of the girders was carried out to obtain a safe live load capacity of the bridges in their current condition and to evaluate the performance of the strengthened girders. Load rating analyses, using LFR and LRFR methodologies were conducted at the design level for inventory strength. The experimental moment capacities for the girders were used in the calculation of the rating factors.

For the LRFR method, a rating factor was obtained for inventory condition for the maximum live load obtained for a design truck load, HL-93, with a uniform design lane load (0.64 kip/ft). Only one line of wheels was considered in the calculations. This is due to the fact that only one line of wheels could fit on one channel at a time. Accurate live load distribution calculations could not be conducted due to the girders being tested individually and not as a system. Numerous factors can affect live load distribution, like transverse tie rod condition or reflective cracking on the surface. A live load distribution factor of 0.5 was obtained from the research conducted on similar type of prestressed concrete channel bridge by WSP report [99]. The rating factor for each girder was

calculated using Equation (A.1) where capacity is equal to the measured moment capacity from each test.

$$RF = \frac{C-(\gamma_{DC})(DC)-(\gamma_{DW})(DW)-(\gamma_P)(P)}{(\gamma_{LL})(LL+IM)} \quad (B.1)$$

where:

RF = Rating Factor

C = Capacity

DC = Dead load effect due to structural components and attachments

DW = Dead load effect due to wearing surface and utilities.

P = Permanent loads other than dead loads

LL = Live load effect

IM = Dynamic load allowance

γ_{DC} = LRFD load factor for structural components and attachments

γ_{DW} = LRFD load factor for wearing surfaces and utilities.

γ_P = LRFD load factor for permanent loads other than dead loads = 1.0

γ_{LL} = Evaluation live load factor

and for strength limit states:

$$C = \emptyset_c \emptyset_s \emptyset R_n \quad (B.2)$$

$\emptyset_c$ = Condition factor

$\emptyset_s$ = System factor

$\emptyset$ = LRFD resistance factor

R_n = Nominal member resistance

Table B.2 displays the results of the LRFR Strength I load ratings of the girders. The results indicate that the strengthened girder (SB) is the only girder with a rating

factor greater than one. This implies the potential of eliminating load postings requirements for this girder and proves the efficacy of the strengthening approach.

Table B.2 LRFR Strength I design load ratings (inventory)

Specimen	Measured moment capacity (kip-ft)	φ_c	φ_s	C (kip-ft)	γ_{DC}	DC (kip-ft)	γ_{DW}	DW (kip-ft)	γ_{LL}	LL (kip-ft)	IM	Rating Factor
U1	177	NA	NA	177	1.25	22.3	1.50	0	1.75	104	0.33	0.61
U2	202	NA	NA	202	1.25	22.3	1.50	0	1.75	104	0.33	0.72
U3	172	NA	NA	172	1.25	22.3	1.50	0	1.75	104	0.33	0.59
U4	184	NA	NA	184	1.25	22.3	1.50	0	1.75	104	0.33	0.64
U5	166	NA	NA	166	1.25	22.3	1.50	0	1.75	104	0.33	0.57
U6	227	NA	NA	227	1.25	22.3	1.50	0	1.75	104	0.33	0.82
SE	190	NA	NA	190	1.25	22.3	1.50	0	1.75	104	0.33	0.66
SEB	246	NA	NA	246	1.25	22.3	1.50	0	1.75	104	0.33	0.90
SB	285	NA	NA	285	1.25	22.3	1.50	0	1.75	104	0.33	1.05

For the LFR method, a rating factor was obtained for inventory condition for the maximum live load obtained for a design truck load, HS20-44. Only one line of wheels was considered in the calculations. This is because only one line of wheels could fit on one channel at a time. Accurate live load distribution calculations could not be conducted due to the girders being tested individually and not as a system. Several factors can affect live load distribution, like transverse tie rod condition or reflective cracking on the surface. A live load distribution factor of 0.5 was obtained from the research conducted on similar type of prestressed concrete channel bridge by WSP report [99]. The rating factor for each girder was calculated using Equation (B.3) where capacity is equal to the measured moment capacity from each test.

$$\mathrm{RF} = \frac{\mathrm{C} - A_1\,\mathrm{D}}{A_2\,(\mathrm{L})(1+\mathrm{I})} \qquad \text{(B.3)}$$

where:

RF = Rating Factor

C = Capacity (ASD)

D = Dead load effect due to structural components and attachments

LL = Live load effect

I = Dynamic load allowance

A_1= Factor for dead loads

A_2= Factor for live loads

Table B.3 displays the results of the LFR design load ratings of the girders. The results indicate that girders U6, SEB, and SB have higher rating factor than one.

Table B.3 LFR design load ratings (inventory)

Specimen	Measured moment capacity (kip-ft)	C (kip-ft)	A1	D (kip-ft)	A2	LL (kip-ft)	I	Rating Factor
U1	177	177	1.3	22.3	2.17	65	0.33	0.75
U2	202	202	1.3	22.3	2.17	65	0.33	0.88
U3	172	172	1.3	22.3	2.17	65	0.33	0.73
U4	184	184	1.3	22.3	2.17	65	0.33	0.79
U5	166	166	1.3	22.3	2.17	65	0.33	0.70
U6	227	227	1.3	22.3	2.17	65	0.33	1.00
SE	190	190	1.3	22.3	2.17	65	0.33	0.82
SEB	246	246	1.3	22.3	2.17	65	0.33	1.10
SB	285	285	1.3	22.3	2.17	65	0.33	1.30

B.5 Nominal capacity of the girders strengthened with fiber reinforced polymers (FRP) (SikaCarboDur S 812):

Material Properties

SikaCarboDur S (812) [100] :

F^*_{fu} = 406 ksi, ε^*_{fu} = 0.0169 in/in, E_f = 23200 ksi, w = 3.15 in, and t = 0.0472 in.

Calculations (ACI 440.2R-17) [101]

Step 1:

$f_{fu} = c_e \times f^*_{fu} = 0.85 \times 406 = 345.1$ *ksi*

$\varepsilon_{fu} = c_e \times \varepsilon^*_{fu} = 0.85 \times 0.0169 = 0.0144$ *in./in.*

Step 2:

E_c = 33000 x $\gamma_c^{1.5}$ x $\sqrt{f_c'}$ = 33000 x $0.15^{1.5}$ x $\sqrt{5}$ = 4287 ksi

ε_{fu} = c_e x ε_{fu}^* = 0.85 x 0.0169 = 0.0144 in./in.

β_1 = 1.05 – 0.05 x f_c' = 1.05 – 0.05 x 5 = 0.8

A_{ps} = n x A_{str} = 10 x 0.08 = 0.8 in^2

A_f = no of strips x t_f x w_f = 2 x 0.0472 x 3.15 = 0.2974 in^2

A_c = 249 in^2

y_t = 5.17 in

I_g = 4823.4 in^4

r = 4.4 in

$\varepsilon_{pe} = \frac{f_{pe}}{E_p} = \frac{140}{28500}$ = 0.00491 in./in.

P_e = f_{pe} x A_{ps} = 140 x 0.8 = 112 ksi

e_c = 7.45 in

y_b = 11.83 in

d_p = 12.625 in

d_f = 13.5 in

$M_{D.L.}$ = 22.3 kip. ft

Step 3:

$\varepsilon_{bi} = \frac{-P_e}{E_c A_c}\left(1 + \frac{e\, y_b}{r^2}\right) + \frac{M_{D.L.}\, y_b}{E_c\, I_g} = \frac{-112}{4287\ x\ 249}\ x\ \left(1 + \frac{7.45\ x\ 11.83}{4.4^2}\right) + \frac{22.3\ x\ 12\ x\ 11.83}{4287\ x\ 4823.4}$ = -0.0004 in./in.

Step 4:

$\varepsilon_{fd} = 0.083\sqrt{\frac{f_c'}{n_f E_f t_f}} = 0.083\ x\ \sqrt{\frac{5}{1\ x\ 23200\ x\ 0.0472}}$ = 0.00561 in./in.

ε_{fu} = 0.0144 in./in.

Check: $\varepsilon_{fd} < 0.9\ x\ \varepsilon_{fu}$

0.00561 in./in. < 0.9 x 0.0144 = 0.0129 in./in.

Step 5:

c_{est} = 2.57 in.

Step 6:

ε_{fe} = 0.003 ($\frac{d_f - c}{c}$) - ε_{bi} = 0.003 ($\frac{13.5-2.57}{2.57}$) – 0.0004 = 0.013 in./in.

$\varepsilon_{fd} < \varepsilon_{fe}$, 0.00561 < 0.013 "Failure is governed by debonding."

$\varepsilon_{fe} = \varepsilon_{fd}$ = 0.00561 in./in.

Step 7:

$\varepsilon_{pnet} = (\varepsilon_{fe} + \varepsilon_{bi}) (\frac{d_p - c}{d_f - c}) = (0.00561 + 0.0004) (\frac{12.625-2.57}{13.5-2.57}) = 0.005$ in./in.

$\varepsilon_{ps} = \varepsilon_{pe} + \varepsilon_{pnet} + = \frac{P_e}{E_c A_c} (1 + \frac{e^2}{r^2}) = 0.00491 + 0.00508 + \frac{112}{4287 \ x \ 249} x (1 + \frac{7.45^2}{4.4^2}) =$ 0.0108 in./in.

Check $\varepsilon_{ps} < \varepsilon_{pu}$

ε_{ps} = 0.0108 in./in. < 0.035 in./in.

Step 8:

for ε_{ps} = 0.0104 in./in. > 0.0076 in./in.

$f_{ps} = 250 - \frac{0.04}{\varepsilon_{ps} - 0.0064} = 250 - \frac{0.04}{0.0108 - 0.0064} = 241$ ksi

$f_{fe} = E_f \ \varepsilon_{fe} = 23200 \ x \ 0.00561 = 130$ ksi

Step 9:

$\varepsilon_c = (\varepsilon_{fe} + \varepsilon_{bi}) (\frac{c}{d_f - c}) = (0.00561 + 0.00039) (\frac{2.57}{13.5-2.57}) = 0.0014$ in./in.

$\varepsilon_c' = \frac{1.7 \ f_c'}{E_c} = \frac{1.7 \ x \ 5}{4287} = 0.002$ in./in.

$\beta_1 = \frac{4\varepsilon_c' - \varepsilon_c}{6\varepsilon_c' - 2\varepsilon_c} = \frac{4 \ x \ 0.002 - 0.0014}{6 \ x \ 0.002 - 2 \ x \ 0.0014} = 0.72$

$\alpha_1 = \frac{3\varepsilon_c'\varepsilon_c - \varepsilon_c \ \varepsilon_c}{3\beta_1 \ \varepsilon_c'^2} = \frac{3 \ x \ 0.002 \ x \ 0.0014 - 0.0014 \ x \ 0.0014}{3 \ x \ 0.72 x \ 0.002 \ x \ \ 0.002} = 0.75$

Step 10:

$c = \frac{A_{ps} f_{ps} + A_f f_{fe}}{\alpha_1 \beta_1 f_c' b} = \frac{0.8 \ x \ 241 + 0.2974 \ x \ 130}{0.75 \ x \ 0.72 \ \ x \ 5 \ x \ 33} = 2.57$ in

Step 11:

$M_{np} = A_{ps} f_{ps} (d_p - 0.5 \ x \ \beta_1 \ x \ c) = 0.8 \ x \ 241 \ x \ (12.625 – 0.5 \ x \ 0.72 \ x \ 2.57) \ x \ 1/12 = 188$ kip-ft

M_{nf} = Ψ$A_f f_{fe}$ (d_f - 0.5 x β_1 x c) = 0.85 x 0.2974 x 130 x (13.5 – 0.5 x 0.72 x 2.653) x 1/12 = 34.5 kip-ft

$M_n = M_{np} + M_{nf}$ = 188 + 34.5 = 222.5 kip. ft

Step 12:

Unstrengthened moment capacity = 188.0 kip. ft

Strengthened moment capacity = 222.5 kip. ft

% Increase in moment capacity = 18 %

Step 13:

For ε_{ps} < 0.010, Φ = 0.75

For ε_{ps} > 0.013, Φ = 1

For ε_{ps} = 0.0104

$\Phi = 0.75 + \frac{0.25\ (\varepsilon_{ps} - 0.010)}{0.013 - 0.010} = 0.75 + \frac{0.25\ (0.0104 - 0.010)}{0.013 - 0.010} = 0.78$

B.6 Cost of aluminum channels and FRP (SikaCarboDur S 812):

Table B.4 presents the materials cost for the strengthening of each girder in the laboratory. Two strengthening materials were investigated aluminum channels and FRP-pultruded strips, to compare the cost of the materials. Table A.7 presents the reason aluminum channels were chosen as the strengthening approach investigated in this study in oppose to FRP-pultruded strips. The price of the aluminum channels was acquired from Xometry Supplies. The cost of the FRP-pultruded strips was acquired from Ram Tool Construction Supply Co. It is worth noting that these materials were acquired in 2022.

Table B.4 Materials cost for strengthening of the girders.

Material	Cost ($/ft)	Total cost for each girder ($)	% Increase in moment capacity**
Aluminum Channel (6061-T6 CH3X258)	7.4	370*	56
FRP (SikaCarboDur S 812)	34	1700*	18

*The total length required to strengthen each girder is 50 ft.
** The increase in nominal moment capacity of strengthened girder with respect to the nominal moment capacity of unstrengthened girder.

B.7 Strain vs time graphs for aluminum channels for girders SEB and SB:

The following graphs present the recorded strain at midspan for the aluminum channels for girders SEB and SB. One strain gauge was attached to each aluminum channel at midspan of each girder.

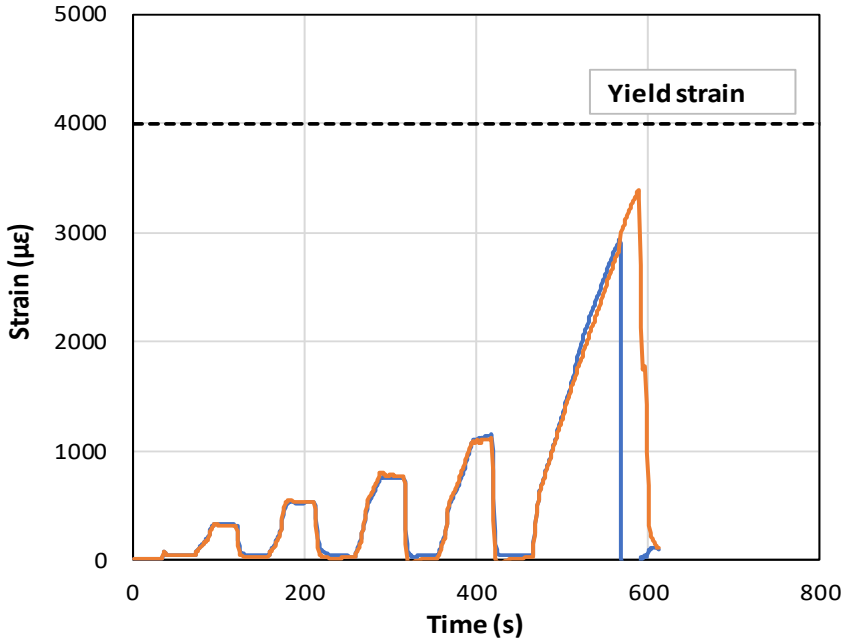

Figure B.2 Strain versus time for aluminum channels at midspan for girder (SEB)

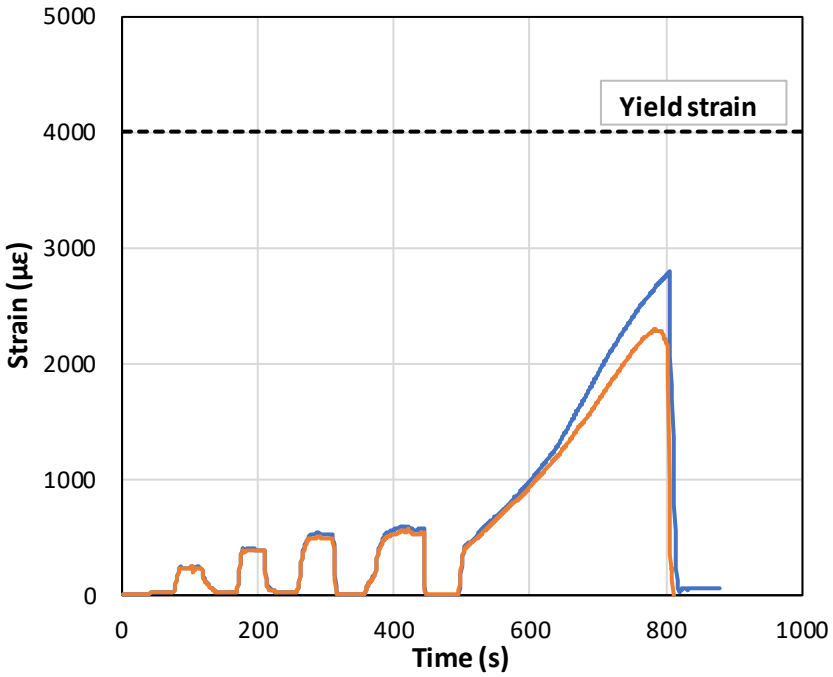

Figure B.3 Strain versus time for aluminum channels at midspan for girder (SB)

Appendix C - Machine Learning Models

C.1 Support Vector Machine (SVM)

The SVM model (Fine Gaussian SVM) was fed with data from the test, which included 30,233 AE hits. AE hits were divided into four data sets, and labeled as L2, L3, L4, and L5. As input, these data sets were fed into the BT-SVM (balanced training SVM). Prior to training and validation, a randomly selected group of AE hits (200 hits) was taken from each data set for testing. Even data from each load step was used to train 288 different models to address the imbalance issue. The SVM model randomly selected 4/5 and 1/5 of the data for training and validation, respectively. Next, the models were tested, and each model cast a vote. AE hits were classified based on the majority of the votes.

First, a group of AE hits (200 hits) was assigned to their corresponding load step according to the maximum number of hits classified to each load step. Figure C.1 displays the results of the BT-SVM and the decision-making process when the AE data produced by the applied loads are input into the model. For the data produced by L2, the number of AE hits accurately classified to L2 was 118, whereas 38, 26, and 18 were misclassified to L3, L4, and L5, respectively. Since the maximum number of AE hits was allocated to L2 for this group of AE hits, the probability of those AE hits being allocated to L2 is the highest. Thus, this group of AE hits was accurately classified as L2. Following the same decision-making process, the AE data generated by L3, L4, and L5 were correctly classified into L3, L4, and L5, respectively. The results show that the BT-SVM model correctly classified each group of AE hits to their corresponding load step.

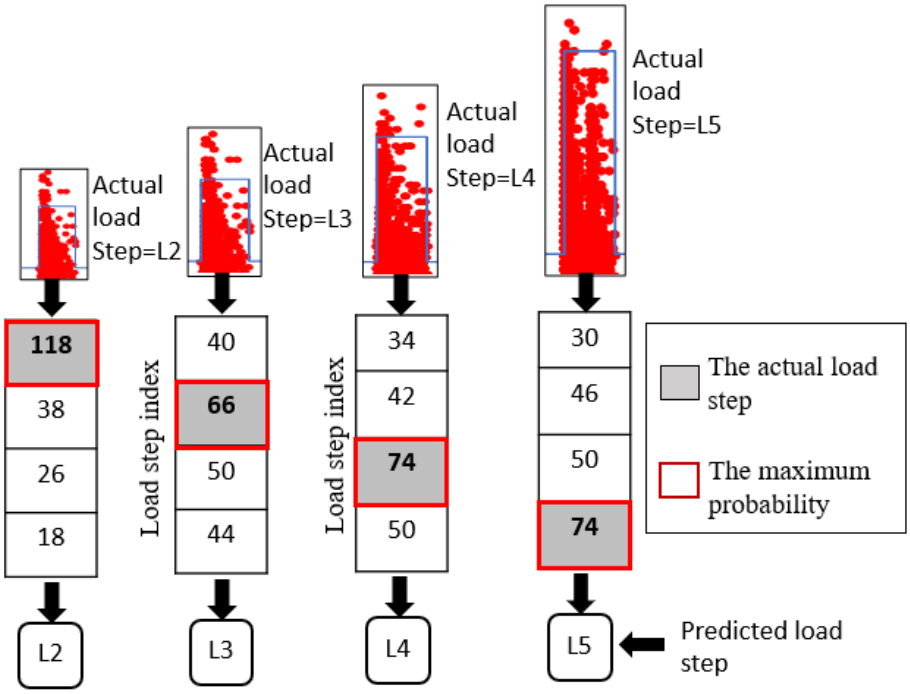

Figure C.1 Output of BT-SVM

Random forest and support vector machine algorithms correctly classified the group of AE hits to their corresponding load steps. Figure C.2 displays the maximum probability computed from BT-RF and BT-SVM. It is evident that the maximum probability for the random forest (BT-RF) is higher than (BT-SVM) in classifying the group of AE hits to their corresponding load step. Although BT-SVM correctly classified the group of AE hits to their corresponding load step, BT-RF is more reliable.

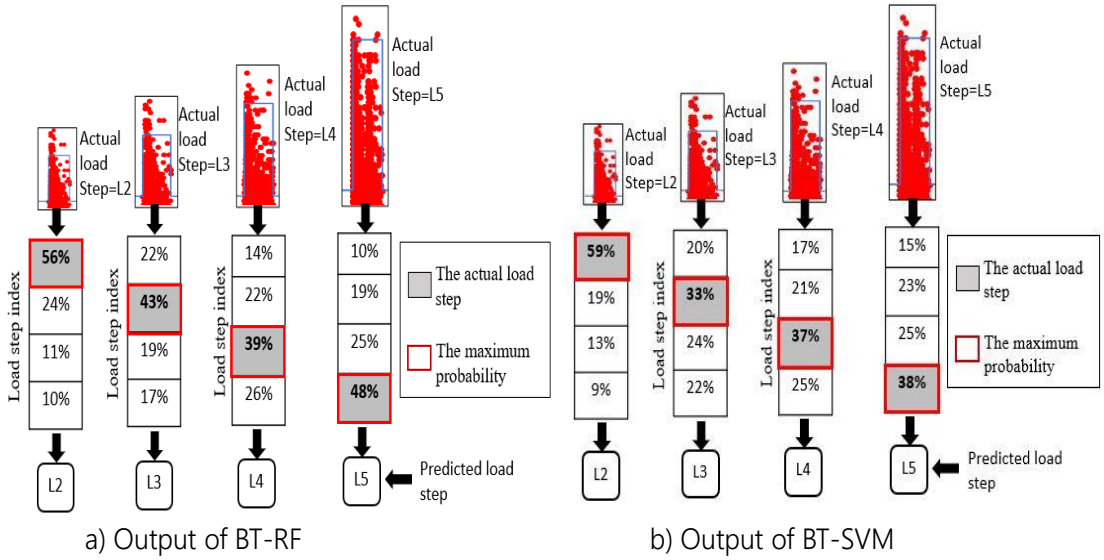

Figure C.2 The maximum probability a) BT-RF; b) BT-SVM

C.2 Robustness of the random forest model

The performance of random forest algorithm was better than the artificial neural network (ANN) and AdaBoost algorithms in classifying the AE hits to their corresponding load steps. Three different scenarios were employed to evaluate the performance of the model when tested on data from another girder. First, the random forest algorithm was trained on the AE data collected from five different girders (U1, U2, U3, U4, and U5) and tested on the AE data collected from another girder (U6). Figure C.3 presents the results of the classification of the AE hits. For the data produced by L2, the number of AE hits accurately classified to L2 was 158, whereas 38, 2, and 0 were misclassified to L3, L4, and L5, respectively. Since the maximum number of AE hits was allocated to L2 for this group of AE hits, the probability of those AE hits being allocated to L2 is the highest. Thus, this group of AE hits was accurately classified as L2. Following the same decision-making process, the AE data generated by L3 and L4 were misclassified into L2. In addition, the AE data generated by L5 was correctly classified into L5.

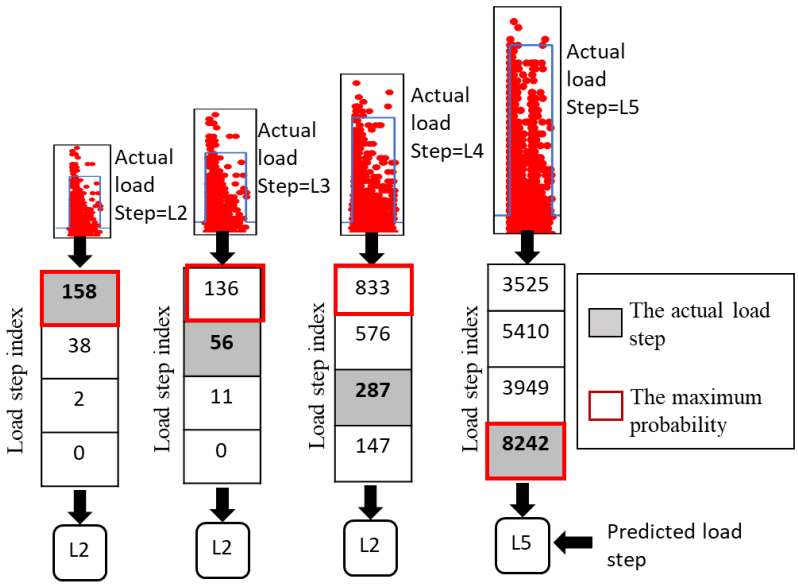

Figure C.3 Output of random forest trained on data from five girders and tested on another girder

Second, the random forest algorithm was trained on the AE data collected from eight different girders (U1, U2, U3, U4, U5, SE, SEB, and SB) and tested on the AE data collected from another girder (U6). Figure C.4 presents the results of the classification of the AE hits. For the data produced by L2, the number of AE hits accurately classified to L2 was 170, whereas 16, 11, and 1 were misclassified to L3, L4, and L5, respectively. Since the maximum number of AE hits was allocated to L2 for this group of AE hits, the probability of those AE hits being allocated to L2 is the highest. Thus, this group of AE hits was accurately classified as L2. Following the same decision-making process, the AE data generated by L4 and L5 were correctly classified into L4 and L5, respectively. In addition, the AE data generated by L3 was incorrectly classified into L2. The results show that increasing the training data of the model provided a better performance for the model to classify AE hits to their corresponding load steps. Hence, a broader and more diverse data set is required to attain further enhancements in performance on different girders.

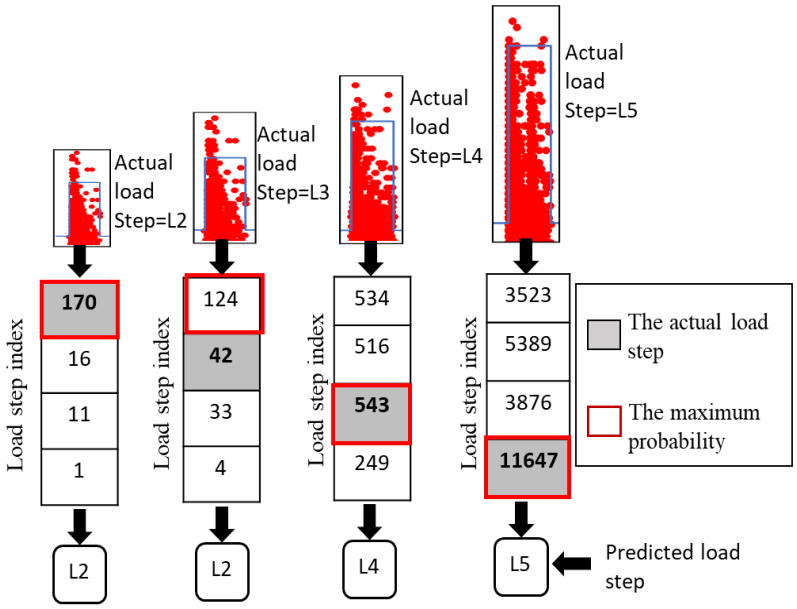

Figure C.4 Output of random forest trained on data from eight girders

Third, the random forest algorithm was trained on the AE data collected from nine different girders (U1, U2, U3, U4, U5, U6, SE, SEB, and SB) and tested on the AE data collected from a random sample from all the girders. Figure C.5 presents the results of the classification of the AE hits. Following the same decision-making process, the AE data generated by L2, L3, L4, and L5 were correctly classified into L2, L3, L4, and L5, respectively. The results show that including representative training data from each girder for the model can help to increase the performance of the model. The model correctly classified the AE hits to their corresponding load steps.

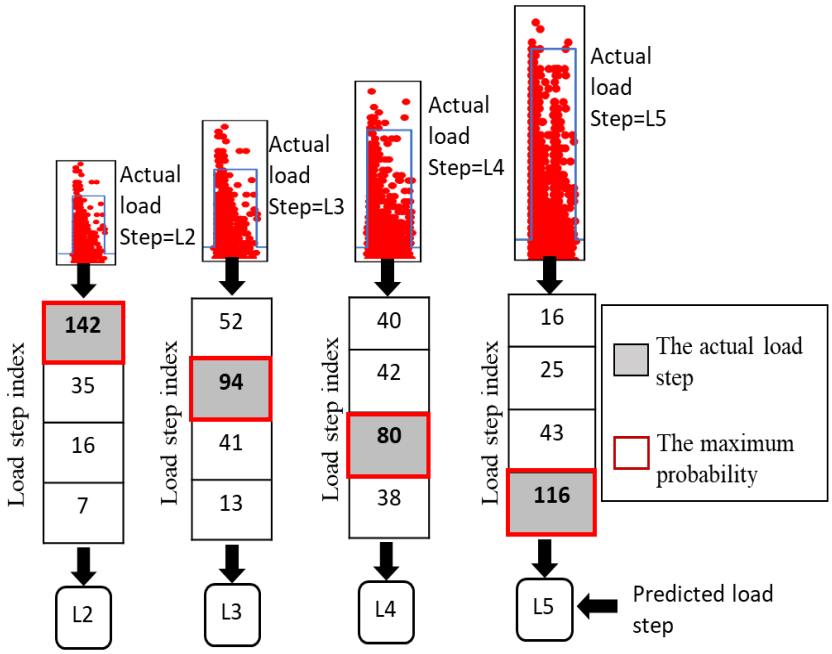

Figure C.5 Output of random forest trained on data from nine girders and tested on random sample

Appendix D - Condition Assessment

D.1 Intensity Analysis

Intensity Analysis was conducted on all the girders utilizing Equations 4.1.a and 4.1.b. The analysis was performed using AE data collected during the loading phases of tests only. The data points for intensity analysis were computed as the maximum historic index and maximum severity recorded during each load step. The intensity analysis chart for the girders in good condition is shown in Figure D.1. Data points in this chart are presented with respect to the theoretical cracking load; therefore, eight different labels are used to show data before and after the theoretical cracking load in the four girders in good condition. For instance, the closed circle is for data points before the theoretical cracking load in girder U6 while the opened circle is for after the theoretical cracking load for the same girder. In accordance with the design criteria for Class U prestressed members, which do not allow cracking, the initiation of cracks was used to determine failure. As depicted in Figure D.1, the intensity analysis distinguishes between data points calculated before and after reaching the theoretical cracking load. The area in the intensity analysis chart where the girders are within the design criteria (did not crack) was determined.

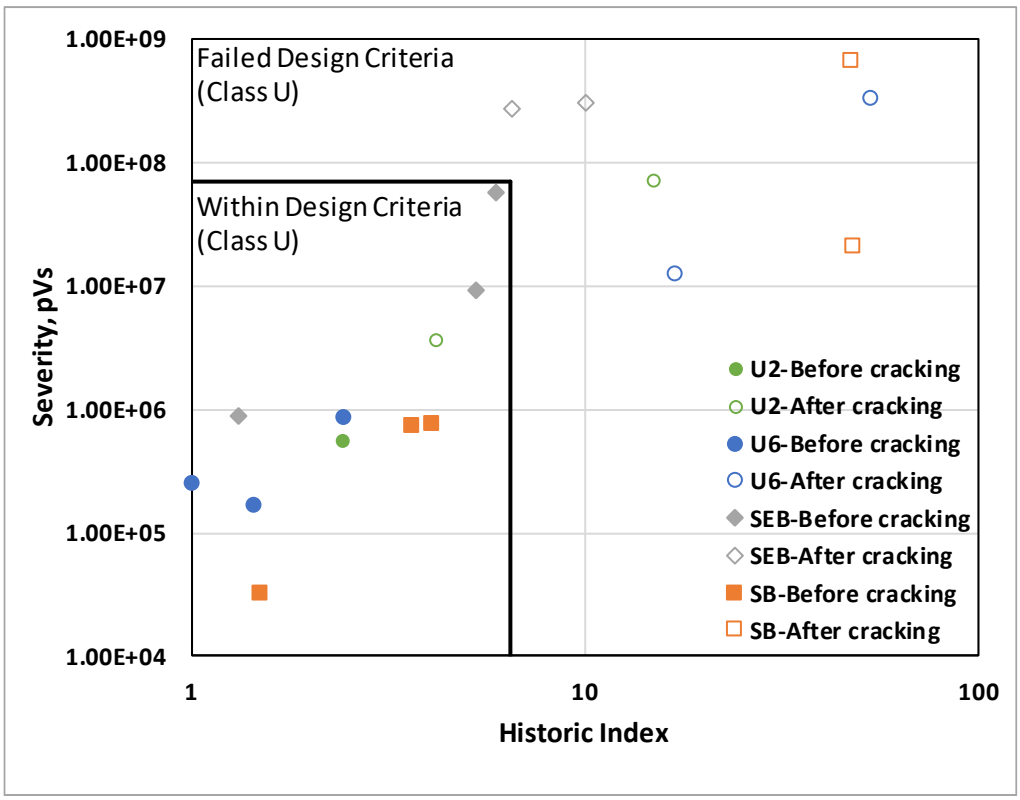

Figure D.1 Intensity analysis chart (girders in good condition)

The intensity analysis chart developed on the girders in good condition was used to assess the deterioration of the girders in poor condition. An intensity analysis chart for girders in poor condition is shown in Figure D.2. Similarly, data points in this chart are presented with respect to the theoretical cracking load; therefore, eight different labels are used to show data before and after the theoretical cracking load in the four girders in poor condition. The results show that the girders in poor condition fail the design criteria at lower loads than the theoretical cracking load. It was noticed that the data points in the red box for the girders in poor condition are plotted in the failed design criteria area; this indicates that the girders have already deteriorated, which is true based on the visual inspection. The results show that the intensity analysis can discriminate between the girders' initial conditions. In addition, the charts consider the existing deterioration in the girders.

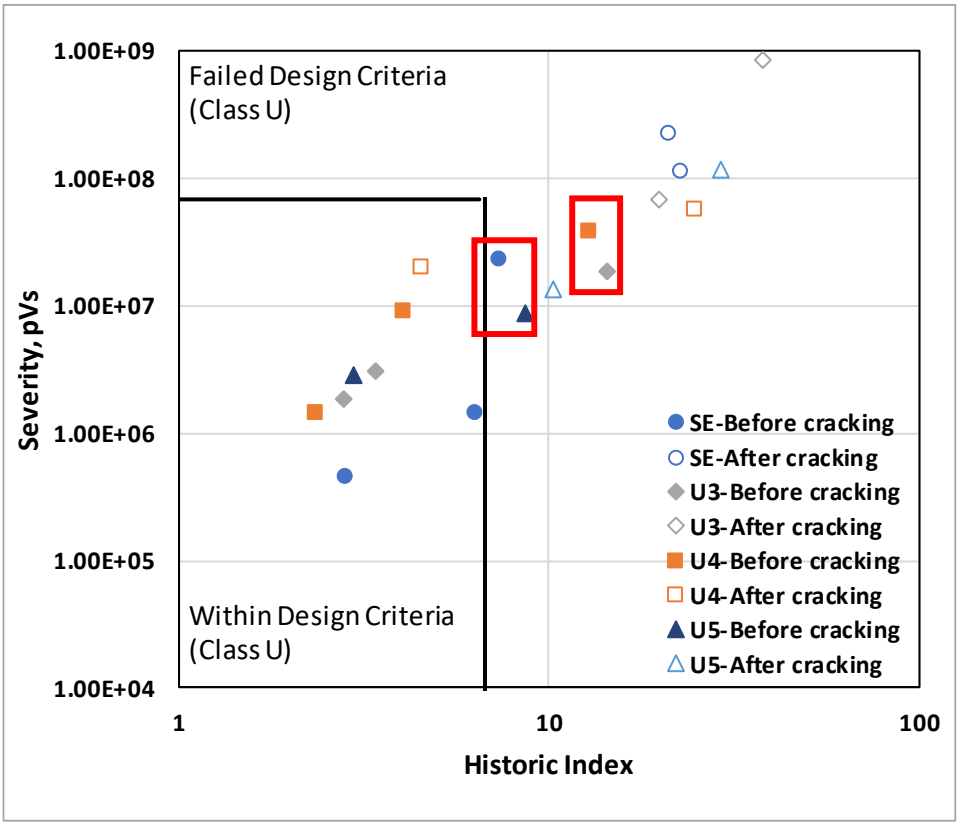

Figure D.2 Intensity analysis chart (girders in poor condition)